STABLY STRATIFIED BUILDING WAKES

by

K. M. Kothari
J. A. Peterka
R. N. Meroney

Prepared for

Site Safety Research Branch
Office of Nuclear Regulatory Research
U.S. Nuclear Regulatory Commission
Washington, D.C. 20555

Fluid Dynamics and Diffusion Laboratory
Department of Civil Engineering
Colorado State University
Fort Collins, Colorado 80523

July 1979

CER78-79KMK-JAP-RNM65

ABSTRACT

STABLY STRATIFIED BUILDING WAKES

The velocity and temperature wake behind an isolated building placed in a stably stratified turbulent boundary layer has been investigated utilizing wind tunnel tests and mathematical analysis. The mean velocity and mean temperature decreases but turbulence intensity and temperature fluctuation intensity increases as a result of the momentum wake. However, the vortex wake increases mean velocity and mean temperature, and decreases turbulence intensity and temperature fluctuation intensity along the centerline of the wake.

A wind tunnel study of the wakes behind six surface-mounted rectangular building models in a stably stratified turbulent boundary layer was performed for wind direction perpendicular to one face of the building. Measurements of mean velocity, mean temperature, turbulence intensity, temperature fluctuation intensity, velocity-temperature correlations, spectra of velocity and temperature were measured at a Reynolds number greater than 2.0×10^4 with and without the buildings in place.

A method for simultaneous measurement of velocity and temperature was developed. Hunt's theory for momentum and vortex wakes was evaluated. An analytical technique for prediction of temperature field in the wake of a building using the energy equation for turbulent flow was developed. The present theory considers momentum and vortex wake effects to determine the mean temperature in the wake of a building.

It was found that Hunt's theories for momentum and vortex wakes give very good agreement for mean velocity on the centerline in the wake of a building. It was also observed that the vortex wake was persistent

and excess velocity was observed in the far wake region. The theory developed for this research for the temperature field shows an excellent agreement for mean temperature in the wake of a building. The excess temperature in the wake of a building increases up to a certain x/H and then decreases. The temperature wake was extremely persistent and even at $x/H = 60$ behind all the buildings the wake displayed an excess temperature. This is the result of the horseshoe vortex which brings higher temperature fluid from the top of the turbulent boundary layer towards the ground along the centerline of the building. Hence, the horseshoe vortex plays a very important role in determining any scalar quantity distribution, such as temperature, in the wake of a building.

The velocity fluctuation spectra are similar at various x/H locations with and without a building and obey a $-5/3$ power law behavior in the inertial subrange. The temperature intensity spectra show a $-5/3$ power law behavior in the inertial subrange for approach-flow conditions; however, spectra of temperature in the wake of a building have approximately a -1 power law behavior in the inertial subrange.

Though refinement is needed, the analytical theory of Hunt for the mean velocity field and the present analytical theory for the mean temperature field in the wake of a building are very useful techniques.

ACKNOWLEDGMENTS

This research was conducted under Contract No. AT(49-24)-0366 with the United States Nuclear Regulatory Commission. Financial support received is greatfully acknowledged. The authors wish to thank Dr. Robert Abbey, Jr., NRC, for the helpful suggestions during the course of the research.

TABLE OF CONTENTS

LIST OF FIGURES

LIST OF SYMBOLS

Symbol	Definition
A, A_1, A_2	calibration constants for hot films
a	virtual origin of wake
B, B_1, B_2	calibration constants for hot films
c, c_1, c_2	calibration constants for hot films
C_1, C_2, C_3, C_4	constants used in Appendix B
c_p	specific heat of fluid at constant pressure
$C_{a_1a_2}(f)$	coincident spectral density function (co-spectrum)
C_{Fx}	force coefficient of the building in x direction
$Co_{a_1a_2}(f)$	coherence
d	width of wake
DELTA T	mean temperature used for nondimensionalizing
Delta T VAR	excess of variance of temperature fluctuation in the wake of a building
Delta U	mean velocity defect in wake of a building
Delta U VAR	excess of variance of velocity fluctuation in wake of a building
E, E_1, E_2	output voltages of contant temperature anemometers
Excess T	excess mean temperature in wake of a building
F	function defined in equation (3.18)
F_1	function defined in equation (2.4)
F_2	function defined in equation (3.24)
f	function defined in equation (3.18)
$G_a(f)$	power spectral density function
$G_{a_1a_2}(f)$	cross spectral density function
g	acceleration due to gravity

Symbol	Definition
$g_a(f)$	normalized power spectral density function
H	building height
h	vertical height of center of vortex
K	von Karman constant
k	molecular diffusivity of fluid
k_1	constant defined in equation (2.4)
k_2	constant defined in equation (3.24)
L	length of wake in longitudinal direction
ℓ	length of bubble region in longitudinal direction
n	mean velocity power law exponent
n_2	mean temperature power law exponent
n'	power law exponent for velocity defect
p, q, r	constants defined in Appendix B
$Q_{a_1 a_2}(f)$	quadrature spectral density function (quad-spectrum)
q_o, q_2	functions defined in equation (3.19)
R, R_1, R_2	resistance of hot films
$R_a(\tau)$	auto-correlation coefficient
R_a, R_{a_1}, R_{a_2}	resistance of hot films corresponding to environment mean temperature T_a, T_{a_1}, and T_{a_2}
R_c, R_{c_1}, R_{c_2}	calibration resistance of hot films corresponding to calibration mean temperature T_c, T_{c_1}, T_{c_2}
$R_{a_1 a_2}(\tau)$	cross-correlation function
$r_a(\tau)$	normalized auto-correlation function
$r_{a_1 a_2}(\tau)$	normalized cross-correlation function
Ri_δ	bulk Richardson number based on boundary layer height
Ri_H	bulk Richardson number based on building height

Symbol	Definition
T	instantaneous fluid temperature
$\overline{T}$	mean fluid temperature
T_w	hot film temperature
$\overline{T}_w$	mean fluid temperature in wake of a building
T_*	reference temperature
$\overline{T}_{z_1}$	mean temperature at the height z_1
t	time
U, V, W	instantaneous velocity components in x, y, and z directions
$\overline{U}, \overline{V}, \overline{W}$	mean velocity components in x, y, and z directions
$\overline{U}_w, \overline{V}_w, \overline{W}_w$	mean velocity components in x, y, and z directions in wake of a building
$\overline{U}_{z_1}$	mean velocity in x direction at the height z_1
u, v, w	perturbations on mean velocity components in x, y, and z directions in wake of a building
u', v', w'	fluctuation of velocity components in x, y, and z directions
u_*	friction velocity
x, y, z	space coordinates, x downwind, y lateral, z vertical
$\overline{x}, \overline{y}, \overline{z}$	nondimensional space coordinates, $\overline{x}$ downwind, $\overline{y}$ lateral, $\overline{z}$ vertical
y_v	lateral distance to center of vortex
z_o	roughness height
z_1	reference height (0.25 cm)
z_2	reference height (δ)

Symbol	Definition
Greek Symbols	
α	temperature coefficient of resistance of hot film
β	constant defined in equation (2.1)
β_T	constant defined in equation (2.2)
Γ	circulation of vortex at $x = 0$
δ	boundary layer thickness
θ	perturbation on mean temperature in wake of a building
θ'	temperature fluctuation
$\theta_{a_1 a_2}(f)$	phase angle between two signals
$\overline{\nu}$	mean eddy viscosity
$\overline{\nu}_1$, $\overline{\nu}_2$, $\overline{\nu}_3$	mean eddy viscosity in x, y and z directions
γ	constant of order one
λ	constant of order one
$\overline{\varepsilon}$	mean eddy diffusivity
ε_1, ε_2, ε_3	mean eddy diffusivity in x, y and z directions
Δ	thickness of wake in z direction
ρ	density of air
μ	viscosity of air
Φ	dissipation function

Chapter I

INTRODUCTION

This research reports a study of momentum and vortex wakes behind surface mounted bluff bodies deeply immersed in a stably stratified turbulent boundary layer. The aims of the present research were to determine the effect of thermal stability in the approach flow on the wake and generate the basic physical models for temperature and velocity distributions in the wake.

A surface obstacle or building in the planetary boundary layer creates a wake behind the obstacle. The wake is generally characterized by increased turbulence intensity and decreased mean longituinal velocity. The loss of velocity in the wake amounts to loss of momentum. Moment of the loss of momentum is then related to the couple acting on the obstacle. The spread of the wake increases as the distance from the building increases, and the difference between the velocity in the approach flow and in the wake becomes smaller. An obstacle wake of this type is known as a Momentum Wake or Normal Wake. Passage of a shear flow around a surface obstacle also creates a system of longitudinal vortices in the wake of the obstacle. An obstacle wake of this type is classified as a vortex wake. The vortex brings higher-momentum, less-turbulent fluid from higher elevations of the turbulent boundary layer to increase the velocity and decrease the turbulence intensity near the wake centerline; however, the vortex brings lower-momentum, high-turbulent fluid from the lower elevation of the turbulent boundary layer to decrease the velocity and increase turbulence intensity on the outboard side of the vortex. Gregory and Walker [1] and Mochizuki [2] observed longitudinal vortices in the wakes of isolated objects in

laminar boundary layer flows. Ostrowski, Marshall and Cermak [3] described the generation of vortices at the leading roof corner of a building placed at an angle of incidence to the approach flow. Similar effects were observed by Hansen, Peterka and Cermak [4] in the wake of a simple structure in a simulated atmospheric flow. Woo, Peterka and Cermak [5] have observed the horseshoe vortex pattern with the wind approaching normal to the one face of the model in a wake of an obstacle placed in a simulated turbulent boundary layer. Thus, in the wake of an obstacle placed in a turbulent boundary layer, the resultant superposition of momentum and vortex wake on fields of temperature and velocity should be determined.

Knowledge of the stucture of building wakes has application to diverse fields. Diffusion of material released in the wake of a building will be strongly altered, particularly if the pollutant is released within the separation bubble in the lee of a building or if the wake contains standing vortices. Modeling the pollutant concentration in the wake of the building requires the knowledge of flow characteristics within the wake. Using the data of Peterka and Cermak [6] for decay rate of excess turbulent intensity, Huber and Snyder [7] have developed a prediction technique for pollutant concentration in building wakes.

In order to reduce congestion at major airports, the need exists for rapid interurban transportation. A promising alternative for solving this problem is to design smaller airports near populated centers operating with V/STOL aircraft. Before constructing the airport in or very near an urban area, the effect of wind in and near the airport on aircraft operation should be determined. A large building

in the proximity will alter the wind patterns in which aircraft must fly. Serious problems for some aircraft, are created due to increased turbulence and mean wind shear. Highly structured vorticity generated by the flow around buildings could subject aircraft to large pitching and rolling moments deteriorating aircraft control and causing passenger discomfort.

Another area in which knowledge of building wakes is important is the effect of nearby building on the wind load requirement of a structure. Local pressure loadings may increase or decrease due to nearby structures and depend on the relative position of approaching wind, the building shapes and separation distance between structures. Zambrano and Peterka [8] have carried out an extensive study of the pressure loading on the building due to adjacent buildings. In addition, pedestrian comfort near buildings is frequently influenced by the wake characteristics of a building.

The present research was divided into two parts viz., wind tunnel experiments in the wakes of six different obstacles and development of a theoretical model for the temperature field. Six simple Plexiglas models were used and placed on the wind tunnel floor in a stably stratified turbulent boundary layer. Measurements of mean velocity and temperature, turbulence intensity of velocity and temperature, and one-dimensional spectra for velocity and temperature were measured. A technique was developed to determine the velocity and temperature from fluctuating voltage outputs of two parallel hot films in a manner conducive to the large volume of data anticipated for this study.

In the second phase, a theory of momentum and vortex wakes developed by Hunt was used to compare the present results for the

velocity field. A similar theory was developed for the temperature field. These theories will be discussed in detail in the next chapters.

A literature survey of related wake studies is presented in Chapter II. Theoretical considerations for determination of temperature field in the building wake are described in Chapter III. Chapter IV presents the modified technique for determination of velocity and temperature from voltage outputs of two parallel hot films. Experimental results are presented in Chapter V and compared with the present theory. The major conclusions of the present study and recommended areas for further investigations are outlined in Chapter VI.

Chapter II

LITERATURE SURVEY

2.1 Introduction

Theoretical and experimental research for wake behavior has been performed behind cylinders, spheres and streamlined bodies. Very little is known concerning wake characteristics behind bluff bodies. Experimental and theoretical research for obstacles placed in turbulent shear layers has been performed only for neutral flow conditions; hence, the present research for stably stratified building wakes will add a new insight to the wake problem. The intent of this chapter is to present and draw together in condensed form the literature for building wakes. It should be noted that the mathematical treatment reviewed does not apply to the entire wake behind a building; nevertheless the concepts describe the physical mechanism and essential features of the far-wake region behind a building. Most of the literature which deals with stable flow concerns turbulent boundary layers only. The pertinent literature for turbulent boundary layers and then the details of neutral wakes behind buildings will be reviewed.

2.2 Turbulent Boundary Layers

Using the basic assumption that the flow is homogeneous in the flow direction and fluxes of heat and momentum remain essentially constant with height, Monin and Obukov [9] developed a similarity theory. Consideration of the pertinent variables leads to three scales, viz., length, L, velocity, u_*, and temperature, T_*. They concluded that the mean and turbulent quantities of flow when nondimensionalized by the proper combination of the above mentioned three scales, must be a universal function of a stratification parameter, z/L.

For the mean velocity and temperature, the theory of Monin and Obukhov predicts log-linear profiles given by

$$\overline{U}(z) - \overline{U}(z_{ref}) = \frac{u_*}{K} \left[\ell n \frac{z}{z_{ref}} + \beta\left(\frac{z - z_{ref}}{L}\right)\right], \tag{2.1}$$

$$\overline{T}(z) - \overline{T}(z_{ref}) = \frac{T_*}{K} \left[\ell n \frac{z}{z_{ref}} + \beta_T\left(\frac{z - z_{ref}}{L}\right)\right], \tag{2.2}$$

in which β and β_T are empirical constants, and K is the von Karman constant.

Arya [10] has examined the stably stratified boundary layer in a meteorological wind tunnel, and the structure of the boundary layer was discussed in light of Monin and Obukhov's similarity theory. It was shown that mean and turbulent characteristics of the flow of the wind tunnel boundary layer are described well by similarity theory.

2.3 Building Wakes

2.3.1 Prototype Measurements

M. J. Colmer [11] reported measurements in the wake of a hanger, 30 m long, 15 m wide, 10 m high, with a roof pitch of 10 degrees, at the Royal Aircraft Establishment at Bedford. Three instrumented towers were located 5H, 14H, and 23H downwind along the anticipated wake centerline and one tower was located at 5H downwind and 5H off the centerline, where H is the height of the hanger. The approach conditions were measured by a tower at 18H upstream of the hanger. The measurements were performed in the planetary boundary layer having a measured power law exponent of 0.18. The thickness of the boundary layer was estimated (but not measured) to be 610 m (2,000 ft). Only one set of experimental measurements was reported; hence, no general conclusion can be drawn for the wake structure. Colmer determined that

the mean speed in the wake was smaller than that in the approach flow at the same height. Colmer also found that this velocity defect reduced rapidly to zero around 14H downstream of the hanger. He discovered that turbulent intensities were still noticeably different from those in the approach flow at the same height even at a distance of 23H downstream.

Frost and Shahabi [12] have made prototype measurements in the wake of rectangular buildings at the NASA George C. Marshall Space Flight Center in Huntsville, Alabama. The facility included an eight tower array located in a large open field. All the towers were instrumented at 3, 6, 12 and 20 m levels. Sixty-two experimental data sets were obtained with no building present, 16 runs were made with a small building 2.4 m deep, 3.2 m high and 7.95 m long, and 12 runs were made with a longer building 2.4 m deep, 3.2 m high and 26.8 m long. The measurements included data to determine mean longitudinal velocity, vertical velocity, wind direction, auto-correlation function and spectra of longitudinal velocity fluctuations. The mean velocity defect behind the larger building decayed with distance at a rate proportional to $x^{-1.5}$. This is in agreement with wind tunnel measurements of Woo et al. [5]; however, the wind-tunnel velocity defects were smaller in magnitude.

2.3.2 Wind-Tunnel Measurements

A large body of literature exists on the two-dimensional wakes of barriers; because two-dimensional wakes differ significantly from the three-dimensional wakes considered in this study, only three-dimensional wake studies will be reported. Wind-tunnel measurements of building wakes have been conducted by Yang and Meroney in 1970 [13],

Counihan in 1971 [14], Lemberg in 1973 [15], Castro and Robins in 1975 [16], Hansen, Peterka, and Cermak in 1975 [4], Peterka and Cermak in 1975 [6], Hansen and Cermak in 1975 [17], Woo, Peterka, and Cermak in 1976 [5], Hatcher, Meroney, Peterka, and Kothari in 1977 [18], and Hunt, Abell, Peterka, and Woo in 1978 [19].

Yang and Meroney [13] measured centerline velocities in the wake of a 15 cm (5.9 inch) cube placed in a stably stratified turbulent boundary layer with one face either perpendicular or 45 degrees to the approach flow. The measurements were performed to establish the velocity profile influencing turbulent diffusion in the wake of a building and no wake characteristics were reported. However, from figures presented it can be concluded that the momentum wake disappeared within 20 to 25 heights downstream of the building.

Counihan [14] made detailed measurements of wakes behind a 1.9 cm (0.75 inch) cube, with one face perpendicular to the flow direction, placed in an artificially simulated thick turbulent boundary layer. The ratio of model height to boundary layer height was 1/8 with a power law exponent of 0.15. Mean longitudinal velocities, three fluctuating components of velocity and spectra of longitudinal velocity fluctuation were measured in the wake of the cube. Similar measurements were made, with the same conditions, for a two-dimensional block 1.9 cm (0.75 inch) high and 1.9 cm (0.75 inch) deep. The main finding of Counihan was that the wake of a two-dimensional block decays at a rate of $x^{-0.47}$. This decay rate was slower than the rate of decay for the cube. Hunt and Smith [20] predicted for a two-dimensional block that the mean velocity defect decreases as x^{-1} whereas for the cube it decreases as $x^{-1.5}$; hence, the experimental measurement

and theoretical prediction do no agree for two-dimensional block. Counihan also noted that turbulent integral length scales were larger in the undisturbed boundary layer than behind the block and cube. He observed that the integral length scale for the block was larger than that of the cube.

At the University of Western Ontario, Lemberg [15] obtained experimental data for several three-dimensional building wakes in a naturally developed turbulent boundary layer in a wind tunnel. Measurements of longitudinal mean velocity and turbulence intensity as well as overturning moments for each building were made. Lemberg also observed the horseshoe vortices during flow visualization studies in a water channel but without boundary layer simulation. No attempt was made to determine the effect on the wake of horseshoe vortices. The velocity defect was found to decay as $x^{-1.58}$ for all of his data, which is close to Hunt's theoretical prediction. The turbulence intensity excess was found to decrease at rates varying from -0.11 to -0.30, much slower rates than the -2.0 predicted by Hunt [21]. Part of Lemberg's work was devoted to modification of Hunt's theory to include variable eddy viscosity.

Castro and Robins [16] observed the wake behind a 0.2 m (0.66 ft) cube in a simulated planetary boundary layer having a power law exponent of 0.24 and a thickness of 2 m (6.6 ft). The measurements were carried out with a pulse-wire anemometer to measure more accurately longitudinal velocity and turbulence intensity in the near wake region. The wake observed by them extended only 4.5 building heights downstream of the building. The reasons suggested for the short wake were high turbulence intensity and strong shear in the approach flow.

Some recent measurements of wakes in wind tunnel studies at Colorado State University were reported by Hansen, Peterka and Cermak [4], and Peterka and Cermak [6]. An interesting feature of these studies was the effect of approach flow direction on the wake structure. It was found that the wake extends about four times farther with the model placed at 45 degrees to the approach flow than with one face normal to the approach flow. Longitudinal vortices were determined to persist for farther distances with the model at approximately 45 degrees to approach flow resulting in a longer wake. A technique for measurement of the horseshoe vortex circulation was also developed.

Hansen and Cermak [17] measured the vortex containing wakes behind hemispheres placed in a thick, simulated planetary boundary layer. The mean longitudinal velocity, mean swirl velocity and vortex strength, longitudinal velocity fluctuation intensity and spectra were measured in the wakes. They developed an inviscid model to predict the strength of the horseshoe vortex. They also determined that the meander caused a rapid decay in the average vortex strength, whereas there was very slow decay of the instantaneous vortex strength. It was observed that the vortex wake was extremely persistent as compared with the momentum wake. The vortex wake was observed up to 100 model heights downstream whereas the momentum wake was observed only up to 15 to 20 model heights downstream. They concluded:

> "As the momentum wake decays in proportion to $x^{-1.5}$ and the vortex wake strength decreases much more slowly as $x^{-0.5}$, it can be expected that at sufficient distance downwind of the obstacle the vortex wake will be dominant and there will be a region of velocity excess."

Woo, Peterka and Cermak [5] have carried out an extensive study of wakes behind twenty different models using four different simulated

thick turbulent boundary layers. The flow pattern around the rectangular block and horseshoe vortex pattern were determined. Measurements of longitudinal mean velocity, turbulence intensity, correlations, and spectra were made in the wake of the buildings and without buildings in place. A general model of mean flow developed in that study is shown in Figure 1. Similar measurements were made with models at 47 degrees to the approach flow to deduce similar effects on the wake structures as noted by Hansen, Peterka and Cermak [4].

Hatcher, Meroney, Peterka and Kothari [18] have carried out extensive measurement of turbulence and dispersion in a wake of a model industrial complex. The mean velocity defect decayed as $x^{-1.13}$ and excess turbulence intensity decayed as $x^{-2.7}$ in the wake. They detected the wake at a distance of $x/H = 30$ at a five percent mean velocity defect level. They concluded that such a long wake region was associated with the low roughness characteristic of the site.

Hunt, Abell, Peterka and Woo [19] have studied kinematical aspects of the flows around free or surface mounted obstacles. They have studied laminar and turbulent flow around surface obstacles such as cuboids and axisymmetric humps. They developed a technique for the surface flow visualization for highly turbulent recirculating flows. From the surface patterns they deduced the mean surface stress streamline. The mean flow streamlines were sketched from velocity measurements near bluff bodies. On the basis of kinematical principles and experimental results they concluded that in the separated flow around surface-mounted obstacles closed streamline surfaces do not exist.

2.3.3 Theoretical and Numerical Methods

A theoretical foundation for wake behavior behind bluff bodies immersed in a thick turbulent boundary layer was pioneered by Hunt and Smith. Hunt and Smith [20] in 1969 proposed a theory to calculate time mean velocity in the wake of two- and three-dimensional bluff bodies immersed in a thick turbulent boundary layer. The theory was improved for two-dimensional bodies by Hunt [21]. In this publication, methods to calculate the root mean square of turbulent velocity and Reynold stress were also described. In 1971, Hunt [22] described a model for two-dimensional laminar wakes and a relation between the moment of momentum defect in the wake and the overturning moment exerted on the body. A detailed summary for such wake theories has been presented in two papers of Hunt [23,24]. Comparison of theory with experiments and a condensation of the analysis are given in another two papers by Hunt [25,26]. In 1975, Hunt [27] developed the theoretical model to account for the influence of longitudinal vortices on wakes.

Momentum wake theory is based on the assumption that only small perturbations to the turbulent boundary layer are caused by obstacle, that the ratio of the model height to the boundary layer height is very small and that velocity defects in the wake are small compared with mean longitudinal velocity. The theory is valid only for the far wake region because the separated region behind the model cannot be considered to be a small perturbation on the approach flow. Hunt's theory also assumes a power-law profile for approach flow mean velocity, with power-law exponent $n << 1$. The mean velocities in the wake were expressed by perturbation on the undisturbed flow and represented by:

$$\overline{U}_w = \overline{U}\ (x,\ z) + u(x,\ y,\ z),$$

$$\overline{V}_w = v\ (x,\ y,\ z),\ \text{and} \qquad (2.3)$$

$$\overline{W}_w = w\ (x,\ y,\ z).$$

The assumption that u, v and w vanishes as $x \to \infty$ implies that farther downstream the effect of the building disappears and the flow field returns to the approach conditions.

For the two-dimensional obstacle case, an empirical relationship was used to obtain the perturbation shear stress by Hunt [20] for closure of the equations of motion. From this, an equation for eddy viscosity was derived. The equation for eddy viscosity was integrated across the boundary layer using the approach flow condition to estimate an average eddy viscosity, $\overline{\nu} = 2K^2 nH\overline{U}(H)/(2+n)$. K and n are the von Karman constant and the power-law profile exponent in the approach flow respectively. For the three-dimensional obstacle case, the constant eddy viscosities, $\overline{\nu}_2$ and $\overline{\nu}_3$ in y and z directions respectively, were then approximated by $\overline{\nu}_3 = \gamma\overline{\nu}$ and $\overline{\nu}_2 = \lambda\overline{\nu}_3 = \lambda\gamma\overline{\nu}$. λ and γ are the constants of order one for the three-dimensional case. Using this approximation, turbulent shear stresses τ_{xz} and τ_{xy} are expressed as $\tau_{xz} = \overline{\nu}_3 \frac{\partial \overline{U}}{\partial z}$ and $\tau_{xy} = \overline{\nu}_2 \frac{\partial \overline{U}}{\partial y}$. Assuming a Gaussian distribution of velocity defect in the lateral directions, the first order solution of the equation of motion was obtained by Hunt and Smith [20].

Hunt's three-dimensional wake solution can be summarized:

$$\frac{u(x,\ y,\ z)}{\overline{U}(H)} = k_1 F_1(z'',\ y'')/[(x - a)/H]^{\frac{3+n}{2+n}} \qquad (2.4)$$

where $u(x, y, z)$ = velocity defect,

$\bar{U}(H)$ = velocity at building height H in the undisturbed flow,

a = virtual origin of the wake to be determined from experiment,

n = boundary layer velocity profile power-law exponent,

$k_1 = 0.21\ C_{Fx}\ (W/H)/\{4\lambda^{1/2}\ \gamma(2K^2n/(2+n))^{\frac{3+n}{2+n}}\}$,

W = width of building,

λ and γ = constants of order one that are adjusted to give optimum agreement with theoretical and experimental results,

K = von Karman constant (0.41),

C_{Fx} = force coefficient of building,

$$F_1(z'', y'') = \frac{\eta^{\frac{1}{2+n}} \mathrm{Exp}[-(\eta + y''^2/(1.5 + \eta))]}{(\eta + 1.5)^{1/2}},$$

$$z'' = (z/H)/[(x - a)/H]^{\frac{1}{2+n}},$$

$$\eta = z''^{(2+n)}/[2(2 + n)\ K^2n\ \gamma],$$

$$y'' = \frac{(y/H)}{[(x - a)/H]^{\frac{1}{(2+n)}}} \left[\frac{2+n}{2\lambda\gamma K^2 n}\right]^{\frac{1}{(2+n)}}.$$

Similar results are available for the two-dimensional case. The perturbation fluctuating velocity were also determined. Briefly, for the three-dimensional case, the mean square longitudinal fluctuating velocity varies as $\Delta u^2_{rms}/\bar{U}(H)^2 \simeq 1.0/(x/H)^2$ and the two-dimensional case varies as $\Delta u^2_{rms}/\bar{U}(H)^2 \simeq 10.0\ (K^2n)^{1/2}/(x/H)^{3/2}$.

Hunt's theory provides a method to plot the experimental data in a universal form. For a three-dimensional case the experimental data can be plotted as $u/\overline{U}(H)$. $(\frac{x-a}{H})^{\frac{3+n}{2+n}}$ against $(z/H)/(\frac{x-a}{H})^{\frac{1}{2+n}}$ to give a universal curve. For n small, Hunt's momentum theory predicts that the mean velocity defect decays as $x^{-3/2}$.

Hunt [21] compared the above momentum wake theory with the results of Counihan [14]. For a two-dimensional block Counihan found that the mean velocity defect decayed as $x^{-0.47}$. Hunt predicted a mean velocity defect decay rate of $x^{-1.0}$. Hunt attributed the difference to the assumption of constant eddy viscosity; however, the experimental values of the mean velocities behind the cube did fit a universal curve as suggested by Hunt's theory.

Lemberg recognized the weakness of the constant eddy viscosity assumption in Hunt's theory. Lemberg assumed a variable viscosity of the form $\overline{\nu}_3 = K' z^b H \overline{U}(H)$, where K' and b are arbitrary constants determined by comparison with experimental data. He also assumed the eddy viscosity in the y direction to be proportional to $\overline{\nu}_3$ and has a form of $\overline{\nu}_2 = \overline{\nu}_3 (W/H)^2$. Lemberg determined the value of "b" to be equivalent to the boundary layer power-law exponent n. Hence, the eddy viscosity used by Lemberg was proportional to the mean longitudinal velocity at the same height in the undisturbed flow. The introduction of variable eddy viscosity did not show significant improvement in ability of the theory to match experiments.

Both Lemberg and Hunt assumed a Gaussian distribution of velocity defect for the lateral direction. Measurements by Peterka and Cermak [6] do not support this hypothesis; hence, improvement is needed in this area. They observed in horizontal profiles of mean velocity defect, the

profile maxima did not occur on the centerline near the model but was displaced from 1/2 to 1 building width to the side. The displaced maxima was short lived in downstream distance. An interesting feature of the profiles is a secondary peak which occurred 2 to 3 W/2 from centerline and observed from 2 to 12-14 H downwind. Similar effects were observed by Hansen, Peterka and Cermak [4] in the wake of a rectangular building in a simulated atmosphere boundary layer wind. Peterka and Cermak concluded that this effect was the result of the well-known horseshoe vortex which was not considered in Hunt's theory.

An extensive study of hemisphere wakes containing organized longitudinal vorticity was conducted by Hansen and Cermak [17]. Simultaneously, Hunt developed a small perturbation theory for the effect of vortices on wakes behind buildings deeply immersed in the planetary boundary layer [27, to be published]. Hansen and Cermak used the results of Hunt's vortex wake theory to determine the perturbation excess velocity induced in the hemisphere wake by an organized line vortex.

Figure 2 is derived from Hunt's vortex wake theory to show the regions of influence of the vortex cores. The region is divided into three regions, viz., E, where the flow is assumed to be inviscid, V_+ and its image V_- is the viscous region surrounding the vortex where there is a balance between Reynolds stress and inertial forces and G where the boundary layer assumptions apply. The growth rates of all these regions were determined by Hunt, and he concluded that downstream from the origin of the vortex all three regions merge together. This means that the vortex core radius is much larger than the height of building. The qualitative and pictorial view of the flow

pattern around the bluff body immersed in the turbulent boundary layer was shown in Figure 1 to illustrate the effect of such a horseshoe vortex.

Hunt's theory considers the interaction of a line vortex with the mean vertical velocity shear. It is in concept similar to the momentum wake theory. The vortex transports higher momentum fluid from a higher elevation to a lower elevation of the turbulent boundary layer and increases the velocity on the inboard side of the vortex. The horseshoe vortex forms in the stagnation region in front of the building and curls around the building to produce a mean vorticity with the axis in the longitudinal direction. The total solution of the multiple vortex system can be obtained by superimposing the result of each vortex in the system. The resultant equations of motion become linear in the perturbation quantities; hence, the solution of momentum wake and vortex wake can be superimposed.

The exact solution of the equations of motion for Hunt's vortex wake solution in terms of perturbation quantities involve triple integration which have not been evaluated. At present only the asymptotic results are available for determining the effect of vortex. Hunt has determined that swirl velocity component, w, decreases as $x^{-1/2}$ when the three regions are distinct and farther downstream where all three regions merge together it decreases as x^{-1}. Hunt has also calculated the asymptotic results for region V_+ and V_- and found that the longitudinal perturbation velocity excess induced by a vortex increases as $x^{1/2}$ until the three regions are distinct. Thereafter, Hunt has indicated (not calculated) for longitudinal perturbation velocity excess, that the asymptotic solution will be proportional to $x^{-1/2}$.

The longitudinal velocity excess in region E was determined by Hunt and given by,

$$u = \frac{n\Gamma}{\pi} \frac{hy'x}{[(y'^2 + h^2 + z^2)^2 - 4z^2h^2]} \qquad (2.5)$$

where $y' = y_v - y$. y_v and h are the locations of the vortex center in lateral and vertical directions respectively and Γ is the circulation of $x = 0$. An interesting feature of the equation (2.5) is that u increases linearly with x in region E; however, this process cannot persist indefinitely. Hunt has concluded that u ceases to vary linearly as soon as the width of the viscous core is approximately equal to y or the depth of the region G equals z.

Hansen and Cermak [17] have investigated the effect of horseshoe vortices without consideration of roof corner vortices. The velocity perturbation predicted by equation (2.5) was doubled to account for two horseshoe vortices, one on each side of the hemisphere, as observed in the wake of the hemisphere. In their result, the effect of u proportional to x is clearly noticeable. The theoretical and experimental results are in fair agreement at $x/R = 8.73$. The comparison deteriorates for large x/R ratios due to the assumption of a continuous increase in u. Hunt's theory requires the strength and position of the vortex, the measurements of which are not always performed.

Frost, Maus and Simpson [28] and Hirt and Cook [29] have been working to develop a numerical model for building wakes. However, due to the complex nature of the problem the progress in the numerical model is slow and relies heavily on experimental data. A survey of such wake models that are in the process of development is given by Frost [30].

Chapter III

THEORETICAL CONSIDERATIONS

The physics of vortex and momentum wake mechanisms can be applied to any passive scalars such as temperature or heat. In this chapter, the theory has been developed to predict the time mean temperature field behind the three-dimensional bluff body immersed deeply in a stratified turbulent boundary layer. Some of the results for the velocity field are obtained from Hunt's Vortex Wake Theory [27] to derive the present model for the temperature field.

3.1 Turbulent Energy Equation

The transport of a scalar quantity such as temperature is governed by the energy equation,

$$\frac{DT}{Dt} = \frac{\partial}{\partial x}\left(\frac{K}{\rho c_p}\frac{\partial T}{\partial x}\right) + \frac{\partial}{\partial y}\left(\frac{K}{\rho c_p}\frac{\partial T}{\partial y}\right) + \frac{\partial}{\partial z}\left(\frac{K}{\rho c_p}\frac{\partial T}{\partial z}\right) + \frac{\mu}{\rho c_p}\Phi \qquad (3.1)$$

where Φ is the dissipation function given by,

$$\Phi = 2\left\{\left(\frac{\partial U}{\partial x}\right)^2 + \left(\frac{\partial V}{\partial y}\right)^2 + \left(\frac{\partial W}{\partial z}\right)^2\right\} + \left(\frac{\partial V}{\partial x} + \frac{\partial U}{\partial y}\right)^2 + \left(\frac{\partial W}{\partial y} + \frac{\partial V}{\partial z}\right)^2 + \left(\frac{\partial U}{\partial z} + \frac{\partial W}{\partial x}\right)^2,$$

U, V, W, = velocity components in x, y and z directions (see Figure 3),

T = temperature of fluid,

K = thermal conductivity of the fluid,

ρ = density of the fluid,

c_p = specific heat of the fluid,

μ = viscosity of the fluid,

and $$\frac{DT}{Dt} = \frac{\partial T}{\partial t} + U\frac{\partial T}{\partial x} + V\frac{\partial T}{\partial y} + W\frac{\partial T}{\partial z} .$$

The fluid is assumed to be incompressible although the density is not uniform. This means that the changes in density are not due to changes in pressure but only due to temperature. Schlichting [31] has shown by the estimation of each term in the energy equations that the dissipation function is small compared with the other terms when the viscosity of the fluid is small. Hence, the dissipation term was negelected in the present analysis, to give,

$$\frac{\partial T}{\partial t} + U\frac{\partial T}{\partial x} + V\frac{\partial T}{\partial y} + W\frac{\partial T}{\partial z} = \frac{\partial}{\partial x}\left(k\frac{\partial T}{\partial x}\right) + \frac{\partial}{\partial y}\left(k\frac{\partial T}{\partial y}\right) + \frac{\partial}{\partial z}\left(k\frac{\partial T}{\partial z}\right) \tag{3.2}$$

where $k = \frac{K}{\rho c_p}$ is the molecular diffusivity of the fluid.

Now, assuming the steady state condition and expressing $T = \overline{T} + \theta'$, $U = \overline{U} + u'$, $V = \overline{V} + v'$ and $W = \overline{W} + w'$, where the overbar represents the time mean value of the quantity and u', v', w' and θ' represent the fluctuations in three components of velocity and temperature respectively. Using the Reynolds averaging procedure, the equation (3.2) can be written as,

$$\overline{U}\frac{\partial \overline{T}}{\partial x} + \overline{V}\frac{\partial \overline{T}}{\partial y} + \overline{W}\frac{\partial \overline{T}}{\partial z} = \frac{\partial}{\partial x}\left[k\frac{\partial \overline{T}}{\partial x} - \overline{\theta' u'}\right] + \frac{\partial}{\partial y}\left[k\frac{\partial \overline{T}}{\partial y} - \overline{\theta' v'}\right] + \frac{\partial}{\partial z}\left[k\frac{\partial \overline{T}}{\partial z} - \overline{\theta' w'}\right]. \tag{3.3}$$

From equation (3.3), it is concluded that the distribution of $\overline{T}$ by the mean motion is affected by the molecular diffusion and by the turbulence convective motions. The latter effect is determined by the velocity and temperature fluctuation correlations. With turbulence or eddy transport coefficients defined as

$$
\begin{aligned}
-\overline{\theta' u'} &= \varepsilon_1 \frac{\partial \overline{T}}{\partial x}, \\
-\overline{\theta' v'} &= \varepsilon_2 \frac{\partial \overline{T}}{\partial y} \quad \text{and} \\
-\overline{\theta' w'} &= \varepsilon_3 \frac{\partial \overline{T}}{\partial z},
\end{aligned}
\tag{3.4}
$$

the equation (3.3) can be written as,

$$
\begin{aligned}
\overline{U}\frac{\partial \overline{T}}{\partial x} + \overline{V}\frac{\partial \overline{T}}{\partial y} + \overline{W}\frac{\partial \overline{T}}{\partial z} &= \frac{\partial}{\partial x}\left[k\frac{\partial \overline{T}}{\partial x} + \varepsilon_1 \frac{\partial \overline{T}}{\partial x} \right] \\
&+ \frac{\partial}{\partial y}\left[k\frac{\partial \overline{T}}{\partial y} + \varepsilon_2 \frac{\partial \overline{T}}{\partial y} \right] + \frac{\partial}{\partial z}\left[k\frac{\partial \overline{T}}{\partial z} + \varepsilon_3 \frac{\partial \overline{T}}{\partial z}\right].
\end{aligned}
\tag{3.5}
$$

It is well known that turbulent transport coefficients ε_1, ε_2 and ε_3 are much greater than the molecular diffusivity k and hence the molecular diffusion terms were neglected and equation (3.5) simplifies to,

$$
\begin{aligned}
\overline{U}\frac{\partial \overline{T}}{\partial x} + \overline{V}\frac{\partial \overline{T}}{\partial y} + \overline{W}\frac{\partial \overline{T}}{\partial z} &= \frac{\partial}{\partial x}\left[\varepsilon_1 \frac{\partial \overline{T}}{\partial x} \right] + \frac{\partial}{\partial y}\left[\varepsilon_2 \frac{\partial \overline{T}}{\partial y} \right] \\
&+ \frac{\partial}{\partial z}\left[\varepsilon_3 \frac{\partial \overline{T}}{\partial z} \right].
\end{aligned}
\tag{3.6}
$$

3.2 Solution of Turbulent Energy Equation for Momentum Wake Analysis

The approximations for the momentum wake analysis in Hunt's theory were $H/\delta << 1$ and $|u|/\overline{U} << 1$, where H is the height of the building, δ is the height of the boundary layer, u is the longitudinal velocity perturbation of mean velocity in the wake and $\overline{U}$ is the mean velocity of flow.

Let L be the distance over which the wake extends. ℓ is the distance over which large changes occur in the flow due to building, then it follows that $\ell << L$. The thickness, Δ, and width, d, of the wake are of the same order of magnitude.

Let $\overline{U}_w$, $\overline{V}_w$, and $\overline{W}_w$ be the time mean velocity components in x, y and z direction respectively and $\overline{T}_w$ be the time mean temperature in the wake. Also let $(\overline{U}(x, z), 0, 0)$ be the mean components of velocity and $\overline{T}(x, z)$ be the mean temperature in the undisturbed boundary layer. Let (see Figure 3),

$$\begin{aligned} \overline{U}_w &= \overline{U}(x, z) + u(x, y, z), \\ \overline{V}_w &= v(x, y, z), \\ \overline{W}_w &= w(x, y, z), \\ \overline{T}_w &= \overline{T}(x, z) + \theta(x, y, z), \end{aligned} \tag{3.7}$$

where u, v, w and θ describe the perturbations of three mean velocity components and the mean temperature respectively due to the building. The assumptions of $|u|/\overline{U} << 1$ and $|\theta|/\overline{T} << 1$ implies that the present analysis is valid only far downstream of the body. The equation (3.6) with equation (3.7), when the terms for the undisturbed boundary layer are removed, becomes,

$$\bar{U}\frac{\partial\theta}{\partial x} + u\frac{\partial\bar{T}}{\partial x} + u\frac{\partial\theta}{\partial x} + v\frac{\partial\bar{T}}{\partial y} + v\frac{\partial\theta}{\partial y} + w\frac{\partial\bar{T}}{\partial z} + w\frac{\partial\theta}{\partial z}$$

$$= \frac{\partial}{\partial x}\left(\varepsilon_1\frac{\partial\theta}{\partial x}\right) + \frac{\partial}{\partial y}\left(\varepsilon_2\frac{\partial\theta}{\partial y}\right) + \frac{\partial}{\partial z}\left(\varepsilon_3\frac{\partial\theta}{\partial z}\right). \qquad (3.8)$$

The continuity equation for the perturbation quantities is given by,

$$\frac{\partial u}{\partial x} + \frac{\partial v}{\partial y} + \frac{\partial w}{\partial z} = 0 \qquad (3.9)$$

The gradients of u, v and w with respect to x, y and z respectively are of the same order of magnitude. Hence, each term of equation (3.9) is proportional to the other, and given by

$$v \sim \frac{ud}{\ell}$$

and (3.10)

$$w \sim \frac{u\Delta}{\ell} \quad ,$$

where ℓ is a length scale in the x direction (say the separated bubble length), d is the wake width, and Δ is the wake height.

Let $\bar{U}_o$ and $\bar{T}_o$ be the mean velocity and temperature at $z = \Delta$ in the undisturbed boundary layer. Assuming, $|\theta|/\bar{T}_o << 1$ and $|u|/\bar{U}_o << 1$, the order of magnitude of each term of equation (3.8) was determined as follows:

$$\bar{U}\frac{\partial\theta}{\partial x} \sim \bar{U}_o\left(\frac{\theta}{\ell}\right) \quad ,$$

$$u\frac{\partial\bar{T}}{\partial x} \sim u\left(\frac{\bar{T}_o}{L}\right) \sim u\left(\frac{\theta}{\ell}\right) << \frac{\bar{U}_o\theta}{\ell} \quad ,$$

$$u\frac{\partial\theta}{\partial x} \sim u\left(\frac{\theta}{\ell}\right) << \frac{\bar{U}_o\theta}{\ell} \quad ,$$

$$v\frac{\partial\theta}{\partial y} \sim \left(\frac{ud}{\ell}\right)\cdot\left(\frac{\theta}{d}\right) \sim \frac{u\theta}{\ell} << \frac{\bar{U}_o\theta}{\ell} \quad ,$$

$$w\frac{\partial\theta}{\partial z} \sim \left(\frac{u\,\Delta}{\ell}\right)\left(\frac{\theta}{\Delta}\right) \sim \frac{u\theta}{\ell} << \frac{\overline{U}_o\theta}{\ell} ,$$

$$\frac{\partial}{\partial x}\left(\varepsilon_1 \frac{\partial\theta}{\partial x}\right) \sim \varepsilon\left(\frac{\theta}{\ell^2}\right) ,$$

$$\frac{\partial}{\partial y}\left(\varepsilon_2 \frac{\partial\theta}{\partial y}\right) \sim \varepsilon\left(\frac{\theta}{d^2}\right) , \tag{3.11}$$

and $$\frac{\partial}{\partial z}\left(\varepsilon_3 \frac{\partial\theta}{\partial z}\right) \sim \varepsilon\left(\frac{\theta}{\Delta^2}\right) .$$

Dropping the terms smaller than $\frac{\overline{U}_o\theta}{\ell}$, noting $\overline{T}$ is not a function of y and $\ell > \Delta, d$, the equation (3.8) reduces to

$$\overline{U}\frac{\partial\theta}{\partial x} + w\frac{\partial\overline{T}}{\partial z} = \frac{\partial}{\partial y}\left(\varepsilon_2 \frac{\partial\theta}{\partial y}\right) + \frac{\partial}{\partial z}\left(\varepsilon_3 \frac{\partial\theta}{\partial z}\right). \tag{3.12}$$

$\overline{T}$ is expressed in power law profile, with exponent $n_2 << 1$, as,

$$\frac{\overline{T}}{\overline{T}_o} = \left(\frac{z}{\Delta}\right)^{n_2} . \tag{3.13}$$

Therefore,

$$w\frac{\partial\overline{T}}{\partial z} = \frac{w\,\overline{T}_o\,n_2}{\Delta^{n_2}}(z)^{n_2-1} \sim \left(\frac{u\Delta}{\ell}\right)\left(\frac{T_o\,n_2}{\Delta}\right) \sim \frac{u\theta}{\ell} << \frac{\overline{U}_o\theta}{\ell} ,$$

is also neglected compared with the other terms of equation (3.12) to give,

$$\overline{U}\frac{\partial\theta}{\partial x} = \frac{\partial}{\partial y}\left(\varepsilon_2 \frac{\partial\theta}{\partial y}\right) + \frac{\partial}{\partial z}\left(\varepsilon_3 \frac{\partial\theta}{\partial z}\right). \tag{3.14}$$

Further analysis is based on constant eddy transport coefficients ε_2 and ε_3, given by $\varepsilon_3 = \gamma\bar{\varepsilon}$ and $\varepsilon_2 = \lambda\varepsilon_3 = \lambda\gamma\bar{\varepsilon}$, where λ and γ are constants of order one and $\bar{\varepsilon}$ is the constant eddy transport coefficient. The assumption of constant eddy diffusivity linearizes the equation (3.14), the solution of which can be obtained. The power-law profile for the undisturbed boundary layer, $n << 1$, is given by,

$$\frac{\bar{U}}{\bar{U}_o} = \left(\frac{z}{\Delta}\right)^n , \tag{3.15}$$

where $\bar{U}_o$ is the mean longitudinal velocity at the height $z = \Delta$ and n is the power-law exponent. The length scale, $\left[\frac{\varepsilon_3 \Delta^n}{\bar{U}_o}\right]^{\frac{1}{(1+n)}}$, proportional to the height of the building was used to nondimensionalize x, y and z variables. Hence with,

$$\bar{x} = \frac{x}{\left(\frac{\varepsilon_3 \Delta^n}{\bar{U}_o}\right)^{\frac{1}{(1+n)}}} ,$$

$$\bar{y} = \frac{y}{\left(\frac{\varepsilon_3 \Delta^n}{\bar{U}_o}\right)^{\frac{1}{(1+n)}}} ,$$

$$\bar{z} = \frac{z}{\left(\frac{\varepsilon_3 \Delta^n}{\bar{U}_o}\right)^{\frac{1}{(1+n)}}} ,$$

the equation (3.14) reduces to,

$$\bar{z}^n \frac{\partial\theta}{\partial\bar{x}} = \lambda \frac{\partial^2\theta}{\partial\bar{y}^2} + \frac{\partial^2\theta}{\partial\bar{z}^2} . \tag{3.16}$$

Before dealing with the solution of equation (3.16), the estimation of ε_3 and ε_2 are outlined. Hinze [32] states that ε_3 is of the same order as eddy viscosity $\bar{\nu}$. Arya [10] has calculated the ratio of $\varepsilon_3/\bar{\nu}$ for the fully developed undisturbed turbulent boundary layer. He found that the ratio is approximately constant and equal to 0.85. Thus, the following was assumed,

$$\varepsilon_3 = \gamma\bar{\varepsilon} = 0.85\ \gamma\ \bar{\nu} \quad \text{and} \quad \varepsilon_2 = 0.85\ \lambda\ \gamma\ \bar{\nu}. \tag{3.17}$$

The eddy viscosity was calculated from the parameters of undisturbed boundary layer neglecting advection and diffusion, the details of which are discussed by Hunt and Smith [20].

The equation (3.16) has the form of a diffusion equation. The procedure adopted for obtaining the solution of equation (3.16) is similar to that of Smith [33] and Hunt and Smith [20]. The salient features of the method to obtain the solution of equation (3.16) are described here and details are given in Appendix A.

The solution of equation (3.16) was assumed to be of the form,

$$\theta(x, y, z) = F(\bar{x}, \bar{z})\ \text{Exp}\ (-\bar{y}^2/f(\bar{x}, \bar{z})). \tag{3.18}$$

Functions $F(\bar{x}, \bar{z})$ and $f(\bar{x}, \bar{z})$ are evaluated using the technique of Hunt and Smith [20] and given by,

$$F(\bar{x}, \bar{z}) = q_o \sqrt{q_o/(2\pi q_2)} \quad \text{and} \tag{3.19}$$

$$f(\bar{x}, \bar{z}) = 2q_2/q_o,$$

where

$$q_o(\bar{x}, \bar{z}) = \int_{-\infty}^{\infty} \theta \, d\bar{y} \quad \text{and}$$

$$q_2(\bar{x}, \bar{z}) = \int_{-\infty}^{\infty} \bar{y}^2 \, \theta \, d\bar{y} \, . \tag{3.20}$$

The functions q_o and q_2 are the solutions of the following differential equations (see Hunt and Smith [20]),

$$\bar{z}^n \frac{\partial q_o}{\partial \bar{x}} = \frac{\partial^2 q_o}{\partial \bar{z}^2} \tag{3.21}$$

and

$$\bar{z}^n \frac{\partial q_2}{\partial \bar{x}} = \frac{\partial^2 q_2}{\partial \bar{z}^2} + 2\lambda q_o \, , \tag{3.22}$$

with boundary conditions,

$$q_o = q_2 = 0 \qquad \text{at} \qquad \bar{z} = 0 \quad \text{and} \quad \bar{z} \to \infty \, ,$$

$$q_o = q_2 = 0 \qquad \text{at} \qquad \bar{y} \to -\infty \quad \text{and} \quad \bar{y} \to +\infty \tag{3.23}$$

and

$$\int_{-\infty}^{\infty} \left(\int_{0}^{\infty} z\bar{U}\theta \, d\bar{z} \right) d\bar{y} = \bar{c} \, ,$$

where $\bar{c}$ is a constant.

The solution of equations (3.21) and (3.22) with boundary conditions given by equation (3.23) was obtained using the method of Hunt and Smith [20]. With equation (3.19), the functions $F(\bar{x}, \bar{z})$ and $f(\bar{x}, \bar{z})$ were then evaluated. The perturbation temperature defect θ is given by

$$\frac{\theta(x,y,z)}{\text{DELTA T}} = k_2 \frac{\bar{T}(H)}{\text{DELTA T}} \frac{F_2(z'',y'')}{\left(\frac{x-a}{H}\right)^{\frac{3+n}{2+n}}} \tag{3.24}$$

where, DELTA T = $\overline{T}_\delta - \overline{T}_{z_1}$ in undisturbed boundary layer and used for nondimensionalizing,

$\overline{T}_\delta$ = mean temperature at the top of the turbulent boundary layer,

$\overline{T}_{z_1}$ = mean temperature at the reference height z_1,

$\overline{T}(H)$ = mean temperature at the building height in the undisturbed flow,

k_2 = constant to be determined by matching with the experimental result,

a = virtual origin of the wake to be determined from experiment,

n = boundary layer velocity profile power law exponent,

$$F_2(z'',y'') = \frac{\eta^{\frac{1}{2+n}}}{(\eta + 1.5)^{1/2}} \text{ Exp } [-(\eta + c_8 \frac{y''^2}{(\eta + 1.5)})],$$

$$z'' = \frac{(z/H)}{[\frac{x-a}{H}]^{\frac{1}{(2+n)}}},$$

$$\eta = \frac{z''^{(2+n)}}{[2(2+n)\ K^2 n\ 0.85\ \gamma]},$$

$$y'' = \frac{(y/H)}{[\frac{x-a}{H}]^{\frac{1}{(2+n)}}} \left[\frac{(2+n)}{2\ \lambda\ 0.85\ \gamma\ K^2 n}\right]^{\frac{1}{(2+n)}}$$

K = von Karman constant (0.41),

c_8 = constant to be determined from experimental results.

3.3 Solution of Turbulent Energy Equation for Vortex Wake Analysis

In the analysis of the momentum wake behind a surface obstacle in a turbulent boundary layer, described in section 3.2, it was assumed

that trailing vortices are weak and hence do not have much effect on the wakes. However, the experiments by Hansen, Peterka and Cermak [4], Hansen and Cermak [17] and Woo, Peterka and Cermak [5] on the wakes behind hemispheres and cubes have shown that the vortices persist much farther downstream. They have significant, sometimes dominant, effects on the wake structures.

The interaction of a line vortex with a stably stratified shear flow for region E (see Figure 2) is developed in this section. The pictorial, qualitative drawing of the flow pattern around a rectangular block in a turbulent boundary layer was shown in Figure 1. The considerations of excess perturbation temperature on the inboard side of the vortex are described in detail in this section. For regions V_+ or V_- and G (see Figure 2) the results for the vortex velocity field were developed by Hunt [27]. Hunt found that the exact solution requires triple integrals to be evaluated. Similar results were obtained for the temperature field. However, due to the difficulty of evaluating the particular triple integrals involved in a closed form, the details of such a solution will not be pursued here.

In order to analyze the effect of vortex on the temperature field behind the bluff body deeply immersed in the turbulent boundary layer, the effect of perturbation in vertical velocity should be taken into account. Equation (3.12) is the start of a vortex wake analysis of temperature perturbation,

$$\overline{U}\,\frac{\partial\theta}{\partial x} + w\,\frac{\partial\overline{T}}{\partial z} = \varepsilon_2\,\frac{\partial^2\theta}{\partial y^2} + \varepsilon_3\,\frac{\partial^2\theta}{\partial z^2} \quad . \tag{3.25}$$

The perturbations u, v, w and θ are expressed in an asymptotic series in n given by,

$$\begin{aligned} u &= u^{(0)} + nu^{(1)} + - - -, \\ v &= v^{(0)} + nv^{(1)} + - - -, \\ w &= w^{(0)} + nw^{(1)} + - - -, \\ \theta &= \theta^{(0)} + n\theta^{(1)} + - - -, \end{aligned} \tag{3.26}$$

where $u^{(0)}$, $v^{(0)}$, $w^{(0)}$, $\theta^{(0)}$ and $u^{(1)}$, $v^{(1)}$, $w^{(1)}$, $\theta^{(1)}$ are all of the order, $0(1)$. The superscript number indicates the power of n with which the perturbation quantity is multiplied. Thus, equation (3.26) represents the descending series of perturbation quantities u, v, w and θ. The undisturbed boundary layer mean velocity $\overline{U}$ and mean temperature $\overline{T}$ and their derivatives $\frac{\partial \overline{U}}{\partial z}$ and $\frac{\partial \overline{T}}{\partial z}$ expressed in terms of asymptotic series of power-law exponents n and n_2 respectively, with assumptions $n << 1$ and $n_2 << 1$, are

$$\overline{U} = \overline{U}(h)\ e^{n\ \ell n(z/h)}, \tag{3.27}$$

$$\overline{U} = \overline{U}(h)\ [1 + n\ \ell n(z/h) + \frac{n^2}{2!}\ (\ell n\ z/h)^2 + - - -], \tag{3.28}$$

$$\frac{\partial \overline{U}}{\partial z} = \frac{n}{z}\ \overline{U}(h)\ [1 + n\ \ell n(z/h) + - - -], \tag{3.29}$$

$$\overline{T} = \overline{T}(h)\ e^{n_2\ \ell n(z/h)} \tag{3.30}$$

$$\overline{T} = \overline{T}(h)\ [1 + n_2\ \ell n(z/h) + \frac{n_2^2}{2!}\ (\ell n\ z/h)^2 + - - -], \tag{3.31}$$

and

$$\frac{\partial \overline{T}}{\partial z} = \frac{n_2 \overline{T}(h)}{z}\ [1 + n_2\ \ell n\ (z/h) + - - -]. \tag{3.32}$$

Using the assumption of $n_2 \sim n$, the equation (3.31) and (3.32) can be written as,

$$\overline{T} = \overline{T}(h)\ [1 + n\ \ell n(z/h) + \frac{n^2}{2!}\ (\ell n\ z/h)^2 + - - -], \tag{3.33}$$

$$\frac{\partial \overline{T}}{\partial z} = \frac{n}{z}\ \overline{T}(h)\ [1 + n\ \ell n(z/h) + - - -]. \tag{3.34}$$

Hunt [27] has proved that for region E, the zeroth order perturbation velocity field is irrotational. Hunt has also concluded that $u^{(0)}$ is zero everywhere and determined, for region E, that

$$w^{(0)} = \frac{\Gamma}{4\pi}\left[-\frac{y'}{y'^2 + (z-h)^2} + \frac{y'}{y'^2 + (z+h)^2}\right] \tag{3.35}$$

for $x/h >> \frac{\sqrt{4x\bar{\nu}/\bar{U}(h)}}{h}$ and $y' = y_v - y$.

y_v and h are the distances to the center of vortex in lateral and vertical directions respectively and Γ is the circulation of vortex at $x = 0$. Substitution of equations (3.26) through (3.34) in equation (3.25) gives,

$$\bar{U}(h)\ [1 + n\ \ell n(z/h)]\ \frac{\partial}{\partial x}(\theta^{(0)} + n\theta^{(1)}) + (w^{(0)} + nw^{(1)})$$

$$\frac{n}{z}\bar{T}(h)\ [1 + n\ \ell n(z/h)] = \varepsilon_2 \frac{\partial^2(\theta^{(0)} + n\theta^{(1)})}{\partial y^2}$$

$$+ \varepsilon_3 \frac{\partial^2(\theta^{(0)} + n\theta^{(1)})}{\partial z^2}\ . \tag{3.36}$$

Now, comparing the coefficients of n^0 and n^1 in equation (3.36) the following equations are obtained,

$$\bar{U}(h)\ \frac{\partial\theta^{(0)}}{\partial x} = \varepsilon_2 \frac{\partial^2\theta^{(0)}}{\partial y^2} + \varepsilon_3 \frac{\partial^2\theta^{(0)}}{\partial z^2}\ , \tag{3.37}$$

$$\bar{U}(h)\ \frac{\partial\theta^{(1)}}{\partial x} + \bar{U}(h)\ \ell n(z/h)\ \frac{\partial\theta^{(0)}}{\partial x} + \frac{\bar{T}(h)}{z}\ w^{(0)}$$

$$= \varepsilon_2 \frac{\partial^2\theta^{(1)}}{\partial y^2} + \varepsilon_3 \frac{\partial^2\theta^{(1)}}{\partial z^2}\ . \tag{3.38}$$

For inviscid region E, it is known that as $\bar{\nu} \simeq 0$, $\varepsilon_3 = \gamma\bar{\varepsilon} = \gamma 0.85\,\bar{\nu} \simeq 0$ and $\varepsilon_2 = \lambda\gamma\bar{\varepsilon} = \lambda\gamma 0.85\,\bar{\nu} \simeq 0$. Hence, ε_2 and ε_3 were assumed zero in the region E to give the simplified equations,

$$\frac{\partial\theta^{(0)}}{\partial x} = 0 \,, \tag{3.39}$$

$$\bar{U}(h)\,\frac{\partial\theta^{(1)}}{\partial x} + \frac{\bar{T}(h)}{z}\,w^{(0)} = 0 \,. \tag{3.40}$$

Since, $\theta^{(0)} \to 0$ as $x \to -\infty$ and since $w^{(0)}$ only induces the temperature perturbation of $0(n)$ as shown by equation (3.40), it can be concluded from equation (3.39) that $\theta^{(0)}$ is zero everywhere. Integration of equation (3.40) with respect to x yields

$$\theta^{(1)} = -\frac{\bar{T}(h)}{\bar{U}(h)} \int_0^x \frac{w^{(0)}}{z}\,dx. \tag{3.41}$$

Now, substituting for $w^{(0)}$ from equation (3.35), the perturbation temperature $\theta^{(1)}$ is,

$$\theta^{(1)} = \frac{\Gamma h y' x}{\pi}\left[\frac{1}{(y'^2 + h^2 + z^2)^2 - 4z^2h^2}\right]\frac{\bar{T}(h)}{\bar{U}(h)} \,. \tag{3.42}$$

Noting that $\theta^{(0)} = 0$, the perturbation temperature excess is given by,

$$\theta = \frac{n\Gamma h y' x}{\pi}\left[\frac{1}{(y'^2 + h^2 + z^2)^2 - 4z^2h^2}\right]\frac{\bar{T}(h)}{\bar{U}(h)} \,. \tag{3.43}$$

To account for the effect of two horseshoe vortices, along the centerline of the building, the equation (3.43) was doubled in the calculation. The total excess perturbation temperature θ is given by differences between the double of equations (3.43) and (3.24).

Chapter IV

DATA ACQUISITION AND ANALYSIS

The present wind tunnel research was conducted to obtain characteristics of wakes behind buildings in a stably stratified approach flow for comparison with theory and neutral flow data. A method for separating velocity and temperature signals from output of hot film anemometer voltages was developed to permit the rapid data acquisition required. This chapter describes the experimental facilities and data acquisition techniques.

4.1 Wind Tunnel Boundary Layer Similarity

The boundary layer simulation criteria has been discussed in detail by Cermak [34], and Cermak and Arya [35]. Requirements sufficient for this research are listed as follows:

1. Geometric similarity: This can be achieved by undistorted scaling of geometry of the prototype into the model.
2. Boundary condition similarity: These kinematical similarities can be generated by modeling the approach flow characteristics. The scaled mean velocity profile and turbulence characteristics should be the same in the approach flow for model and prototype. The effective surface roughness also should be scaled by a typical reference length. The distributions of scaled mean and fluctuating temperatures should be the same for model and prototype. The turbulence integral scale and boundary layer depth are also scaled by a typical reference length.
3. Reynolds number equality: Equal Reynolds number are not attainable for model and prototype. However, this does not

seriously limit capabilities for modeling the atmospheric boundary layer as the significant flow characteristics are weakly dependent upon large Reynolds number ($> 2 \times 10^4$) as shown by Schlichting [31]. For the present research, Reynolds numbers were greater than 2×10^4 based on velocity at the height of building.

4. Rossby number equality: For the investigation of the localized flow characteristics behind a typical surface obstacle the coriolis effects are not important; hence, Rossby number equality is not necessary.

5. Bulk Richardson number equality: This equality is important for stable or unstable flow, whereas for neutral flow with strong wind the similarity can be achieved using isothermal flow. The model bulk Richardson number was held equal to typical prototype conditions for present research.

The atmospheric boundary layer flows can be modeled by satisfying the above criteria.

4.2 The Wind Tunnel Facility

All the measurements were performed in the Meteorological Wind Tunnel in the Fluid Dynamics and Diffusion Laboratory at Colorado State University. The facility has been described in detail by Plate and Cermak [36]. The wind tunnel plan view is shown in Figure 4 and the salient features of it are described here.

The wind tunnel is a closed circuit facility driven by a 250 h.p. variable pitch, variable speed propeller with a 9:1 contraction ratio. The test section is 1.83 m (6 ft) square and 26.8 m (88 ft) in length. The roof of the test section is adjustable to obtain zero pressure gradient along the test section. The test section velocities range

from .3 m/sec (1 ft/sec) to 36.5 m/sec (120 ft/sec) and ambient temperature can be varied from 0°c (32°F) to 82°c (180°F) at medium speeds.

The tunnel has a 22 m (67 ft) section of the test section floor which can be heated or cooled to permit temperature differences between the cold plate and hot air of 65.5°c (150°F) and the hot plate and cold air of approximately 93°c (200°F). The refrigeration system maintains the air temperature at a constant level ($\pm$ 1/2°c) and wind speed does not deviate from that set by the speed controller by more than 1/2 percent.

The probe mounting mechanism is shown in Figure 5. The carriage is mounted on two tracks on each side of the wind tunnel wall and can be moved manually along the test section. The probe can be traversed vertically and laterally approximately 50.8 cm (20 inches) in both directions with the aid of electric motor drive operated from outside the wind tunnel. Limit switches trip the power to the drive motor when extreme positions are reached. The vertical and lateral positions of the probe can be read from digital voltmeters, with an accuracy of several thousands of a centimeter.

A 3.8 cm (1.50 inches) high sawtooth was installed at the test section entrance to insure prompt formation and growth of the boundary layer. The measurements made in this dissertation were 15.2 m (50 ft) from the test section entrance where a similarity profile was obtained (see Zoric [37]). However, due to persistence of vortices in the wakes there was a slight change in the boundary layer thickness. In order to account for this, all velocity defect and temperatures excess reported in this research were calculated by finding the differences between the

velocity or temperature at a point in the wake and the velocity or temperature at the same point in the absence of the building. Before dealing with the description of the thermal and velocity boundary layers used in the present research it is appropriate to derive the relationships to separate velocity and temperature signals.

4.3 Velocity and Temperature Measurements

Measurements of mean velocity and temperature can be accomplished with the pitot tube and thermocouple without much difficulty, see Arya [10]. Unfortunately, the hot wire or film anemometer responds simultaneously to velocity and temperature fluctuations; a technique to separate their respective voltages becomes more involved. Chao and Sandborn [38] utilized a very small diameter cold platinum resistance thermometer for temperature fluctuation measurement and two constant-temperature hot wires to obtain the velocity fluctuations. The details of the technique are outlined by Sandborn [39]. The major disadvantages of this method are the constant danger of breakage of a very small diameter cold wire and the requirement for interpolation of calibration data to obtain the hot wire sensitivities.

A modified technique has been developed for this experiment to permit rapid and extensive measurements under thermally stratified conditions. The measurements of mean and fluctuating velocity and temperature were made using two parallel hot film sensors each operated at a different but constant temperature. Convective heat transfer from a film is governed by Kings law:

$$\frac{E^2}{R\,(R - R_a)} = A + B\,U^C \qquad (4.1)$$

where,

$$R_a = R_c\ (1 + \alpha(T - T_c)), \tag{4.2}$$

E = output voltage from constant temperature hot film,

A, B, c = calibration constants ,

U = velocity ,

R = hot resistance of the film ,

R_a = resistance of hot film corresponding to environmental temperature T ,

R_c = calibration resistance of the film corresponding to calibration temperature T_c ,

α = temperature coefficient of resistance for the hot film.

Substitution of equation (4.2) in equation (4.1) results in

$$\frac{E^2}{R[R - R_c(1 + \ (T - T_c))]} = A + BU^c \quad . \tag{4.3}$$

Equation (4.3) has two unknowns, velocity U, and fluid temperature T. Values of E, R, R_c are known from measurement and A, B and c are determined from calibration procedures.

Calibration of the hot films were performed using a Thermo-Systems, Inc. Model 1125 calibrator, a Model 1050 anemometer and a MKS Baratron pressure meter. The output voltages from the two hot film anemometers were conditioned by an averaging circuit Model 1047 of Thermo-Systems, Inc., and displayed on digital voltmeters. In the analysis of obtaining the velocity and temperature, A and B were assumed constant; however, as the temperature T varies from 0°c (32°F) near the wind tunnel floor to 46°c (115°F) in the free stream,

the A and B are not actually constant throughout the range of interest. This normally would require calibrations to be performed over the complete range of temperatures expected. This difficulty was overcome by noting that the output of a hot film is primarily dependent on velocity and temperature difference $(T_w - T)$, where T_w and T are hot film temperature and environmental temperature respectively. Thus, nearly equivalent results may be obtained by holding T constant and varying T_w as by holding T_w constant and varying T. The films were calibrated with $(T_w - T)$ values such that the effective calibration temperatures of 26.7°c (80°F), 37.8°c (100°F) and 48.9°c (120°F) were obtained relative to a constant test film temperature T_w. The constants A and B were assumed to be constant over a range $\pm$ 5.56°c ($\pm$ 10°F) about these temperatures.

A, B and c are constants determined by a least squares analysis to fit the calibration data. However, such a procedure will produce an exponent c which varies depending upon the fixed effective calibration temperature. The determination of U and T when there is a variable constant c would require a trial and error method. To obtain the direct solution of the equation (4.3) in a computationally efficient manner an average value of c was used. Once the c value was chosen, a least square fit of calibration data was performed to obtain A and B for each effective calibration temperature. The details of evaluating velocity U and temperature T are outlined in Appendix B using the constant c. Digitized voltage outputs of the two hot films were converted to digital time series of velocity and temperature. The mean and root mean square value of the velocity and temperature were calculated from them.

4.4 Approach Flow and Preliminary Measurements

The wind tunnel floor temperature was set at 0°c (32°F) using the refrigeration circuit. The first 10 m (30.5 ft) of cooled floor was slightly rougher than the rest of the cooled floor with 1.59 mm (0.0625 inch) high ribs carrying coolant. The air was heated before it entered the test section so as to obtain approximately 48.9°c (120°F) temperature in the free stream, with the free stream velocity of approximately 6.1 m/sec (20 ft/sec). This established a stable stratification in the wind tunnel. Initial temperatures were measured with thermocouples and tunnel velocities were initially established with a Datametrics probe, Model 800-LV. The fully developed profiles of velocity and temperature were measured at 15.2 m (50 ft) from the test section entrance.

The bulk Richardson number, a measure of atmospheric stability relating the tendency for the atmosphere to enhance or subdue turbulence, is given by,

$$Ri = \frac{g}{\overline{T}} \frac{\Delta T \ \Delta z}{(\Delta U)^2} \quad , \tag{4.4}$$

where

g = acceleration due to gravity

$\Delta z = z_2 - z_1$, the vertical height difference for which the bulk Richardson number is calculated

ΔT = the difference between the mean temperature at heights z_2 and z_1

ΔU = the difference between the mean velocities at heights z_2 and z_1

$\overline{T}$ = the average of the mean temperatures at heights z_1 and z_2, expressed in absolute units.

In this form the bulk Richardson number is an indication of the stability of the atmosphere over a finite layer. The initial results of velocity and temperature profiles were used to calculate the bulk Richardson number using equation (4.4). The tunnel free stream temperature was varied until the approximate required bulk Richardson number equal to 0.023 was obtained. In calculation of bulk Richardson Δz was used such that $z_2 = 50.8$ cm and $z_1 = 0.25$ cm.

A Systems Development, Inc., digital-data-acquisition system was used for the measurement of velocity and temperature. A block diagram of the total system is shown in Figure 6. Two parallel hot films were operated by two constant temperature anemometers adjusted for overheat ratios of 1.5 and 1.2. The voltage signals from the anemometers were processed by signal conditioners, where voltages were suppressed (offset) by predetermined fixed voltages. The suppressed voltages were displayed on oscilloscopes and voltmeters. The suppressed voltages were sent to an analog-to-digital converter. The digital signals were stored on magnetic tape for reduction and interpretation by the University CDC 6400 computer.

The major input requirements for operation of the system were the number of channels, sample rate, total sampling time and details of the digital tape format. For velocity and temperature measurements, data was digitized at 250 samples/sec on each channel, except when evaluating spectra. Preliminary data were recorded with the analog-digital system at 250 samples/sec on each channel for a period of five minutes. Time series of velocity and temperature were calculated using the method described in section 4.3 and mean and rms velocities and temperatures were calculated by the method of section 4.5 for various averaging

times. The results of these calculations are shown in Figure 7. It was concluded that mean values could be obtained within one percent and rms values within two percent using a 30 second length of record. Data for spectral calculations were digitized at 2000 samples/sec on each channel for 35 seconds. The higher rate of sampling increases the Nyquist frequency, whereas longer record gives better estimate of energy at lower frequency.

4.5 Data Reduction

The digital tape contained two voltage signals $e_1(t)$ and $e_2(t)$ consisting of N values sampled at time intervals of Δt seconds. The records are denoted by $e_1(t_i)$ and $e_2(t_i)$, $t_i = \Delta t, 2\Delta t, \ldots N\Delta t$. The total length of the record in seconds is given by $\tilde{T}$ (equal to $N\Delta t$). Initially $e_1(t_i)$ and $e_2(t_i)$ were converted to the physical units of velocity and temperature using the technique described in section 4.3. The converted values of velocity and temperature were stored as a time series on the magnetic tape. The discrete form of each time series, either velocity or temperature, can be expressed as a_i, $i = 1, 2, 3, \ldots N$.

The mean of the signal is

$$\overline{a} = \frac{1}{\tilde{T}} \int_0^{\tilde{T}} a(t)\, dt \tag{4.5}$$

or in the discrete form

$$\overline{a} = \frac{1}{N} \sum_{i=1}^{N} a_i \tag{4.6}$$

The variance of the signal is

$$\overline{a^2} = \frac{1}{\tilde{T}} \int_0^{\tilde{T}} (a(t) - \bar{a})^2 \, dt \tag{4.7}$$

and in discrete form,

$$\overline{a^2} = \frac{1}{(N-1)} \sum_{i=1}^{N} (a_i - \bar{a})^2 \quad . \tag{4.8}$$

The root mean square of the signal is the square root of the variance.

The auto-correlation function or power spectral density function of the fluctuations of a_i are generally carried out using a signal with a zero mean. Hence, define, $\hat{a}_i$,

$$\hat{a}_i = a_i - \bar{a} \quad . \tag{4.9}$$

Now the auto-correlation function is defined as,

$$R_a(\tau) = \underset{\tilde{T}\to\infty}{\text{Lim}} \frac{1}{\tilde{T}} \int_0^{\tilde{T}} \hat{a}(t) \; \hat{a}(t+\tau) \, dt \quad , \tag{4.10}$$

and in discrete form

$$R_a(\tau) = \frac{1}{N-r} \sum_{i=1}^{N-r} \hat{a}_i \, \hat{a}_{i+r} \quad , \tag{4.11}$$

where $r = 0, 1, 2 \ldots N-r$ and $\tau = r\Delta t$.

The power spectral density function is defined as the Fourier transform of the auto-correlation function and given by,

$$G_a(f) = 2 \int_{-\infty}^{\infty} R_a(\tau) \; e^{-i2\pi f\tau} \, d\tau \qquad f \geq 0 \quad . \tag{4.12}$$

This function describes contributions of the fluctuations at a given frequency, f, to the variance of the signal. The auto-correlation and

power spectral density function were normalized with the variance of the signal to obtain auto-correlation coefficient,

$$r_a(\tau) = R_a(\tau)/\overline{a^2} \quad , \tag{4.13}$$

and the normalized power spectral density function,

$$g_a(f) = G_a(f)/\overline{a^2} \quad . \tag{4.14}$$

The normalized power spectral density function was computed directly from the data record using a Fast Fourier Transform Technique (see Bendat and Piersal [40]). The details of the computer programs used for calculations are described by Akins and Peterka [41]. The programs were modified to be suitable for the present research. The normalized power spectral density function was calculated directly from the digital signal. The auto-correlation coefficients were obtained by performing an inverse Fourier transform of the normalized power spectral density function. This technique used much less time compared with calculating auto-correlation functions using equation (4.10) and then calculating power spectral density function using equation (4.12).

The two-channel analysis of velocity and temperature can be analyzed in a similar way. Let $\hat{a}_{1,i}$ and $\hat{a}_{2,i}$ represent the digital records of velocity and temperature with the mean removed. The cross-correlation function between the two signals is

$$R_{a_1 a_2}(\tau) = \underset{\tilde{T}\to\infty}{\text{Lim}} \frac{1}{T} \int_0^T \hat{a}_{1,i}(t) \; \hat{a}_{2,i}(t + \tau) \, dt \tag{4.15}$$

or in discrete form

$$R_{a_1a_2}(\tau) = \frac{1}{(N-r)} \sum_{i=1}^{N-r} \hat{a}_{1,i}\, \hat{a}_{2,i+r} \qquad (4.16)$$

where $r = 0, 1, 2, \ldots N-r$ and $\tau = r\Delta t$.

The normalized cross correlation function was obtained by dividing the cross correlation function by the product of the root mean square value of the individual channels to give

$$r_{a_1a_2}(\tau) = \frac{R_{a_1a_2}(\tau)}{\sqrt{\overline{a_1^2}}\sqrt{\overline{a_2^2}}} \quad . \qquad (4.17)$$

The cross-spectral density function of two signals is the Fourier transform of the cross correlation function and is defined as,

$$G_{a_1a_2}(f) = 2 \int_{-\infty}^{\infty} R_{a_1a_2}(\tau)\, e^{-i2\pi f\tau}\, d\tau \,, \qquad f \geq 0 \quad . \qquad (4.18)$$

The cross correlation function is normally not an even function, and must be expressed as a complex quantity,

$$G_{a_1a_2}(f) = C_{a_1a_2}(f) - i\, Q_{a_1a_2}(f) \quad . \qquad (4.19)$$

$C_{a_1a_2}(f)$ is known as the coincident spectral density function or co-spectrum, and $Q_{a_1a_2}(f)$ is called the quadrature spectral density function or quad-spectrum. The phase angle between the two signals is defined as,

$$\theta_{a_1a_2}(f) = \tan^{-1}\left[\frac{Q_{a_1a_2}(f)}{C_{a_1a_2}(f)}\right] \quad . \qquad (4.20)$$

In many applications a real valued quantity, coherence, is used as a measure of how well the two signals are correlated at a particular frequency and defined as,

$$Co_{a_1 a_2}(f) = \frac{|G_{a_1 a_2}(f)|^2}{G_{a_1}(f)\ G_{a_2}(f)} \quad . \tag{4.21}$$

The cross spectral density function was obtained directly from the digital signals of two channels. The cross correlation function was obtained by taking the inverse Fourier transform of the cross spectral density function, the details of which are given by Akins and Peterka [41].

4.6 Description of the Models and Test Program

The stratified wakes from a number of building shapes were included in the present research program. The models were made out of plexiglas. Details of dimensions of the models are shown in Table 1.

Detailed wake measurements for one wind direction (with one face of the model normal to the flow direction) were obtained rather than a series of less-detailed measurements at many wind directions. The coordinate system and definition of symbols used is shown in Figure 3. The series of wake measurements were made at x/H values of 1.0, 2.5, 7.5, 10.0, 15.0, 20.0, 30.0, 40.0 and 60.0 at various z/H locations for $y/H = 0.0$ with and without the model in place. The off-centerline data were observed for x/H equal to 1.0, 2.5, 7.5, 10.0 and 15.0 at $z/H = 1.0$ and various values of y/H with and without model 2 in place. The data for spectra were also observed in the wake of model 2 at $z/H = 1.0$, $y/H = 0.0$ and various x/H locations.

Chapter V

RESULTS AND DISCUSSION

Wind tunnel measurements of velocity and temperature, using the technique described in Chapter IV, in the wakes of six idealized buildings deeply immersed in the stable turbulent boundary layer were performed and are reported in this chapter. The mean velocity and temperature measurement results are discussed in the first part of this chapter. Next, mean velocity and temperature measurements are compared with the theories described in Chapters II and III. The effects of longitudinal vortices in the wake of the building are evaluated. The method to calculate the circulation, Γ, at $x = 0$ for the buildings has been generalized. Measurements of turbulences statistics will be reported in the second part of this chapter.

5.1 The Approach Flow Characteristics

For stable stratification that is not too severe, it can be determined from dimensional arguments that,

$$\frac{\partial \overline{U}(z)}{\partial z} = \frac{u_*}{Kz} \quad , \tag{5.1}$$

and

$$\frac{\partial \overline{T}(z)}{\partial z} = \frac{T_*}{Kz} \quad , \tag{5.2}$$

where

$\overline{U}(z)$ = mean velocity at height z,

$\overline{T}(z)$ = mean temperature at height z,

u_* = velocity scale,

T_* = temperature scale, and

K = von Karman constant.

Integrating equations (5.1) and (5.2) gives,

$$\frac{\overline{U}(z)}{u_*} = \frac{1}{K} \ln (z/z_o) \tag{5.3}$$

and

$$\frac{\overline{T}(z)}{T_*} = \frac{1}{K} \ln (z/z_o) \tag{5.4}$$

where z_o is the characteristic roughness length.

It can be concluded from equations (5.3) and (5.4) that,

$$\overline{U}(z) \alpha \ln z \tag{5.5}$$

and

$$\overline{T}(z) \alpha \ln z. \tag{5.6}$$

The vertical profiles of mean velocity and temperature, measured by the method described in Chapter IV, were plotted according to equations (5.5) and (5.6) respectively, and are shown in Figure 8. The lower reference temperature, $\overline{T}_{z_1}$, and lower reference velocity, $\overline{U}_{z_1}$, are at the height z_1, 0.25 cm (0.1 inch), and are equal to 21.1°c (70°F) and 1.68 m/sec (5.5 ft/sec), respectively. The bulk gradient Richardson number calculated across the boundary layer, from z_1 to the outer edge of the boundary layer z_2, was 0.023. The bulk Richardson number with z_2 as the height of building was about 0.005. This bulk Richardson number characterizes the moderately stable atmosphere. The approach flow characteristics are plotted in Figure 9, where,

$$\text{DELTA T} = (\overline{T}(\delta) - \overline{T}_{z_1})_{\text{without building}},$$

$\overline{T}(\delta)$ = mean temperature at the top of the turbulent boundary layer,

$\overline{T}_{z_1}$ = mean temperature at height z_1, and

δ = turbulent boundary layer thickness.

Table 1 shows additional details of the approach profiles.

The mean velocity defect, Delta U, turbulence variance excess, Delta U VAR, Mean temperature excess, Excess T, and temperature variance excess, Delta T VAR are defined as follows:

$$\text{Delta U} = \left(\frac{\overline{U}(z)}{\overline{U}(\delta)}\right)_{\text{without building}} - \left(\frac{\overline{U}(z)}{\overline{U}(\delta)}\right)_{\text{with building}},$$

$$\text{Delta U VAR} = \left(\frac{u_{rms}(z)}{\overline{U}(z)}\right)^2_{\text{with building}} - \left(\frac{u_{rms}(z)}{\overline{U}(z)}\right)^2_{\text{without building}},$$

$$\text{Excess T} = \frac{\overline{T}(z)_{\text{with building}} - \overline{T}(z)_{\text{without building}}}{\text{DELTA T}},$$

$$\text{Delta T VAR} = \frac{T^2_{rms}(z)_{\text{with building}} - T^2_{rms}(z)_{\text{without building}}}{(\text{DELTA T})^2},$$

where $u_{rms}(z)$ and $T_{rms}(z)$ are the root mean square (rms) of velocity and temperature at height z respectively.

5.2 The Experimental Measurements of Mean Velocity in the Wakes of Buildings

The mean velocity measurements in the wakes of six idealized buildings were made in the stable turbulent boundary layer over the smooth floor. Detailed wake measurements for one wind direction, viz., one face perpendicular to the flow, were obtained rather than a series of less-detailed measurements at many wind directions. This provided an optimum set of limited data to make a comparison with the wake theory.

Figures 10 through 15 show the vertical profiles of mean velocity defect, Delta U, for buildings 1 through 6 respectively. The measurements were taken from x/H = 1.0 to 60.0 downwind for various z/H ratios. The measurements were made with and without building in place at all locations. The maximum vertical extent of the velocity defect wake is 2 to 3H near the building and about 4 to 5H in the far wake for buildings 1 and 2. This is of the same order of magnitude as reported by Woo, Peterka and Cermak [5] for building 2. However, for the buildings 3 through 6 the maximum vertical extent is about 2 to 3H for the entire wake. Flow visualization studies by Woo et al. [5] have shown that the separated region extends to about 3H*downstream of the building. Measurements with a hot film anemometer are not suitable for this region. Thus, the results in this region should be only used as qualitative information.

The interesting feature of all the wakes is that they extend much farther than those reported by Counihan [14], Colmer [11], Lemburg [15] and Castro and Robins [16]. However, the extension of the wakes behind the buildings do agree with the results of Hansen et al. [4] and Woo et al. [5]. The momentum wake diffuses in about 10 to 15H downstream of the buildings. However, the effect of the vortex wake persisted to 60 heights downstream of the buildings. The measurements were not performed beyond the distance of 60H downstream and hence the total length of the wake was not known. It is concluded from the present results that the effect of horseshoe vortices play an important role in determining the wake behind an isolated building. Horseshoe vortices bring higher momentum fluid from the top of the boundary layer to

*Estimation of cavity size, see Hosker "Empirical Estimation of Wake Cavity Size Behind Block-Type Structures," A.M.S. 4th Symposium on Turbulence, Diffusion, Air Pollution, January 15-18, 1979, Reno, Nevada.

increase mean velocity along the centerline of the building and results in excess velocity in the far wake region. In the region characterized by the vortex wake velocity profiles, the maximum velocity excess moves upward indicating that the wake is diffusing upward. A similar conclusion was drawn by Hansen et al. [17] for the wakes behind hemispheres.

The maximum velocity defect occurring at each x/H for the buildings are shown in Figures 16, 17 and 18. This maximum velocity defect did not occur at the same z/H for each x/H value. The mean velocity defect decays with a power-law exponent -0.87, -1.20, -1.65, -1.08, -1.91 and -2.06 for buildings 1 through 6 respectively. The theory for neutrally stable wakes of Hunt and Smith [20] would predict a power-law decay of about -1.5. The decay rate near -2 originates from the action of two horseshoe vortices bringing higher momentum fluid down toward the surface on the centerline. Examination of Figures 10 through 15 also show that some of these decay curves actually go negative before asymptoting to zero. Thus, the high power-law exponent does not necessarily imply a rapid dissipation of the wake. Due to stable atmospheric condition, horseshoe vortices persisted for a longer distance resulting in stronger subsidence of high-momentum fluid on the centerline. Thus, neither the theory of a momentum wake nor the power-law decay description of the wake maximum velocity defect is really an appropriate means of characterizing the wake. The comparisons of wake data of Woo et al. [5] in neutral turbulent boundary layer with velocity profile power-law exponent of 0.12 are also shown in Figures 16, 17 and 18. The decay rates compared very well with the present results, although for building 4 the actual numbers are different.

Horizontal profiles of the mean velocity defect in the wake of building 2 are shown in Figure 19. The profile maxima did not occur at the centerline but were displaced about 0.25H to 0.5H in lateral direction. Similar results were observed by Woo et al. [5] and Peterka et al. [6]. However, the displacement was larger in their observations. Another interesting feature of the profiles is the secondary peak, also observed by Woo et al. [5] and Peterka et al. [6], observed between 2H and 4H from the wake centerline. The horseshoe vortex carried high momentum fluid from a higher elevation towards the ground near the centerline of wake and decreases the velocity defect. However, it brings lower momentum fluid from lower elevations on the outboard side of the vortex to increase the velocity defect resulting in the secondary peak. Hence, the assumption of a Gaussian lateral velocity defect profile in the theories of Hunt [21] and Lemburg [15] is not justified and requires further modifications.

5.3 Comparison of the Experimental Measurements of Mean Velocity with Hunt's Theories

The theory of wakes behind buildings deeply immersed in a turbulent boundary layer was developed by Hunt and was reviewed in Chapter II. In this section Hunt's theories [21, 27] of momentum and vortex wakes behind the buildings have been evaluated. Since Hunt's theories contain the basic physical models for momentum and vortex wake representations, the theories should present a reasonable prediction of the velocity wake. The assumptions that $n << 1$ and $H/\delta << 1$ used in the theory are satisfied for the present measurements.

The theory requires the knowledge of the force coefficient on the building, C_{Fx}. C_{Fx} for the test buildings were derived from the

measurements of mean forces on buildings by Akins, Peterka and Cermak [42]. The force coefficients, C_{Fx}, for buildings 1 through 6 were estimated to be 1.3, 1.4, 1.3, 1.35, 1.35 and 1.3 respectively. The constants γ and λ in Hunt's theory were assumed equal to one for all the calculations. The virtual origin, a, for the building wakes were determined from the variation of the experimental data along the wake centerline by a method proposed by Hunt [21] as shown in Figures 20 and 21. The data in these figures, unfortunately, are not very linear. Castro and Robins [16] also found that their wind tunnel results did not follow a straight line. Nonetheless the data has been approximated by a straight line, and virtual origins for buildings 1 through 6 were determined as -2.5H, -1.75H, -0.30H, -1.35H, -1.5H and -1.0H respectively. The theoretical predictions for mean velocity defect suggested by the momentum wake theory of Hunt were then calculated using equation (2.4). The vertical profiles of the mean velocity defect, Delta U, due to the momentum wake for various x/H locations for buildings 1 through 6 are shown in Figures 22 through 27 respectively. It should be noted that any mean velocity excess observed in the wake will never be predicted by the momentum wake theory.

The measurements of Peterka et al. [6] clearly indicated the effect of horseshoe vortices in the wake of a building. Noting the results of Peterka et al. [6] Hunt developed the vortex wake theory [27]; the details of the theory were described in Chapter II. On the centerline the effect of both branches of horseshoe vortices are identical and additive. Hence, the result for one branch was calculated and the results were doubled to get the net effect.

Hunt's model requires the position of the vortex in the wake and circulation, Γ, at $x = 0$. Hunt assumed the location of the center of vortex constant with respect to the x axis, although the results of Hansen et al. [17] have shown that the vortex moves laterally and vertically with increasing x. In the present calculations the observed values of y_v, lateral center of vortex, were obtained from the measurements of Hansen et al. [17] behind hemispheres. The vertical center of vortex, h, was assumed constant and equal to 0.3H. The assumptions of constant h and the use of the variation of lateral position of vortex y_v obtained from Hansen et al. [17] may be questionable, but no other data was available for the estimation of these parameters. The magnitude of any errors introduced due to these approximations are left to future investigations.

The vortex circulation at $x = 0$ was evaluated by the following technique. It was assumed that part of the circulation in the approach flow is converted into the circulation of horseshoe vortex. The circulation in the approach flow, Γ_a, up to the height z is given by $\overline{U}(\delta)\ x_L(\frac{z}{\delta})^n$, where x_L is the reference longitudinal length. During calculation of the strength of horseshoe vortex z was assumed to be 0.3H. The horseshoe vortex, in front of the building, rolls as a circular tube. The diameter of this tube was assumed to be 0.8W, where W is the width of the building. The reference length, x_L, was assumed to be the circumference of this tube or equal to π (0.8W). Using this method, $\Gamma_{x=0}$ for buildings 1 through 6 were calculated and were found equal to 0.45, 1.44, 0.71, 0.49, 1.0, 1.0 m^2/sec (4.8, 15.5, 7.6, 5.3, 10.7, 10.7 ft^2/sec) respectively. The results of the calculations of the vortex wake using equation (2.5), along the centerline of the

buildings for various x/H for buildings 1 through 6 are also shown in Figures 22 through 27 respectively.

The sum of the momentum wake velocity defect and the vortex wake velocity excess are also shown in Figures 22 through 27 for buildings 1 through 6. The experimental observations of velocity defect in the wakes behind these buildings are plotted on the same figures. The comparison between the measurements and combined momentum and vortex wake theory is very satisfactory for buildings 2, 3, 5 and 6. However, for buildings 1 and 4 with W/D equal to 0.31 and 0.5 respectively, the vertical profiles of velocity defect have more momentum-like wake characteristics. The comparisons also deteriorate in the separated region (near wake region) behind the buildings, as expected, since this region cannot be considered as a small perturbation on the approach flow. A better agreement between theory and experiment might exist if Hunt's complete results were available. But the asymptotic results predict the shape of velocity profiles quite satisfactorily even including a region of net excess velocity. The theory appears to incorporate the more important physical concepts of the wake behind a building and needs only fine refinement.

5.4 The Experimental Measurements of Mean Temperature in the Wakes of Buildings

Mean temperature measurements in the wakes of six idealized buildings, with one face normal to the flow direction, deeply immersed in a stably stratified turbulent boundary layer were made. Figures 28 through 33 show the vertical profiles of mean temperature excess, Excess T, for buildings 1 through 6 respectively. The maximum vertical extent of the temperature excess is 2 to 3H for buildings 1, 2 and 4;

whereas, it is about 1 to 2H in the near wake and 2 to 4H in the far wake for buildings 3, 5 and 6. The measurements of temperature in the separation bubble region (about 3H downstream of the building) should only be used as qualitative information since the hot film anemometer interpretation utilized is not suitable for this region. The hot film anemometer indicates higher mean velocity in this region than actually exists; hence, from equation (B.3) it can be concluded that the mean temperature measurement will also be high and result in an overestimate of Excess T. An interesting feature of the temperature wake is that it tends to extend much farther than the velocity wake. Even at a distance of x/H equal to 60, all the building wakes displayed higher temperatures than the approach flow temperatures at a given height.

The maximum mean temperature excess occurring at each x/H is shown in Figure 34 for all buildings. This maximum did not occur at the same z/H at different values of x/H. For all buildings studied this maximum increases until approximately 8 to 15H downstream of the buildings and then decreases. Similar increases in the mean temperature magnitudes were reported by Alexopoulos and Keffer [43] on the off-centerline data for flow behind a cylinder in a uniform flow with a linear temperature gradient. For buildings 2, 3 and 6 the maximum mean temperature excess increases with a power-law exponent of 0.40, 0.53 and 0.18 and then decreases with an exponent of -0.36, -0.70, and -0.22 respectively. For buildings 1, 4 and 5 the initial increase in the form of a power-law exponent was difficult to determine; however, beyond certain x/H it decreases with a power-law exponent of -0.67, -0.73, -0.33, respectively. It should be concluded that the decay of temperature excess is slower than the decay of velocity defect; hence,

the horseshoe vortices play more important roles for temperature wakes than for velocity wakes.

5.5 Comparison of the Experimental Measurements of Mean Temperature with the Present Theories

The theory of mean temperature behind buildings deeply immersed in a stably stratified turbulent boundary layer was developed and described in detail in Chapter III. The results of calculations of this theory have been evaluated in this section. The theory contains the basic physical representation of the wake, viz., momentum and vortex wake. The assumption of $n_2 << 1$ and $H/\delta << 1$ are also satisfied for present measurements.

The effect of the horseshoe vortex in the wake of a building on the mean temperature was to increase the mean temperature on the centerline of a building as predicted by equation (3·43) for region E. The results of calculations for region E were extrapolated into the regions of G and V_+ where the assumptions of $\varepsilon_3 \neq 0$ and $\varepsilon_2 \doteq 0$ are not valid at all. In the absence of other available methods, it was thought appropriate to perform such an operation. The action of two horseshoe vortices along the centerline of a building was the same and additive; hence, the result of equation (3.43) was doubled to obtain the net excess temperature due to vortices. In calculation, the circulation, Γ, at $x = 0$ and the position of the vortex were taken the same as in the velocity calculation and described in section 5.3. Figures 35 through 40 show by dashed lines the excess temperature due to the vortex behind buildings 1 through 6 respectively.

The momentum wake theory for the mean temperature was developed in section 3.2 of Chapter III. This wake theory results in a mean

temperature defect in the wake behind a building and is analogous to the velocity defect in the momentum wake theory of Hunt. The mean temperature defect due to the building is given by equation (3.24). To be consistent with velocity defect profile calculations, the constants λ and γ were assumed equal to one for the mean temperature calculations. It was felt reasonable to assume that velocity and temperature wakes originate from the same point. With this assumption the virtual origin "a" for temperature wake is the same as the velocity wake. The constant k_2 in the equation (3.24) was evaluated by matching the experimental observation of excess temperature on the centerline of each building at $x/H = 10$ and $z/H = 1$ with the sum of excess temperature due to vortex wake given by equation (3.43) and the momentum wake temperature defect given by equation (3.24). Knowing k_2 for each building, the calculations for temperature defect in the wake were performed according to equation (3.24). The results of calculations are shown in Figures 35 through 40 for buildings 1 through 6 respectively.

The sum of vortex wake temperature excess and momentum wake temperature defect are shown in Figures 35 through 40 for buildings 1 through 6 respectively. The experimental observations of temperature excess in the wakes behind buildings are plotted on these same figures. The comparison between the measurements and combined momentum and vortex wake theory is excellent for all buildings, except in the near wake. Even for buildings 1 and 4, where the results of velocity calculations were not as satisfactory as for the other buildings, agreement between the measurements and theoretical predictions of temperature were very satisfactory. The evaluation of the triple integrals, explained in

section 3.3, for the calculations of excess temperature due to the vortex may improve the present theory. The constant, k_2, used in the above calculations, shows a variation apparently influenced by the building geometry. The constant, k_2, for buildings of W/H ratio of one was $\doteq$ 8.7. However, it was not possible to determine the trend for various W/H ratio buildings. Thus, the present theory requires only one experimental measurement to determine the temperature field in the wake behind a building.

Knowing the temperature field behind a building, the local bulk Richardson number can be evaluated to determine the local stability of the flow field. As a result of observed excess temperature in the wake, the local stability will move towards the unstable regions of the Pasquill-Gifford curves. This results in larger dispersion coefficients in the y and z directions and should increase diffusion downwind of a building as compared with that predicted by the unperturbed Pasquill-Gifford curves. This may explain the shift of ground level concentrations measured by Allwine, Meroney and Peterka [44], during a study of nuclear power station wake effects on atmospheric diffusion.

5.6 Turbulence Measurements

Extensive measurements of longitudinal fluctuating velocity and temperature fluctuation in the wakes of the same six idealized buildings were also performed. Only the longitudinal fluctuations of velocity were recorded and hence the word "longitudinal" will be omitted from the subsequent discussion with the understanding that is is implied in all further material.

The vertical profiles of turbulence variance excess, Delta U VAR, in the wakes of buildings 1 through 6 are shown in Figures 41 through 46 respectively. The mean square values of turbulent velocity fluctuation return to the undisturbed state in approximately 7.5 to 10H downstream of the buildings. This return is much more rapid than the mean velocity field. Similar findings were reported by Peterka et al. [6], Hansen et al. [17] and Woo et al. [5]. The maximum vertical extent of the turbulence wake extends to about 1 to 2H for the entire wake for all buildings. Also, the turbulence variance excess was approximately constant from the lowest z/H measured to the height of $z/H \doteq 1.0$, at a given x/H location. The Delta U VAR also approaches zero within $z/H \doteq 2.0$ for all buildings. The results of Woo et al. [5] in the neutral flow did not show such characteristics. The present results suggest that the stable atmospheric condition inhibits the effects of building wakes in the vertical direction for the turbulence wake.

The maximum Delta U VAR occurring at each x/H is plotted in Figures 47 through 49 for buildings 1 through 6. Similar to the behavior of the maximum Delta U this maximum did not occur at the same z/H at different values of x/H. The figures also display the neutral flow data of Woo et al. [5] for comparison. The maximum Delta U VAR decays with a power-law exponent of -1.67, -2.15, -2.30, -2.02, -2.47 and -2.30 for buildings 1 through 6 respectively. The decay rate of Hunt's theory is -2. The slightly higher decay rates seem to originate from the action of the two horseshoe vortices bringing less turbulent fluid down toward the surface on the centerline. The maximum Delta U VAR also compare very well with the neutral flow data of Woo et al. [5] for

buildings 2, 5 and 6. For buildings 3 and 4 the decay rates of Woo et al. [5] show similar trends; however, the actual numbers are different.

Horizontal profiles of Delta U VAR behind building 2 at $z/H = 1.0$ are shown in Figure 50. The result of horseshoe vortices is evident with the observation of a dip in the profiles near the centerline. No regions of negative Delta U VAR were observed and, in this aspect, the results are different than than observed by Hansen et al. [17] in the wake of a hemisphere. Perhaps the reason is that the strength of the horseshoe vortex, $\Gamma_{x=0}$, calculated in the present research was about one-half to one-third of that observed by Hansen et al. [17], in the wake of a hemisphere. The strong vortex action behind the hemisphere brought low turbulence fluid from above the hemisphere down into the wake region resulting in less turbulence intensity than that which existed without the hemisphere in place.

The maximum temperature excess variance, Delta T VAR, on the centerline of the buildings occurring at each x/H is shown in Figure 51. Similar to maximum Delta U VAR, this maximum did not occur at the same z/H for all x/H. The effect of horseshoe vortices, which were not very clear from the results of maximum Delta U VAR, is obvious from this figure. In the absence of horseshoe vortices, it would be expected that the temperature excess variance asymptotically approaches zero. The results show that the maximum Delta T VAR becomes negative before asymptoting to zero. The longitudinal vortices, which bring fluid having less fluctuation in temperature from the top of the turbulent boundary layer toward the ground on the centerline of the building,

result in the negative Delta T VAR. For Delta T VAR the vortex wake is dominant in the near wake compared with the momentum wake, and Delta T VAR is still strong at a distance of x/H = 60. Thus, the effect of horseshoe vortices play an important role in determining the pattern of temperature fluctuations in the wake of the buildings. The long wake of Delta T VAR as compared to the small wake of Delta U VAR, suggests the need to use local temperature field characteristics for evaluation of diffusion of pollutants from power plants.

Figure 52 compares normalized longitudinal velocity spectra in the wake of building 2 at various x/H locations with the undisturbed boundary layer velocity spectrum. Kolmogorov [45], using dimensional arguments and the concept of local isotropy, determined that the velocity fluctuation spectrum obeys a -5/3 law power-law behavior in the inertial subrange. A line having a slope of -5/3 is also shown on the same figure. The velocity fluctuation spectra measured obey a -5/3 power-law behavior in the inertial subrange. It must be concluded that the velocity spectrum does not change much in the wake of the model building. The slight variation in the velocity spectrum near the building compared with the undisturbed boundary layer velocity spectrum may be the result of measurement inaccuracies in the near wake. The velocity spectra show a shift of energy from lower frequency to higher frequency in the near wake and a gradual return to undisturbed conditions with increasing x/H.

A comparison of normalized temperature spectra in the wake of building 2 at different x/H locations with the undisturbed boundary layer spectrum is shown in Figure 53. Corrsin [46] and Batchelor [47]

have extended Kolmogorov's idea of local isotropy and determined a -5/3 power-law behavior for the spectrum of temperature fluctuations in the inertial subrange. The line of -5/3 slope is also shown in this figure. Laboratory measurements by Arya [10] for a stably stratified turbulent boundary layer also show a -5/3 power-law behavior. Lin, Panchev and Cermak [48] have calculated the -5/3 power-law behavior for temperature spectrum in the inertial subrange. Okamoto and Webb [49] have reported a -5/3 power-law behavior for temperature fluctuation spectrum in the inertial subrange for their measurement at a height of 2 m over flat grassland in stable conditions. Kaimal, Wyngaard, Izumi and Cote [50] have also reported a -5/3 power-law behavior in their Kansas experiments. The present results for temperature spectra reproduce the -5/3 power-law behavior in the inertial subrange for the undisturbed boundary layer. The temperature spectra do not vary greatly with x/H in the wake of the building. The temperature spectra show approximately -1 power-law behavior in the inertial subrange in the wake of a building. The temperature spectra also show a shift of energy from lower frequency to higher frequency in the near wake and a gradual return to undisturbed conditions with increasing x/H. The rate of return of the temperature spectra to upwind conditions seems to be slower than the velocity spectra.

Figures 54 and 55 show the comparison of auto-correlation coefficients derived from velocity and temperature spectra respectively in the wake of building 2 with undisturbed boundary layer auto-correlation coefficients for various x/H ratios. The integral time scale of the motion is reduced with the building in place. This implies, using

Taylor's frozen hypothesis, that the integral length scale of the motion is reduced with the building in place. Similar findings were also reported by Counihan [14], Hansen et al. [4], Woo et al. [5], and Hansen et al. [17].

The velocity and temperature spectra have been compared in Figures 56 and 57 for the undisturbed boundary layer and in the wake of building 2 respectively. The velocity and temperature spectra are more similar for undisturbed boundary layer than in the wake of a building. Figure 56 also includes velocity fluctuation spectrum of Hansen et al. [17] in neutral flow and temperature fluctuation spectrum of Arya [10] in stable flow. The present results compare very well with Hansen et al. [17] for velocity fluctuation spectrum. However, Arya's [10] measurements of temperature spectrum tend to become flat at higher frequency than the present results. The auto-correlation coefficients derived from velocity and temperature spectra respectively in the undisturbed boundary layer and behind building 2 are shown in Figures 58 and 59. The integral length scale, using Taylor's frozen hypothesis, calculated respectively from velocity and temperature spectrum were 0.18 m (0.6 ft) and 0.14 m (0.45 ft) in undisturbed boundary layer and 0.06 m (.18 ft) and 0.04 (0.12 ft) in the wake of building. Thus, it can be concluded that the length scale calculated from velocity and temperature differ by a small amount.

Chapter VI

CONCLUSIONS AND RECOMMENDATIONS

The velocity and temperature wakes behind rectangular, surface-mounted building models with one face perpendicular to approach flow deeply submerged in a stable turbulent boundary layer have been investigated using wind tunnel tests and mathematical analysis. The effects of a building on the approach stable turbulent boundary layer were determined utilizing superposition of momentum and vortex wake perturbation models. Several conclusions were drawn during the discussion of the results, and, hence, only primary considerations are outlined here.

The effects of a momentum-type wake behind a building in a stable turbulent boundary layer are to decrease mean velocity and mean temperature but to increase turbulence intensity and temperature fluctuation intensity. On the other hand, along the centerline of a building, a vortex wake brings higher-momentum, higher-temperature, less-turbulent and less-temperature-flucutation-intensity fluid from the top of the boundary layer to increase mean velocity and mean temperature and decrease turbulent intensity and temperature-fluctuation intensity. In stable flow trailing vortices were observed to a distance of $x/H \doteq 60$, beyond which measurements were not performed; hence, the total length of the votex wake was not known. The wake of an isolated structure, in neutral flow, with one face perpendicular to flow, is less extensive. This characteristic makes the wake structure quite different for stable and neutral flow. Thus, in the wake of an isolated building, particularly in stable flow, both momentum and vortex perturbation effects should be taken into consideration.

A theory for temperature distribution in the wakes of buildings was developed considering both of these effects. The method to calculate the circulation of horseshoe vortices at x = 0 was generalized. With a single free constant, determined from experimental results, the theory predicts the temperature distribution in the far wake of an isolated building. The theory for velocity distribution in the wake of a building (see Hunt [20]) was given a careful evaluation. The present velocity measurements show good agreement with Hunt's theory.

The experimental measurements were compared with the neutral flow data of Woo et al. [5]. The decay rates for the velocity field compared very well in both of these experiments; however, the actual magnitude of velocity defect was different. The temperature wake extends much farther then the velocity wake with all the buildings, showing higher temperature in the wake even at x/H = 60 than the approach flow temperature distribution. The high temperatures and excess velocities observed in the far wake strongly suggest that the horseshoe vortices play a very important role in a wake of an isolated building.

The approach flow and building wake integral time scale and integral length scale derived from velocity or temperature signals were slightly different. Both these scales were reduced in the wake of the building as compared to approach flow values confirming the results of previous researchers. The velocity fluctuation spectra are approximately same at various x/H locations, except in the very near wake, with and without a building in place and obey a -5/3 power-law behavior in the inertial subrange. The temperature fluctuation spectra are different in the approach flow and in the wake, with the -5/3 power-law behavior in the inertial subrange observed only for approach flow. The power-law

behavior in the inertial subrange for temperature spectra was close to -1 in the wake region.

A technique was developed for sensitive measurements of mean and turbulent fluctuation of velocity and temperature. The method makes it possible to collect large amounts of data in a reasonable amount of time.

The differential equations governing velocity, temperature and concentrations of pollutants in the wake of a building have significant similarities. The analytical predictions of temperature distribution, a scalar quantity, shows better agreement then the velocity distribution. Hence, a similar theory for predicting the diffusion of concentration, a scalar quantity, should be considered. In determining the velocity and temperature distribution for vortex wake analysis, the results for the viscous core region (V_+) in which there is a balance between the Reynolds stress and the inertial forces and boundary layer region (G) induced by vortices should be determined numerically to obtain better results. The advantages of using variable eddy viscosity and eddy diffusivity in the perturbation models should be evaluated.

REFERENCES

1. Gregory, N. and Walker, W. S., 1951, "The Effect of Isolated Surface Excrescenes in the Boundary Layer," ARC R&M 2779, October.

2. Mochizuki, M., 1961, "Smoke Observation on Boundary Layer Transition Caused by a Spherical Roughness Element," Journal of the Physical Society of Japan (Nippon Batsuri Gakkai), Vol. 16, No. 5, May, pp. 995-1008.

3. Ostrowski, J. S., Marshall, R. D. and Cermak, J. E., 1967, "Vortex Formation and Pressure Fluctuations on Buildings," Proceedings of the International Seminar on Wind Effects on Buildings and Structures, Ottawa, Canada, September. Also Fluid Dynamics and Diffusion Laboratory Report CEP67-68-JSO-RDM-JEC80, Colorado State University, Fort Collins, Colorado.

4. Hansen, A. C., Peterka, J. A. and Cermak, J. E., 1975, "Wind-Tunnel Measurements in the Wake of a Simple Structure in a Simulated Atmospheric Flow," Fluid Dynamics and Diffusion Laboratory Report CER73-74-ACH-JAP-JEC43, Colorado State University, Fort Collins, Colorado.

5. Woo, H. G. C., Peterka, J. A. and Cermak, J. E., 1976, "Wind-Tunnel Measurements in the Wakes of Structures," Fluid Dynamics and Diffusion Laboratory Report CER75-76-HGCW-JAP-JEC40, Colorado State University, Fort Collins, Colorado.

6. Peterka, J. A. and Cermak, J. E., 1975, "Turbulence in Building Wakes," Fourth International Conference on Wind Effects on Buildings and Structures, London, September.

7. Huber, A. H. and Snyder, W. H., 1976, "Building Wake Effects on Short Stack Effluents," Third Symposium on Atmospheric Turbulence Diffusion and Air Quality, October, Raleigh, N.C.

8. Zambrano, T. G. and Peterka, J. A., 1978, "Wind Load Interaction on an Adjacent Building," Fluid Dynamics and Diffusion Laboratory Report CER77-78-TGZ-JAP26, Colorado State University, Fort Collins, Colorado.

9. Monin, A. S. and Obukhov, A. M., 1954, "Basic Regularity in Turbulent Mixing in the Surface Layer of the Atmosphere," Trans. of the Geophys. Inst. Acad. Sci., USSR, No. 24.

10. Arya, S. P. S., 1968, "Structure of Stably Stratified Turbulent Boundary Layer," Fluid Dynamics and Diffusion Laboratory Report CER68-69 SPSA10, Colorado State University, Fort Collins, Colorado.

11. Colmer, M. J., 1971, "Some Full-Scale Measurements of the Flow in the Wake of a Hanger," ARC-CP-1166.

12. Frost, W. and Shahabi, A. M., 1977, "A Field Study of Wind Over a Simulated Block Building," NASA Report CR-2804.

13. Yang, B. T. and Meroney, R. N., 1970, "Gaseous Dispersion into Stratified Building Wakes," Fluid Dynamics and Diffusion Laboratory Report CER70-71BTY-RNM-8, Colorado State University, Fort Collins, Colorado.

14. Counihan, J., 1971, "An Experimental Investigation of the Wake behind a Two-Dimensional Block and behind a Cube in a Simulated Boundary Layer Flow," CERL Lab. Note: RD/L/N115/71.

15. Lemberg, R., 1973, "On the Wakes Behind Bluff Bodies in a Turbulent Boundary Layer," University of Western Ontario Report BLWT-3-73.

16. Castro, I. P. and Robins, A. G., 1975, "The Effect of a Thick Incident Boundary Layer on the Flow Around a Small Surface Mounted Cube," Central Electricity Generating Board Report R/M/N795.

17. Hansen, A. C. and Cermak, J. E., 1975, "Vortex-Containing Wakes of Surface Obstacles," Fluid Dynamics and Diffusion Laboratory Report CER75-76-ACH-JEC16, Colorado State University, Fort Collins, Colorado.

18. Hatcher, R. V., Meroney, R. N., Peterka, J. A. and Kothari, K., 1977, "Dispersion in the Wake of a Model Industrial Complex," Fluid Dynamics and Diffusion Laboratory Report 76-77-RVH-RNM-JAP-KK35, Colorado State University, Fort Collins, Colorado.

19. Hunt, J. C. R., Abell, C. J., Peterka, J. A. and Woo, H., 1978, "Kinematical Studies of the Flows Around Free or Surface-Mounted Obstacles; Applying Topology to Flow Visualization," Journal of Fluid Mechanics, Vol. 86, Part 1, pp. 179-200.

20. Hunt, J. C. R. and Smith, J. P., 1969, "A Theory of Wakes behind Buildings and some Provisional Experimental Results," Central Electricity Research Laboratory Report RD/L/N31/69.

21. Hunt, J. C. R., 1971, "Further Aspects of the Theory of Wakes behind Buildings and Comparison of Theory with Experiment," Central Electricity Research Laboratory Report RD/L/R/1665.

22. Hunt, J. C. R., 1971b, "A Theory for the Laminar Wake of a Two-Dimensional Body in a Boundary Layer," Journal of Fluid Mechanics, Vol. 49, Part 1, pp. 159-178.

23. Hunt, J. C. R., 1974, "Wakes behind Buildings," A paper presented to Environmental Committee of the Aeronautical Research Council, Great Britain, October.

24. Counihan, J., Hunt, J. C. R. and Jackson, P. S., 1974, "Wakes behind Two-Dimensional Surface Obstacles in Turbulent Boundary Layers," Journal of Fluid Mechanics, Vol. 64, Part 3, pp. 529-563.

25. Hunt, J. C. R., 1971, "The Effect of Single Building and Structures," Phil. Trans. Roy. Soc. Lond., A269, pp. 457-467.

26. Hunt, J. C. R., 1972, "Some Theories for the Mean and Turbulent Velocity Distributions in Flows around Bluff Bodies," A paper presented at the Symposium on External Flows, University of Bristol, July.

27. Hunt, J. C. R., 1975, "Vortex and Momentum Wakes behind Surface Obstacles in Turbulent Boundary Layers," to be published.

28. Frost, W., Maus, J. R. and Simpson, W. R., 1973, "A Boundary Layer Approach to the Analysis of Atmospheric Motion over a Surface Obstruction," NASA CR-2182.

29. Hirt, C. N. and Cook, J. L., 1971, "Calculating Three-Dimensional Flows around Structures and over Rough Terrain," Los Alamos Scientific Laboratory, LA-DC-13289.

30. Frost, W., 1973, "Review of Data and Prediction Techniques for Wind Profiles around a Man-Made Surface Obstruction," Flight in Turbulence, AGARD Conference Proceedings No. 140.

31. Schlichting, H., 1968, Boundary Layer Theory, McGraw-Hill Book Co., New York, N.Y.

32. Hinze, J. O., 1975, Turbulence, McGraw-Hill Book Co., New York, N.Y.

33. Smith, F. B., 1957, "The Diffusion of Smoke from a Continuous Elevated Point-Source into a Turbulent Atmosphere," Journal of Fluid Mechanics, Vol. 2, Part 1, pp. 49-76.

34. Cermak, J. E., 1975, "Applications of Fluid Mechanics to Wind Engineering--A Freeman Scholar Lecture," Journal of Fluids Engineering, Trans. of the ASME, Vol. 97, pp. 9-38.

35. Cermak, J. E. and Arya, S. P. S., 1970, "Problems of Atmospheric Shear Flows and their Laboratory Simulations," AGARD Conference Proceedings, No. 48, pp. 12.1-12.16.

36. Plate, E. J. and Cermak, J. E., 1963, "Micrometeorological Wind Tunnel Facility, Description and Characteristics," Fluid Dynamics and Diffusion Laboratory Report CER63-EJP-JEC9, Colorado State University, Fort Collins, Colorado.

37. Zoric, D. L., 1969, "Approach of Turbulent Boundary Layer to Similarity," Fluid Dynamics and Diffusion Laboratory Report CER68-69DLZ9, Colorado State University, Fort Collins, Colorado.

38. Chao, J. L. and Sandborn, V. A., 1964, "A Resistance Thermometer for Transient Temperature Measurements," Fluid Mechanics Paper No. 1, Colorado State University, Fort Collins, Colorado.

39. Sandborn, V. A., 1972, Resistance Temperature Transducer, Metrology Press, Fort Collins, Colorado.

40. Bendat, J. S. and Piersal, A. G., 1971, Random Data: Analysis and Measurement Procedures, Wiley-Interscience.

41. Akins, R. E. and Peterka, J. A., 1975, "Computation of Power Spectral Densities and Correlations Using Digital FFT Techniques," Fluid Dynamics and Diffusion Report CER75-76REA-JAP13, Colorado State University, Fort Collins, Colorado.

42. Akins, R. E., Peterka, J. A. and Cermak, J. E., 1977, "Mean Force and Moment Coefficients for Buildings in Turbulent Boundary Layers," Journal of Industrial Aerodynamics, Vol. 2, pp. 195-209.

43. Alexopoulos, C. C. and Keffer, J. F., 1971, "Turbulent Wake in a Passively Stratified Field," The Physics of Fluids, Vol. 14, No. 2, pp. 216-224.

44. Allwine, K. J., Meroney, R. N. and Peterka, J. A., 1978, "Rancho Seco Building Wake Effects on Atmospheric Diffusion: Simulation in a Meteorological Wind Tunnel," Fluid Dynamics and Diffusion Laboratory Report CER77-78KJA-RNM-JAP25, Colorado State University, Fort Collins, Colorado.

45. Kolmogorov, A. N., 1941, "The Local Structure of Turbulence in an Incompressible Viscous Fluid for Very Large Reynolds Numbers," C. R. Acad. Sci., URSS, Vol. 30, pp. 301-305.

46. Corrsin, S., 1964, "Further Generalization of Onsagar's Cascade Mode for Turbulent Spectra," Physics of Fluids, Vol. 7, pp. 1156-1159.

47 Batchelor, G. K., 1959, "Small Scale Variations of Convected Quantities like Temperature in Turbulent Fluids--Part I," Journal of Fluid Mechanics, Vol. 5, pp. 113-133.

48. Lin, J. T., Panchev, S. and Cermak, J. E., 1969, "A Modified Hypothesis on Turbulence Spectra in the Buoyancy Subrange of Stably Stratified Shear Flow," Radio Science, December, Vol. 4, No. 12, pp. 1333-1337.

49. Okamoto, M. and Webb, E. K., 1970, "The Temperature Fluctuations in Stable Stratification," Quarterly Journal of Royal Meteorological Society, Vol. 96, pp. 591-600.

50. Kaimal, J. C., Wyngaard, J. C., Izumi, Y. and Cote, O. R., 1972, "Spectral Characteristics of Surface-Layer Turbulence," Quarterly Journal of Royal Meteorological Society, Vol. 98, pp. 563-589.

51. Abramowitz, M. and Stegun, I. A., 1968, Handbook of Mathematical Functions, National Bureau of Standards, Applied Mathematics Series 55, Washington, D.C.

Appendix A

THE SOLUTION TECHNIQUE FOR TURBULENT ENERGY EQUATION FOR MOMENTUM WAKE ANALYSIS

The temperature defect, θ, in the wake of a building is governed by equation (3.16) and this appendix describes the method for obtaining the solution of the same equation. The equation (3.16) is repeated here for completeness and is given by,

$$\bar{z}^{n} \frac{\partial \theta}{\partial \bar{x}} = \lambda \frac{\partial^2 \theta}{\partial \bar{y}^2} + \frac{\partial^2 \theta}{\partial \bar{z}^2} \cdot \tag{A.1}$$

The nondimensional distances $\bar{x}$, $\bar{y}$, and $\bar{z}$ are given by,

$$\bar{x} = \frac{x}{c_1}, \quad \bar{y} = \frac{y}{c_1}, \quad \text{and} \quad \bar{z} = \frac{z}{c_1},$$

where c_1 is the length scale proportional to the building height and given by,

$$c_1 = \left(\frac{\varepsilon_3 \Delta^n}{\bar{U}_o} \right)^{\frac{1}{1+n}} . \tag{A.2}$$

The solution of equation (A.1) was assumed to be of the form,

$$\theta(x,y,z) = F(\bar{x},\bar{z}) \, \mathrm{Exp}\left[- \frac{\bar{y}^2}{f(\bar{x},\bar{z})} \right] . \tag{A.3}$$

The functions $F(\bar{x},\bar{z})$ and $f(\bar{x},\bar{z})$ are evaluated using the technique of Hunt and Smith [20] and given by,

$$F(\bar{x},\bar{z}) = q_o \sqrt{q_o/(2\pi q_2)} \quad \text{and}$$

$$f(\bar{x},\bar{z}) = \frac{2q_2}{q_o}, \tag{A.4}$$

where q_o and q_2 are defined in equation (3.20).

The functions q_o and q_2 are the solutions of the following differential equations (see Hunt and Smith [20]),

$$\bar{z}^n \frac{\partial q_o}{\partial \bar{x}} = \frac{\partial^2 q_o}{\partial \bar{z}^2} \tag{A.5}$$

and

$$\bar{z}^n \frac{\partial q_2}{\partial \bar{x}} = \frac{\partial^2 q_2}{\partial \bar{z}^2} + 2\lambda q_o \, . \tag{A.6}$$

The boundary conditions for equations (A.5) and (A.6) are given by,

$$q_o = q_2 = 0 \quad \text{at} \quad \bar{z} = 0 \quad \text{and} \quad \bar{z} \to \infty \, ,$$

$$q_o = q_2 = 0 \quad \text{at} \quad \bar{y} \to -\infty \quad \text{and} \quad \bar{y} \to +\infty \quad \text{and}$$

$$\int_0^\infty z \, \bar{U} \, q_o \, d\bar{z} = \bar{c}, \tag{A.7}$$

where $\bar{c}$ is a constant.

Assuming that a similarity solution is possible for equation (A.5) and given by,

$$q_o = \bar{x}^{\beta} f(\bar{\eta}) \, , \tag{A.8}$$

where β is a constant, $\bar{\eta} = \bar{z}^{(2+n)}/\bar{x}$ and n is the power-law velocity profile index in the approach flow. Substitution of equation (A.8) in equation (A.5) gives,

$$(2+n)^2 \bar{\eta} \frac{d^2 f}{d\bar{\eta}^2} + \left[(1+n)(2+n) + \bar{\eta}\right] \frac{df}{d\bar{\eta}} - \beta f = 0. \tag{A.9}$$

The value of β was determined using boundary condition (A-7) and knowing the approach velocity profile. Substitution of equation (A.8) and power-law velocity profile in boundary condition (A-7) gives,

$$\bar{x}^{\beta+1} \int_0^{\infty} f(\bar{\eta})\, d\bar{\eta} = c_2, \tag{A.10}$$

where c_2 is a constant. Now, if c_2 is a constant as $\bar{x}$ changes then $\beta = -1$. Therefore, $q_o = f(\bar{\eta})/\bar{x}$ and equation (A.9) can be written as,

$$(2+n)^2 \bar{\eta} \frac{d^2 f}{d\bar{\eta}^2} + \left[(1+n)(2+n) + \bar{\eta}\right] \frac{df}{d\bar{\eta}} + f = 0. \tag{A.11}$$

The solution of equation (A.11) is given by,

$$f(\eta) = c_3 (\eta)^{\frac{1}{(2+n)}} e^{-\eta}, \tag{A.12}$$

where c_3 is a constant and $\eta = \bar{\eta}/(2+n)^2$.

The constant c_3 is determined with the use of boundary condition (A.7). Substitution of q_o in (A.7) and changing the variables to η gives,

$$(2+n)\, \varepsilon_3 c_3 \int_0^{\infty} \eta^{\frac{1}{(2+n)}} e^{-\eta}\, d\eta = \bar{c}. \tag{A.13}$$

The integral in equation (A.13) can be put in the form of the gamma function (see Abramowitz and Stegun [51]) and equals $\Gamma((3+n)/(2+n))$. Hence, constant c_3 is given by,

$$c_3 = \frac{\bar{c}}{(2+n)\, \varepsilon_3\, \Gamma((3+n)/(2+n))}, \tag{A.14}$$

and the solution of equation (A.5) is,

$$q_o = \frac{\bar{c}}{(2+n)\ \varepsilon_3\ \Gamma((3+n)/(2+n))}\ \frac{\eta^{\frac{1}{(2+n)}}\ e^{-\eta}}{\bar{x}} \ . \qquad (A.15)$$

The solution q_o when substitued in equation (A.6) gives,

$$\bar{z}^{\,n}\ \frac{\partial q_2}{\partial \bar{x}} = \frac{\partial^2 q_2}{\partial \bar{z}^{\,2}} + \bar{\lambda}\ (\eta)^{\frac{1}{(2+n)}}\ e^{-\eta}\ \bar{x}^{\,-1} \ , \qquad (A.16)$$

where

$$\bar{\lambda} = 2\lambda\bar{c}/[(2+n)\ \varepsilon_3\ \Gamma((3+n)/(2+n))] .$$

A similarity solution of equation (A.16) was assumed with a form given by,

$$q_2 = \bar{x}^{\,\alpha}\ G(\eta), \qquad (A.17)$$

where α is a constant to be determined. The equation (A.17) when substituted in equation (A.16) gives,

$$\bar{x}^{(\alpha-1\ +\ \frac{n}{2+n})} \left[\eta\ \frac{d^2G}{d\eta^2} + \left\{ \frac{(1+n)}{(2+n)} + \eta \right\} \frac{dG}{d\eta} - \alpha G \right] (2+n)^{\frac{2n}{2+n}}\ \eta^{\frac{n}{2+n}}$$

$$= -\bar{\lambda}\ \eta^{\frac{1}{(2+n)}}\ e^{-\eta}\ \bar{x}^{\,-1} \ . \qquad (A.18)$$

In order that $G(\eta)$ be a function of η only, powers of $\bar{x}$ on both sides of equation (A.18) are equated to obtain,

$$\alpha = -\frac{n}{(2+n)} \ . \qquad (A.19)$$

Therefore, the solution of equation (A.18) is given by,

$$q_2 = \bar{x}^{\,-\frac{n}{(2+n)}}\ G(\eta) \ , \qquad (A.20)$$

where $G(\eta)$ satisfies the following differential equation,

$$\eta \frac{d^2G}{d\eta^2} + \left[\frac{(1+n)}{(2+n)} + \eta \right] \frac{dG}{d\eta} + \frac{n}{(2+n)} G = - \frac{\bar{\lambda}}{(2+n)^{\frac{2n}{(2+n)}}} e^{-\eta} \eta^{\left(\frac{1-n}{2+n}\right)}. \tag{A.21}$$

The transformation,

$$H(\eta) = e^{\eta} G(\eta), \tag{A.22}$$

reduces equation (A.21) to,

$$\eta \frac{d^2H}{d\eta^2} + \left[\frac{(1+n)}{(2+n)} - \eta \right] \frac{dH}{d\eta} - \frac{1}{(2+n)} H = \frac{\bar{\lambda}}{(2+n)^{\frac{2n}{2+n}}} \eta^{\left(\frac{1-n}{2+n}\right)}. \tag{A.23}$$

The equation (A.23) is a non-homogeneous confluent hypergeometric equation (see Abramowitz and Stegun [51]). The solution of equation (A.23) was obtained (see Hunt and Smith [20]) using the method of variation of parameters and is given by,

$$H(\eta) = \frac{\bar{\lambda}\, \Gamma\, (1/(2+n))}{2(2+n)^{\left(\frac{2n}{2+n}\right)}\, \Gamma\, ((1+n)/(2+n))} \eta^{1/2}\, (1.5+\eta). \tag{A.24}$$

Hence, with equations (A.17), (A.22) and (A.24), the solution of equation (A.6) is,

$$q_2 = \frac{\bar{x}^{-\frac{n}{2+n}}\, \bar{\lambda}\, \Gamma\, (1/(2+n))}{2\, (2+n)^{\frac{2n}{2+n}}\, \Gamma\, ((1+n)/(2+n))} \eta^{1/2}\, (1.5+\eta)\, e^{-\eta}. \tag{A.25}$$

Knowing q_o and q_2, the functions $F(\bar{x},\bar{z})$ and $f(\bar{x},\bar{z})$ are,

$$f(\bar{x},\bar{z}) = c_4 \, \bar{x}^{\left(\frac{2}{2+n}\right)} \, \eta^{\left(\frac{n}{2+n}\right)} \, (1.5+\eta), \tag{A.26}$$

$$F(\bar{x},\bar{z}) = \frac{c_5 \, e^{-\eta} \, \eta^{\frac{1-(n/4)}{(2+n)}}}{\bar{x}^{\left(\frac{3+n}{2+n}\right)} \sqrt{1.5+\eta}} \quad , \tag{A.27}$$

where

$$c_4 = \frac{2\lambda}{(2+n)^{\left(\frac{2n}{2+n}\right)}} \qquad \text{and}$$

$$c_5 = \frac{\bar{c}}{\sqrt{2\lambda}\,\pi\,\varepsilon_3} \quad .$$

For $n \ll 1$, $\frac{n}{2+n} \simeq 0$ and $\frac{1-(n/4)}{(2+n)} \simeq \frac{1}{2+n}$ and hence equations (A.26) and (A.27) reduce to,

$$f(\bar{x},\bar{z}) = c_4 \, \bar{x}^{\left(\frac{2}{2+n}\right)} \, (1.5+\eta), \tag{A.28}$$

$$F(\bar{x},\bar{z}) = \frac{c_5 \, \eta^{\left(\frac{1}{2+n}\right)} \, e^{-\eta}}{\bar{x}^{\left(\frac{3+n}{2+n}\right)} \sqrt{1.5+\eta}} \quad . \tag{A.29}$$

Hunt and Smith [20] calculated eddy viscosity, $\bar{\nu}$, using the approach flow conditions to deduce that

$$\bar{\nu} = \frac{2}{(2+n)} \, K^2 n \, \bar{U}(H) \, H. \tag{A.30}$$

In the present analysis it was assumed eddy diffusivity, $\bar{\varepsilon}$, is proportional to eddy viscosity, $\bar{\nu}$, and $\bar{\varepsilon} = 0.85\,\bar{\nu}$ (see Arya [10]). Now, with the assumption that the eddy diffusivity in the z direction $\varepsilon_3 = \gamma\bar{\varepsilon}$ gives,

$$\varepsilon_3 = \frac{2}{(2+n)} K^2 n \, \overline{U}(H) \, H \, \gamma \, 0.85. \tag{A.31}$$

The magnitude of $\overline{c}$ in equation (A.7) was derived using a method similar to Hunt and Smith [20] to conclude that,

$$\overline{c} \doteq c_6 \left(\frac{H}{2}\right) \overline{T}(H) \, \overline{U}(H) \left[\frac{2+n}{2 \, K^2 0.85 \, \gamma n}\right]^{\frac{2}{1+n}} \tag{A.32}$$

where c_6 is a constant.

With equations (A.31) and (A.32), the constant c_5 is given by,

$$c_5 = c_7 \, \overline{T}(H) \, , \tag{A.33}$$

where c_7 is a constant. Hence, the temperature defect θ is,

$$\theta(x,y,z) = c_7 \frac{\overline{T}(H) \, \eta^{\frac{1}{2+n}}}{\overline{x}^{\left(\frac{3+n}{2+n}\right)} \sqrt{1.5+\eta}} \, \mathrm{Exp}\left[-\left(\eta + \frac{\overline{y}^{\,2}}{c_4 \, \overline{x}^{\left(\frac{2}{2+n}\right)} (1.5+\eta)}\right)\right]. \tag{A.34}$$

Now, the non dimensional variables $\overline{x}$, $\overline{y}$, and $\overline{z}$ are replaced with real variables, x, y and z, given by,

$$\begin{aligned}
\overline{x} &= \frac{(x/H)}{\left[\left(\frac{2}{2+n}\right) K^2 n \, \gamma \, 0.85\right]^{\left(\frac{1}{1+n}\right)}} \, , \\
\overline{y} &= \frac{(y/H)}{\left[\left(\frac{2}{2+n}\right) K^2 n \, \lambda \, \gamma \, 0.85\right]^{\left(\frac{1}{1+n}\right)}} \, , \\
\overline{z} &= \frac{(z/H)}{\left[\left(\frac{2}{2+n}\right) K^2 n \, \gamma \, 0.85\right]^{\left(\frac{1}{1+n}\right)}} \, ,
\end{aligned} \tag{A.35}$$

to obtain,

$$\theta(x,y,z) = \frac{k_2\ \overline{T}(H)\ \eta^{\frac{1}{2+n}}}{(x/H)^{\left(\frac{3+n}{2+n}\right)}\sqrt{1.5+\eta}}\ \text{Exp}\left[-\left(\eta + c_8\ \frac{(y/H)^2\left(\frac{2+n}{2K^2n\ \gamma\ \lambda\ 0.85}\right)^{\frac{2}{2+n}}}{(x/H)^{\frac{2}{2+n}}\ (1.5+\eta)}\right)\right] \tag{A.36}$$

where c_8 is another constant. With the assumptions that the wake originate from $x = -a$ and hence replacing x by $(x-a)$ and dividing both sides of equation (A.36) by DELTA T, the temperature defect θ is,

$$\frac{\theta(x,y,z)}{\text{DELTA T}} = k_2\ \frac{\overline{T}(H)}{\text{DELTA T}}\ \frac{F_2(z'',y'')}{\left(\frac{x-a}{H}\right)^{\left(\frac{3+n}{2+n}\right)}}\ , \tag{A.37}$$

where

DELTA T = $\overline{T}_\delta - \overline{T}_{z_1}$ in the undisturbed boundary layer and is used for nondimensionalizing,

$\overline{T}_\delta$ = mean temperature at the top of the turbulent boundary layer,

$\overline{T}_{z_1}$ = mean temperature at the reference height z_1,

$\overline{T}(H)$ = mean temperature at the building height in the undisturbed flow,

k_2 = constant to be determined by matching with the experimental result,

a = virtual origin of the wake to be determined from experiment,

n = boundary layer velocity profile power-law exponent,

$$F_2(z'',y'') = \frac{\eta^{\left(\frac{1}{2+n}\right)}}{(\eta+1.5)^{1/2}}\ \text{Exp}\left[-\left(\eta + c_8\ \frac{y''^2}{(\eta+1.5)}\right)\right]\ ,$$

$$z'' = \frac{(z/H)}{\left(\frac{x-a}{H}\right)^{\frac{1}{2+n}}} ,$$

$$\eta = \frac{z''^{(2+n)}}{(2(2+n)\ K^2\ n\ 0.85\ \gamma)} ,$$

$$y'' = \frac{(y/H)}{\left(\frac{x-a}{H}\right)^{\left(\frac{1}{2+n}\right)}} - \left[\frac{2+n}{2\ \lambda\ 0.85\ \gamma\ K^2 n}\right]^{\frac{1}{2+n}} ,$$

K = von Karman constant (0.41), and

c_8 = a constant and along the centerline of building (y=0) it drops out of the equation.

Appendix B

CALCULATIONS OF VELOCITY AND TEMPERATURE FROM HOT FILM DATA

Calculation of velocity and temperature variation from the voltage output of two hot films is described here.

Equation (4.3) with the output of two hot film sensors, each operated at a different but constant temperature, will be:

$$\frac{E_1^2}{R_1[R_1 - R_{c_1}(1 + \alpha(T - T_{c_1}))]} = A_1 + B_1 U^C \qquad (B.1)$$

and

$$\frac{E_2^2}{R_2[R_2 - R_{c_2}(1 + \alpha(T - T_{c_2}))]} = A_2 + B_2 U^C \qquad (B.2)$$

where suffix 1 and 2 corresponds to the different overheat ratios of 1.5 and 1.2 respectively. Equations (B.1) and (B.2) with

$$C_1 = R_1^2 - R_1 R_{c_1} + R_1 R_{c_1} \alpha T_{c_1}$$

$$C_2 = R_1 R_{c_1} \alpha$$

$$C_3 = R_2^2 - R_2 R_{c_2} + R_2 R_{c_2} \alpha T_{c_2}$$

$$C_4 = R_2 R_{c_2} \alpha$$

becomes,

$$\frac{E_1^2}{C_1 - C_2 T} = A_1 + B_1 U^C \qquad (B.3)$$

and $$\frac{E_2^2}{C_3 - C_4 T} = A_2 + B_2 U^C . \qquad (B.4)$$

Elimination of U from equations (B.3) and (B.4) gives

$$p T^2 - q T + r = 0 \qquad (B.5)$$

where,

$$p = A_2B_1C_2C_4 - A_1B_2C_2C_4 ,$$

$$q = - (A_1B_2C_1C_4 + A_1B_2C_2C_3 - E_1^2B_2C_4 + E_2^2B_1C_2 - A_2B_1C_1C_4 - A_2B_1C_2C_3) ,$$

$$r = E_1^2B_2C_3 - A_1B_2C_1C_3 - E_2^2B_1C_1 + A_2B_1C_1C_3 .$$

From several initial calibrations it was determined that $p \doteq 0$ and hence for all calculations p was set equal to zero. Therefore, the instantaneous fluid temperature T is given by,

$$T = r/q . \qquad (B.6)$$

knowing the T, U was determined from equations (B.3) or (B.4). The time series of T and U were then used to calculate the root mean square values T_{rms} and u_{rms} and mean quantities $\overline{T}$ and $\overline{U}$, respectively.

Table 1. Building model dimensions, boundary layer parameters and constants.

Building	Height (H) cm	Width (W) cm	Depth (D) cm	$\bar{U}(\delta)$ m/sec	$\bar{U}(H)$ m/sec	$\bar{T}(\delta)$ °C	$\bar{T}(H)$ °C	$\frac{u_*}{\bar{U}(H)}$	$\frac{z_o}{H}$	Re_H	Ri_δ	Ri_H	C_{Fx}	k_2	a/H	$\Gamma_{x=0}$ m^2/sec
1	6.25	4.88	15.88	5.96	4.26	47.19	36.89	0.053	5.6×10^{-3}	2.1×10^4	0.0229	4.6×10^{-3}	1.30	11.3	-2.50	0.45
2	6.25	15.88	4.88	5.96	4.26	47.19	36.89	0.053	5.6×10^{-3}	2.1×10^4	0.0229	4.6×10^{-3}	1.40	13.1	-1.75	1.44
3	7.62	7.62	7.62	5.67	4.27	44.16	35.18	0.053	4.6×10^{-3}	2.5×10^4	0.0235	5.0×10^{-3}	1.30	8.7	-0.30	0.71
4	10.16	5.08	10.16	5.85	4.74	45.51	38.01	0.047	3.4×10^{-3}	3.7×10^4	0.0227	5.8×10^{-3}	1.35	5.5	-1.35	0.49
5	10.16	10.16	5.08	5.85	4.74	45.51	38.01	0.047	3.4×10^{-3}	3.7×10^4	0.0227	5.8×10^{-3}	1.35	8.5	-1.50	1.0
6	10.16	10.16	10.16	5.85	4.74	45.51	38.01	0.047	3.4×10^{-3}	3.7×10^4	0.0227	5.8×10^{-3}	1.30	8.6	-1.0	1.0

Boundary layer height = 50.8 cm

$\bar{U}_{z_1}$ = 1.68 m/sec, $\bar{T}_{z_1}$ = 21.1°C at reference height of 0.25 cm

Average mean velocity profile power-law index, n = 0.16

λ = 1.0, γ = 1.0

FIGURES

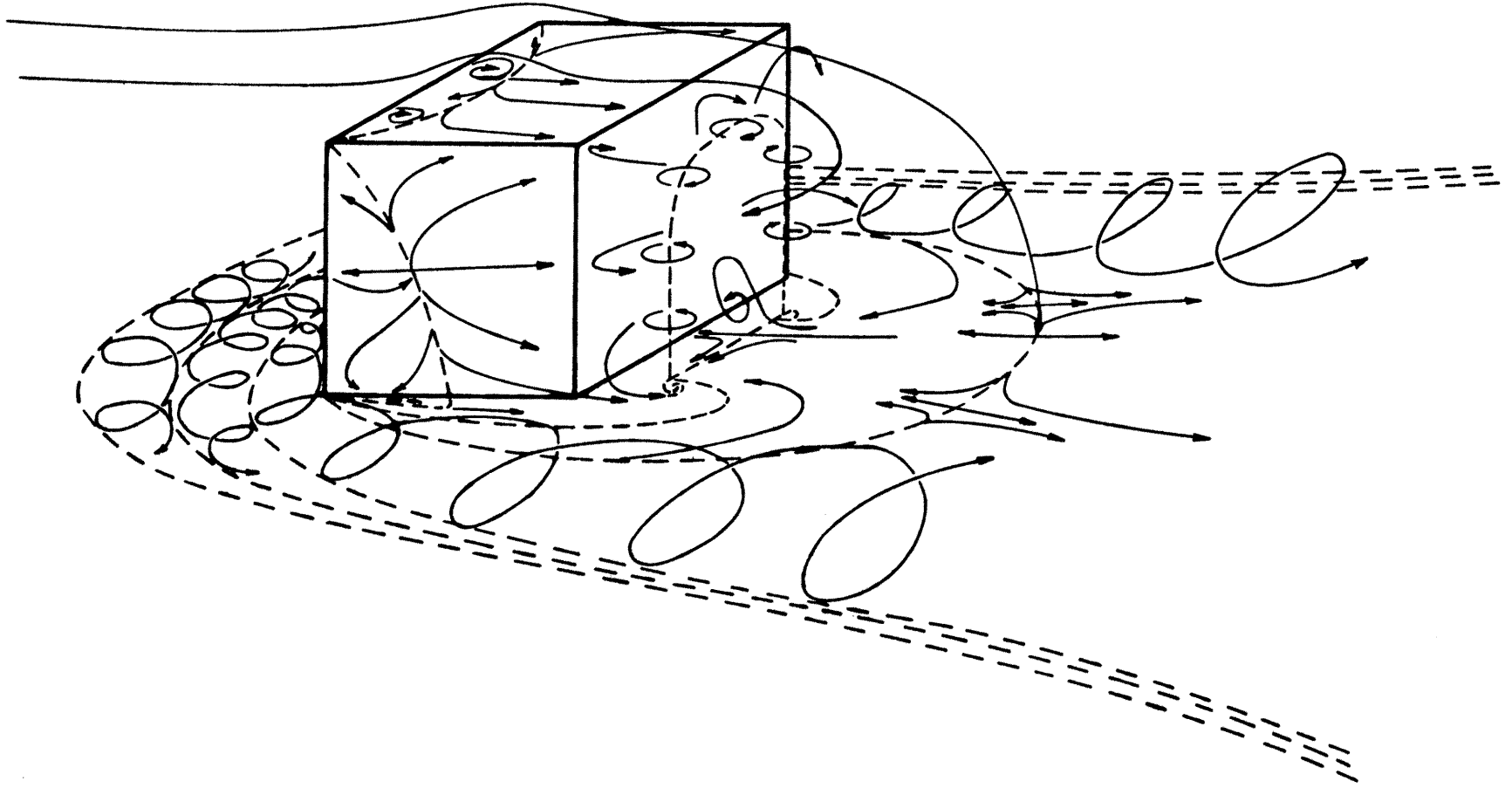

Figure 1. Flow pattern around a rectangular block with reattachment of the free shear layer (from wind tunnel measurements in the wakes of structures by Woo, H. G. C., Peterka, J. A., and Cermak, J. E., 1976 [5]).

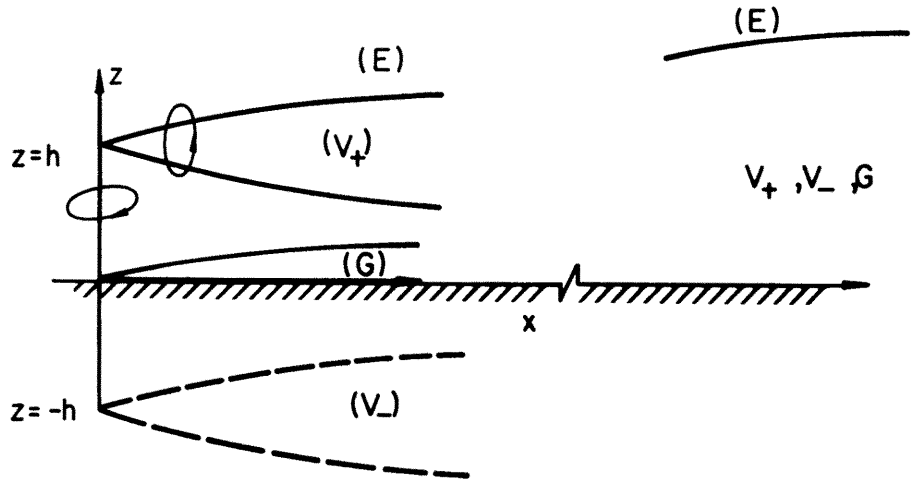

(a) Side View

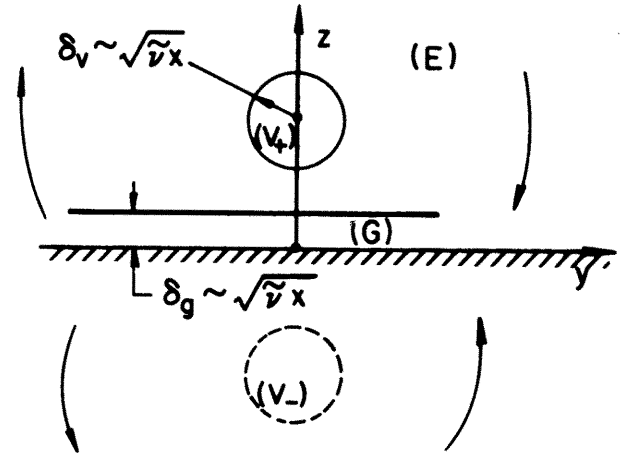

(b) Looking Upwind $h \gg \sqrt{\tilde{\nu} x}$

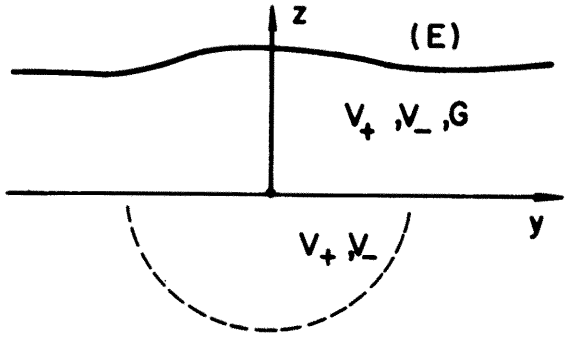

(c) Looking Upwind , $h \ll \sqrt{\tilde{\nu} x}$

Figure 2. Schematics of the regions of influence of the vortex core and the vortex-induced boundary layer (from the vortex wake theory of Hunt, 1975 [27]).

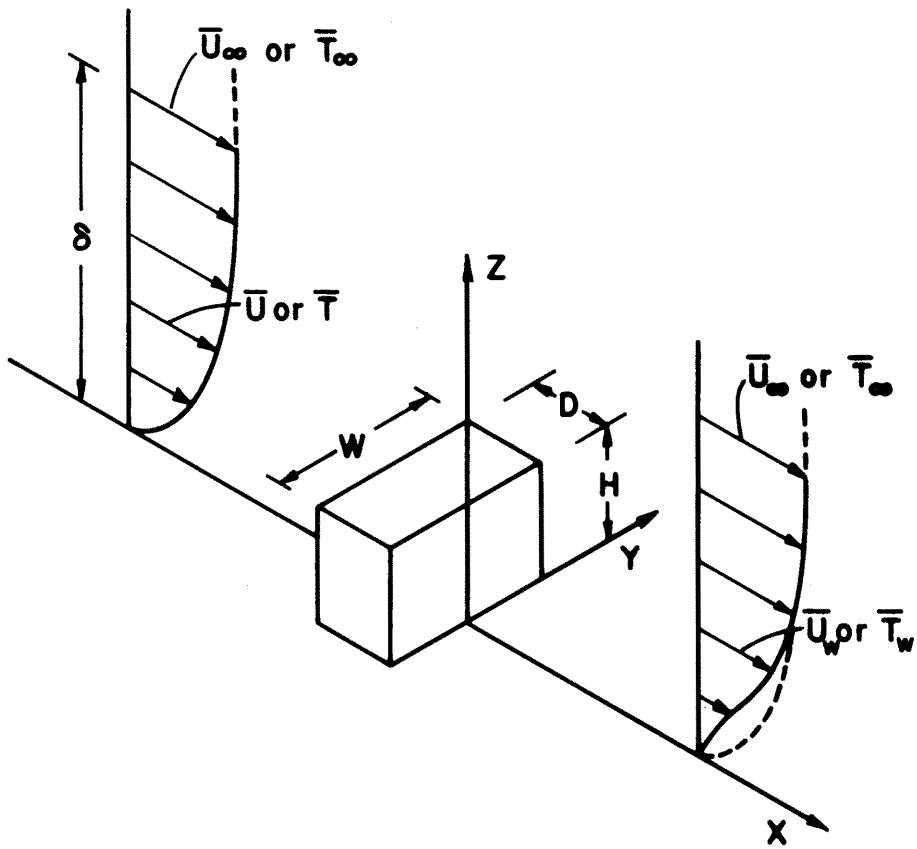

Figure 3. Experimental configuration showing the coordinate system and definitions of symbols.

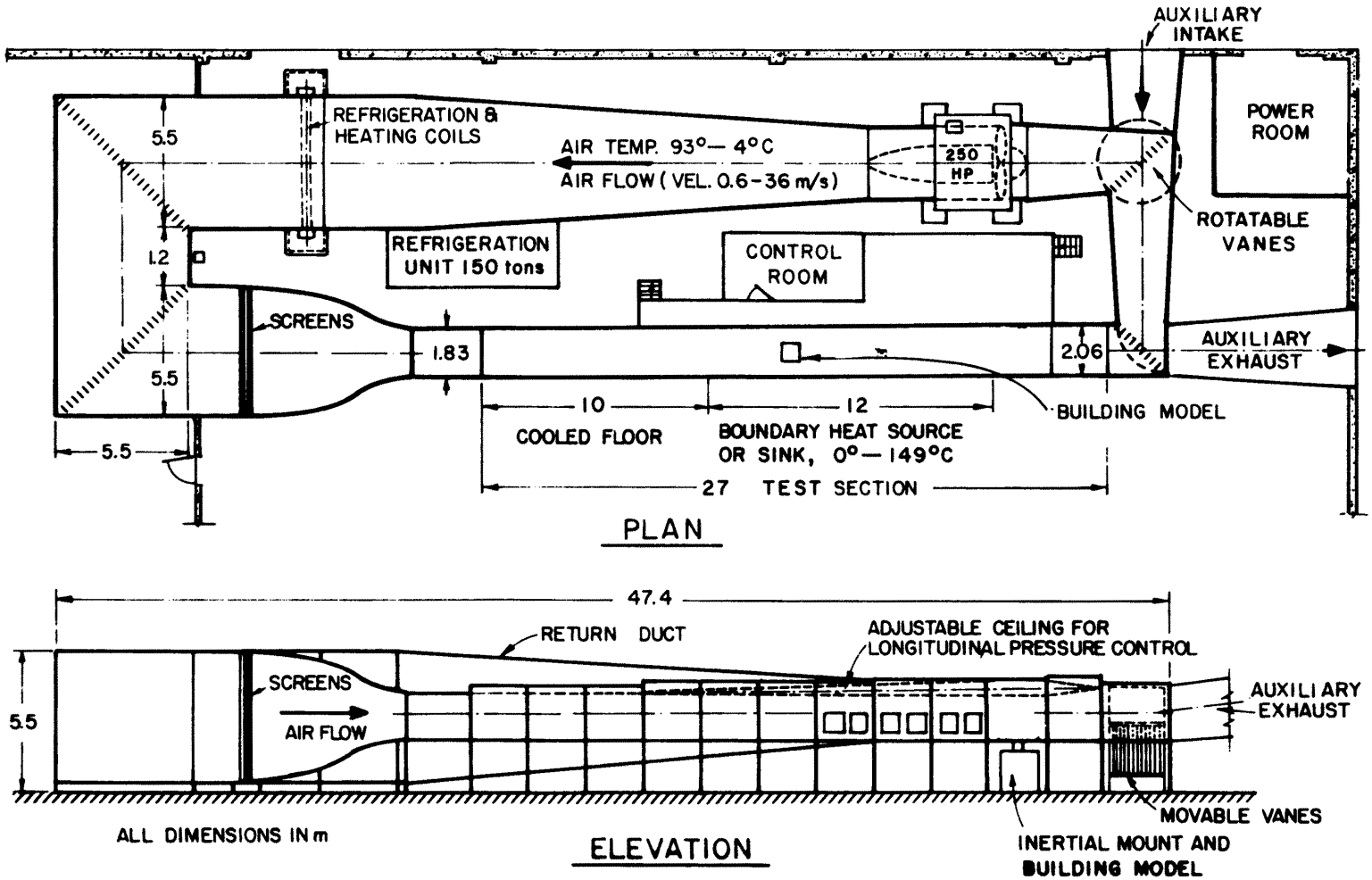

Figure 4. Meteorological wind tunnel, Fluid Dynamics and Diffusion Laboratory, Colorado State University.

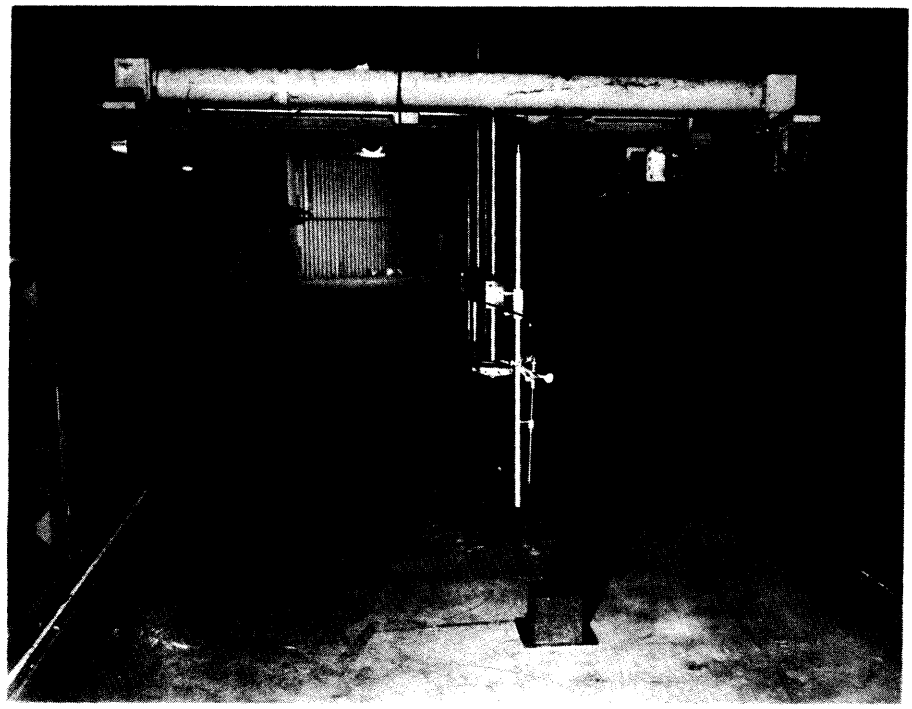

Figure 5. Probe traversing mechanism.

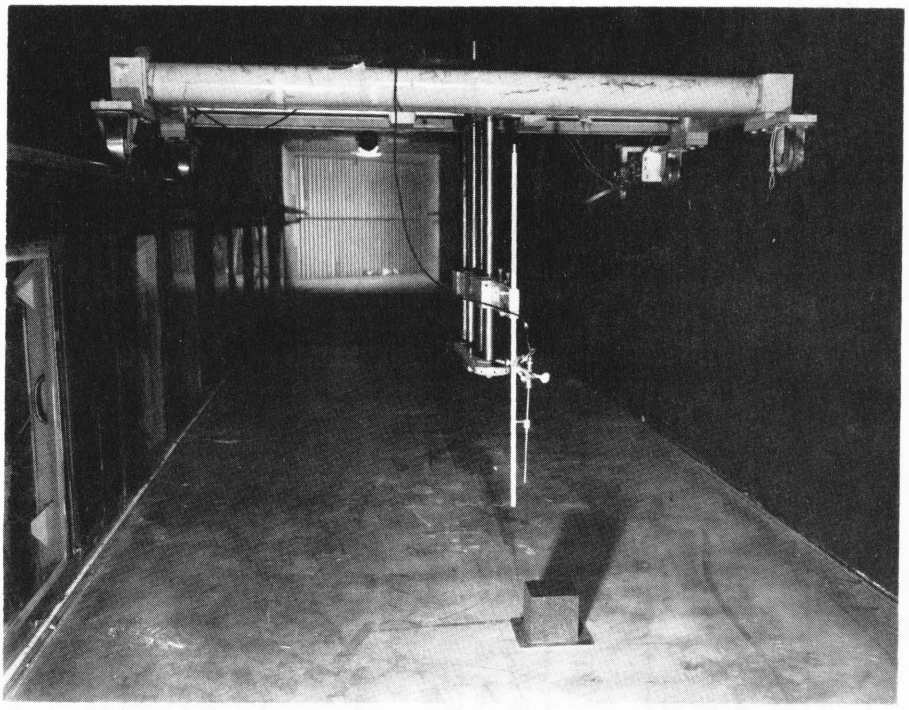

Figure 5. Probe traversing mechanism.

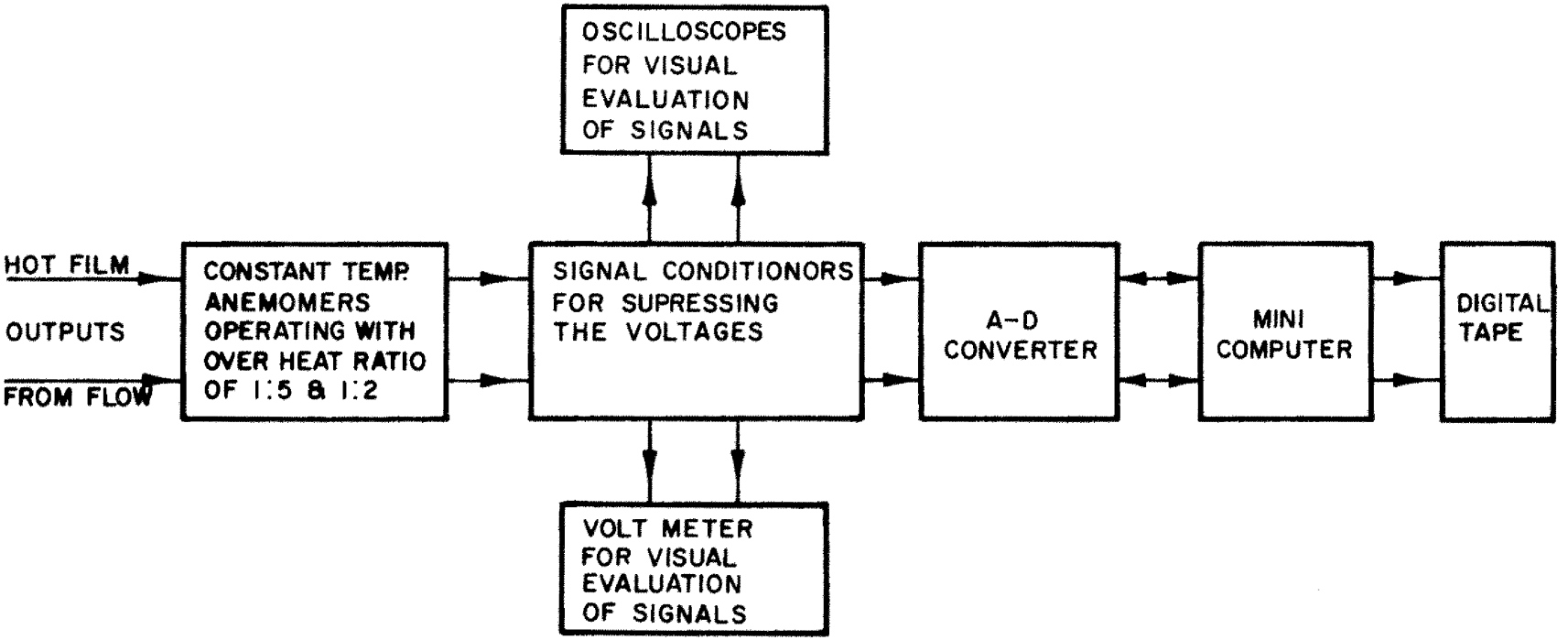

Figure 6. Schematic of data-acquisition system.

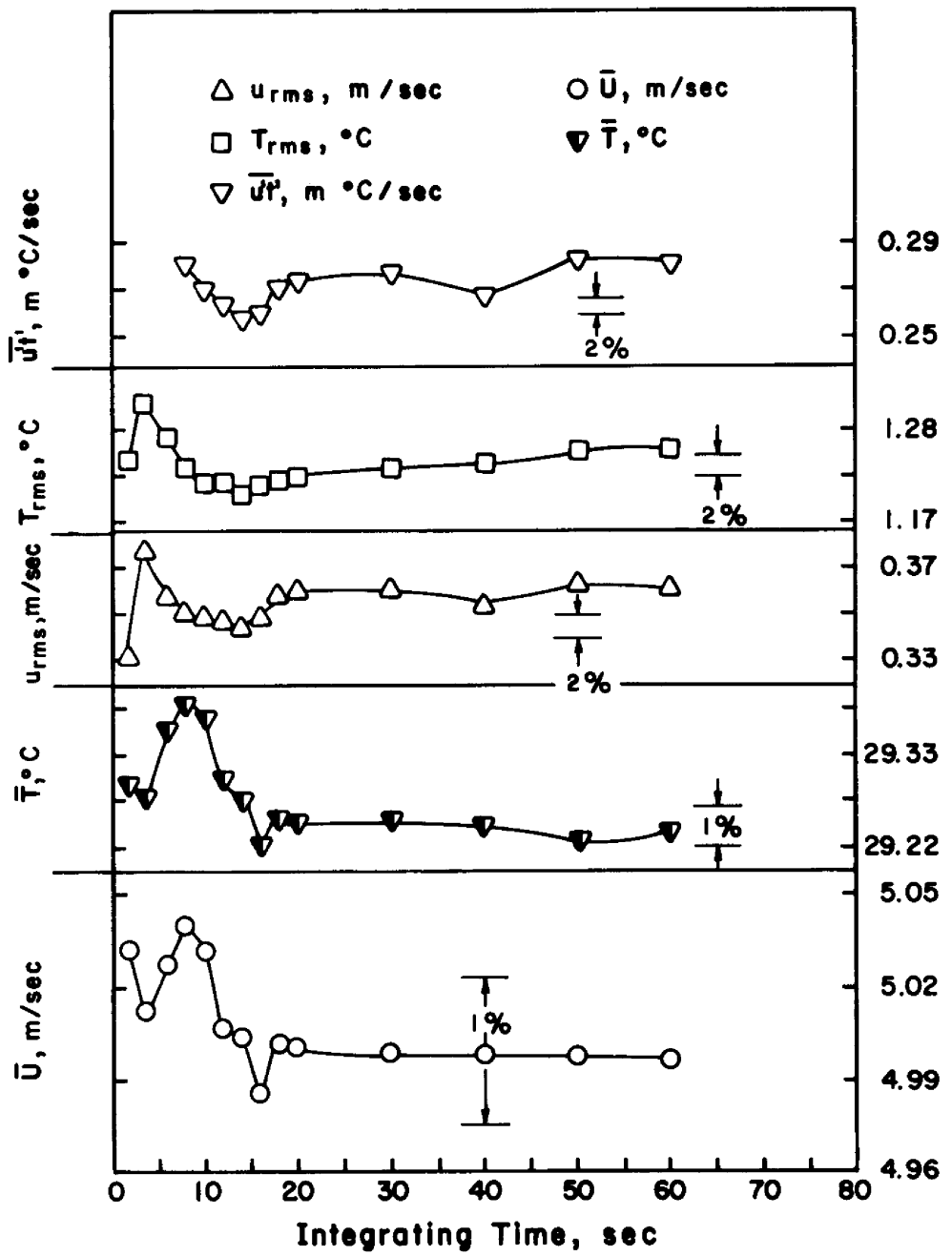

Figure 7. Data sampling time verification.

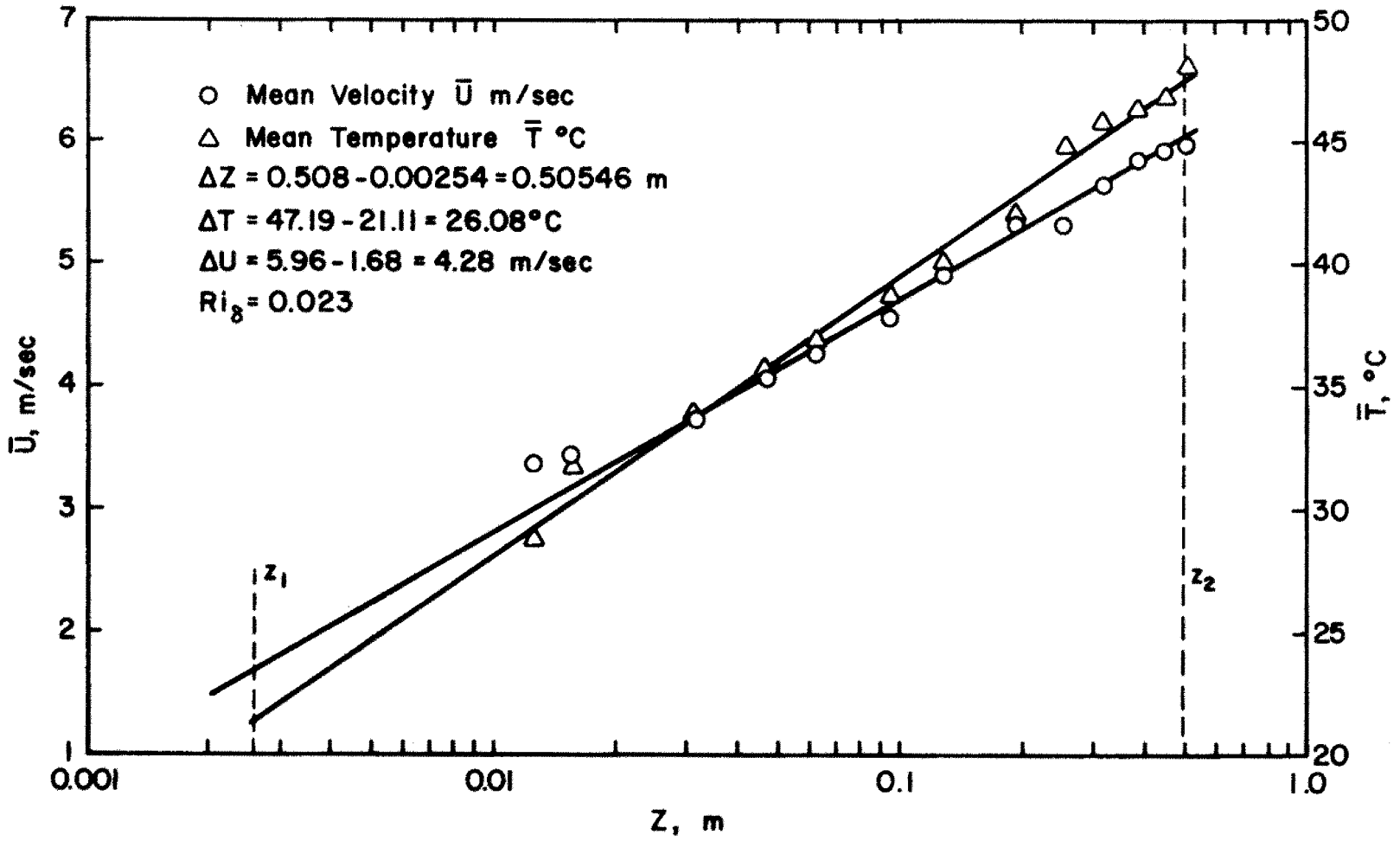

Figure 8. Determination of mean velocity and temperature at z_1 and z_2.

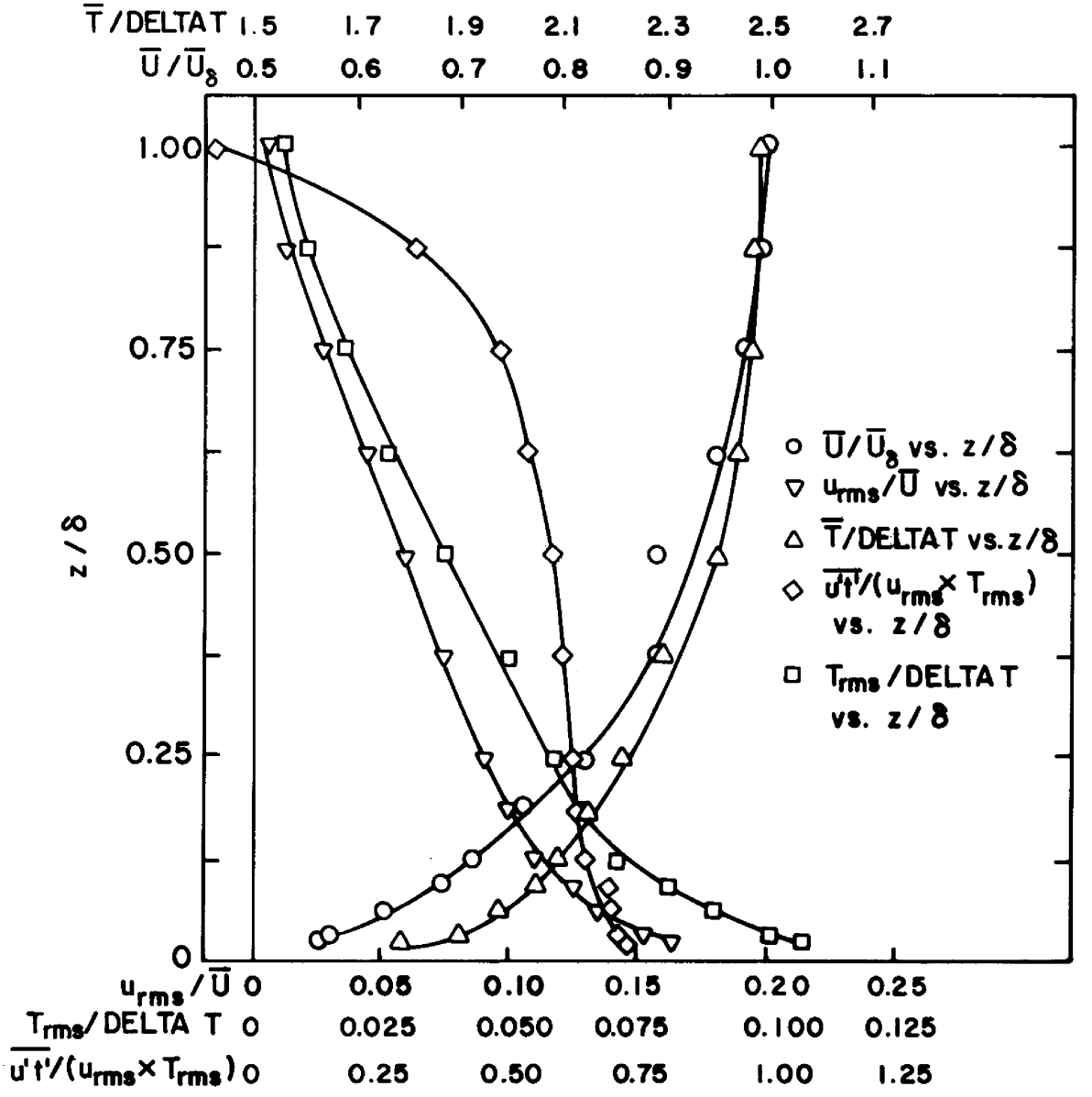

Figure 9. Approach flow characteristics.

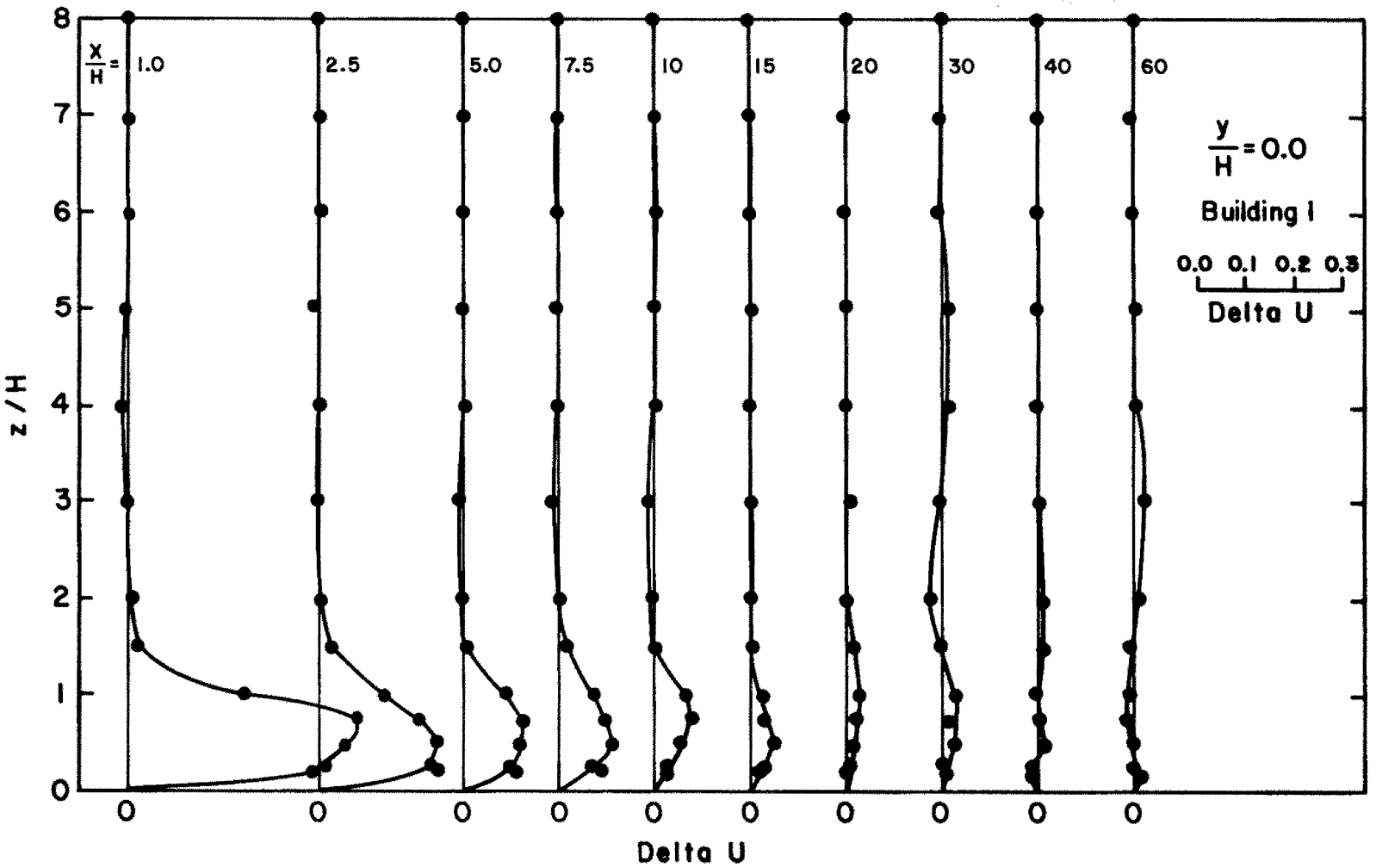

Figure 10. Vertical profiles of mean velocity defect behind building 1.

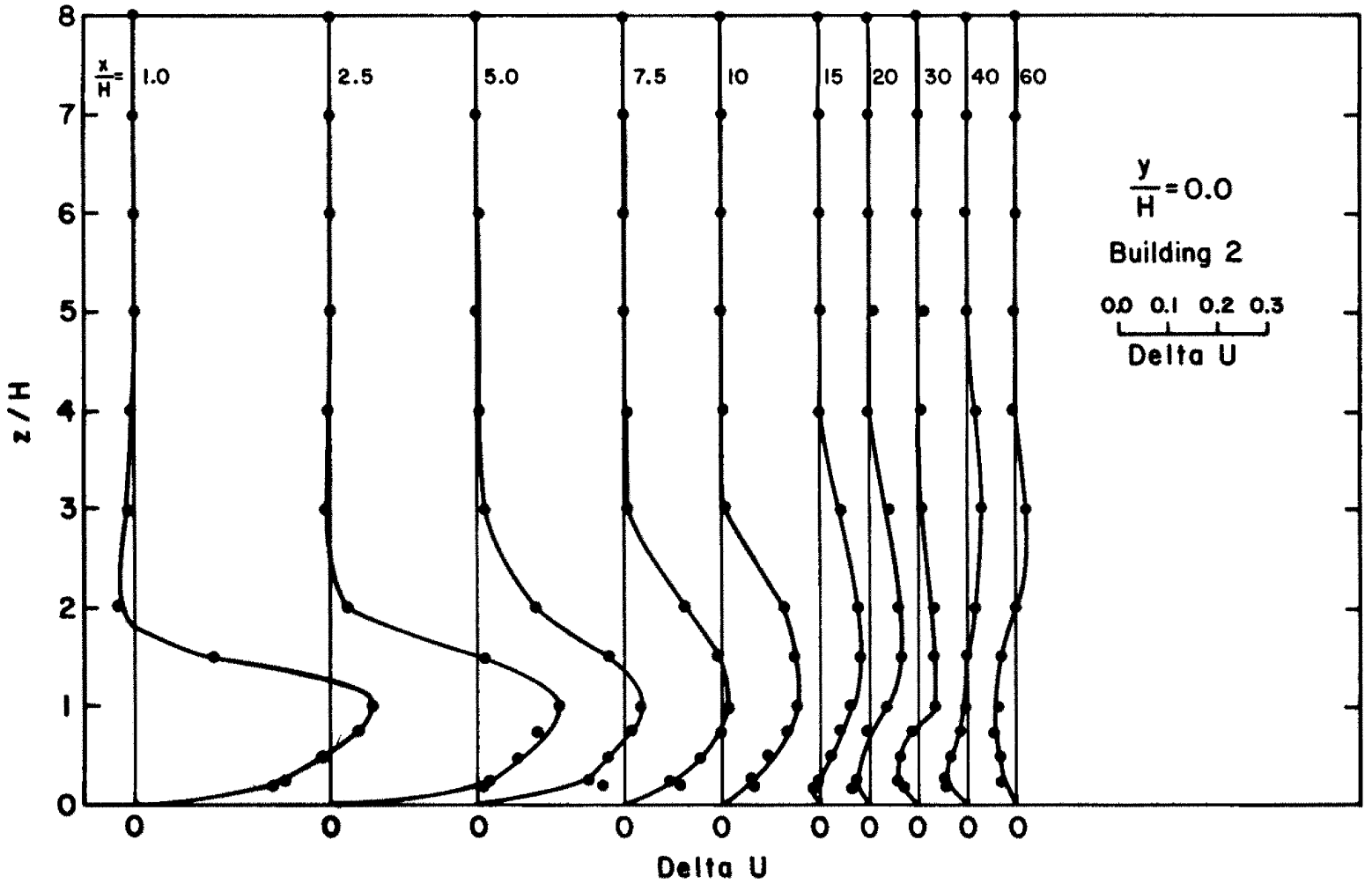

Figure 11. Vertical profiles of mean velocity defect behind building 2.

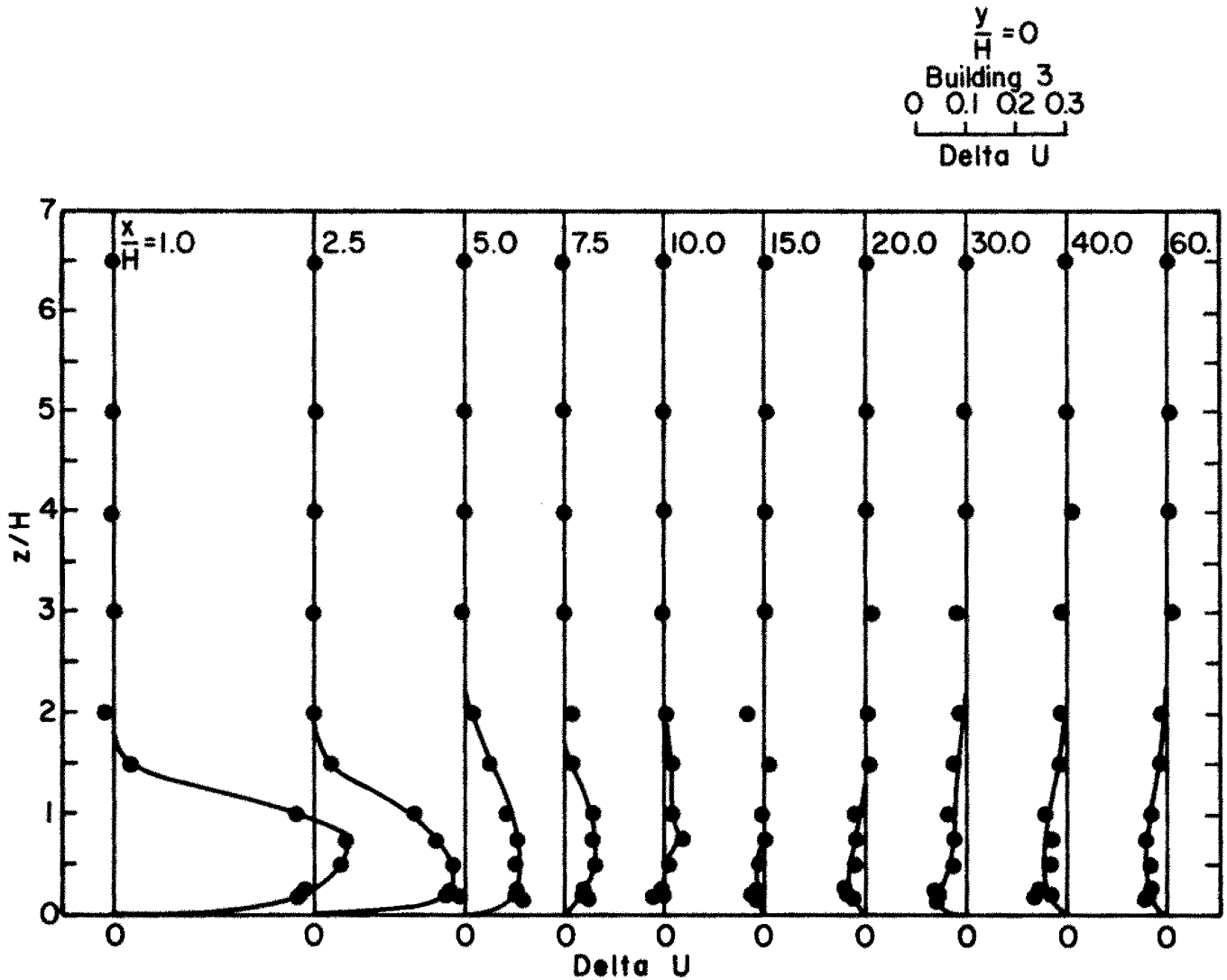

Figure 12. Vertical profiles of mean velocity defect behind building 3.

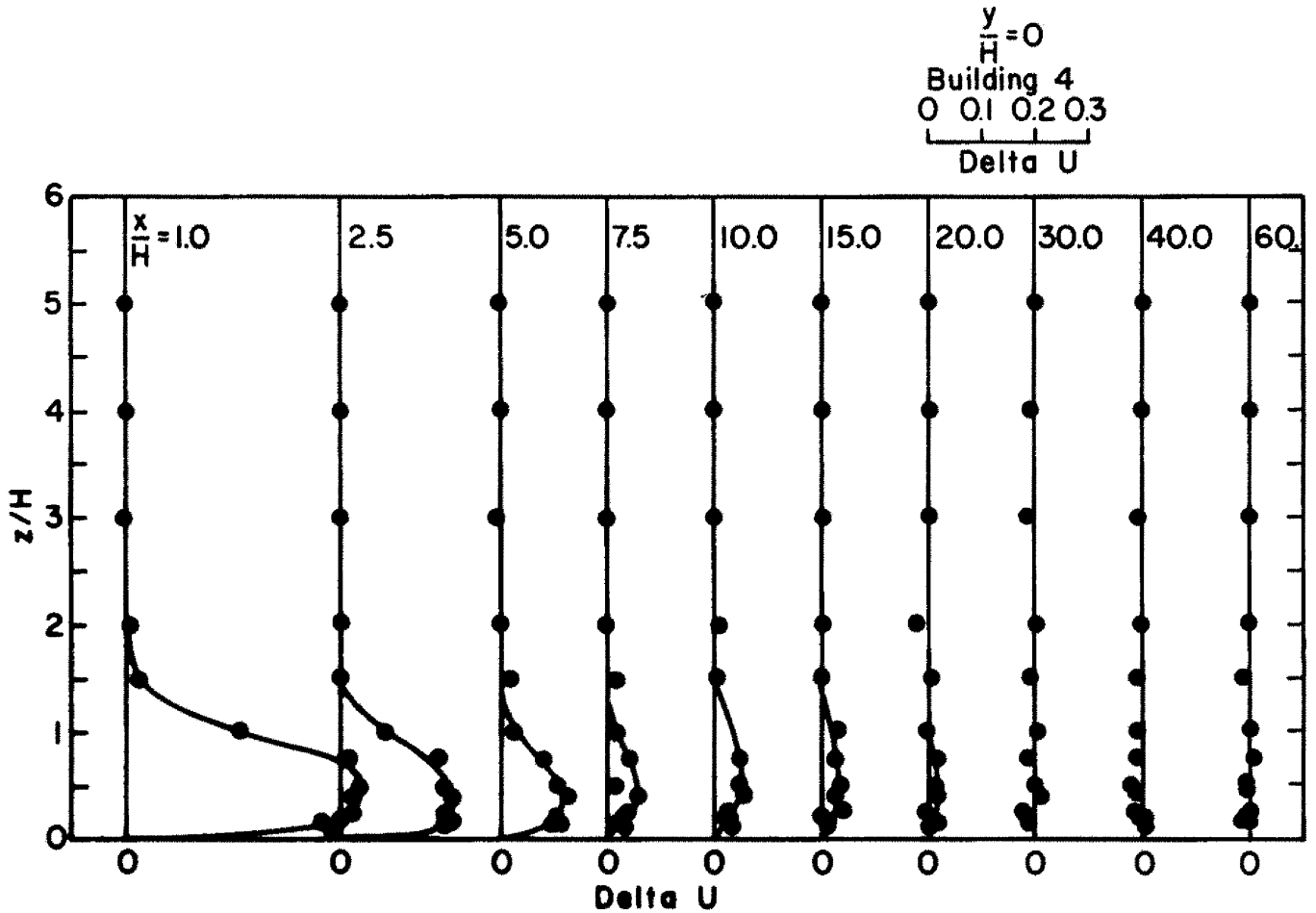

Figure 13. Vertical profiles of mean velocity defect behind building 4.

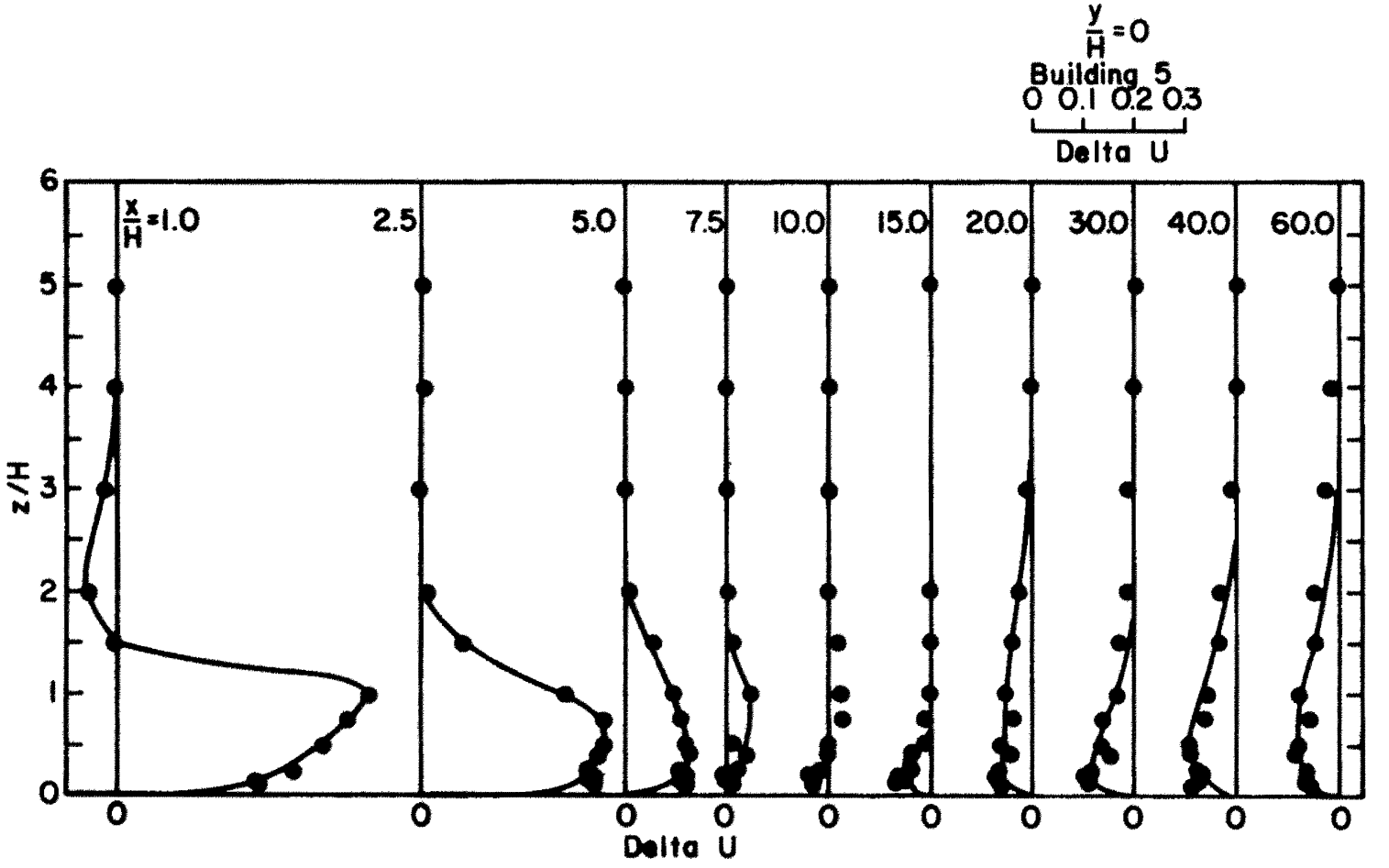

Figure 14. Vertical profiles of mean velocity defect behind building 5.

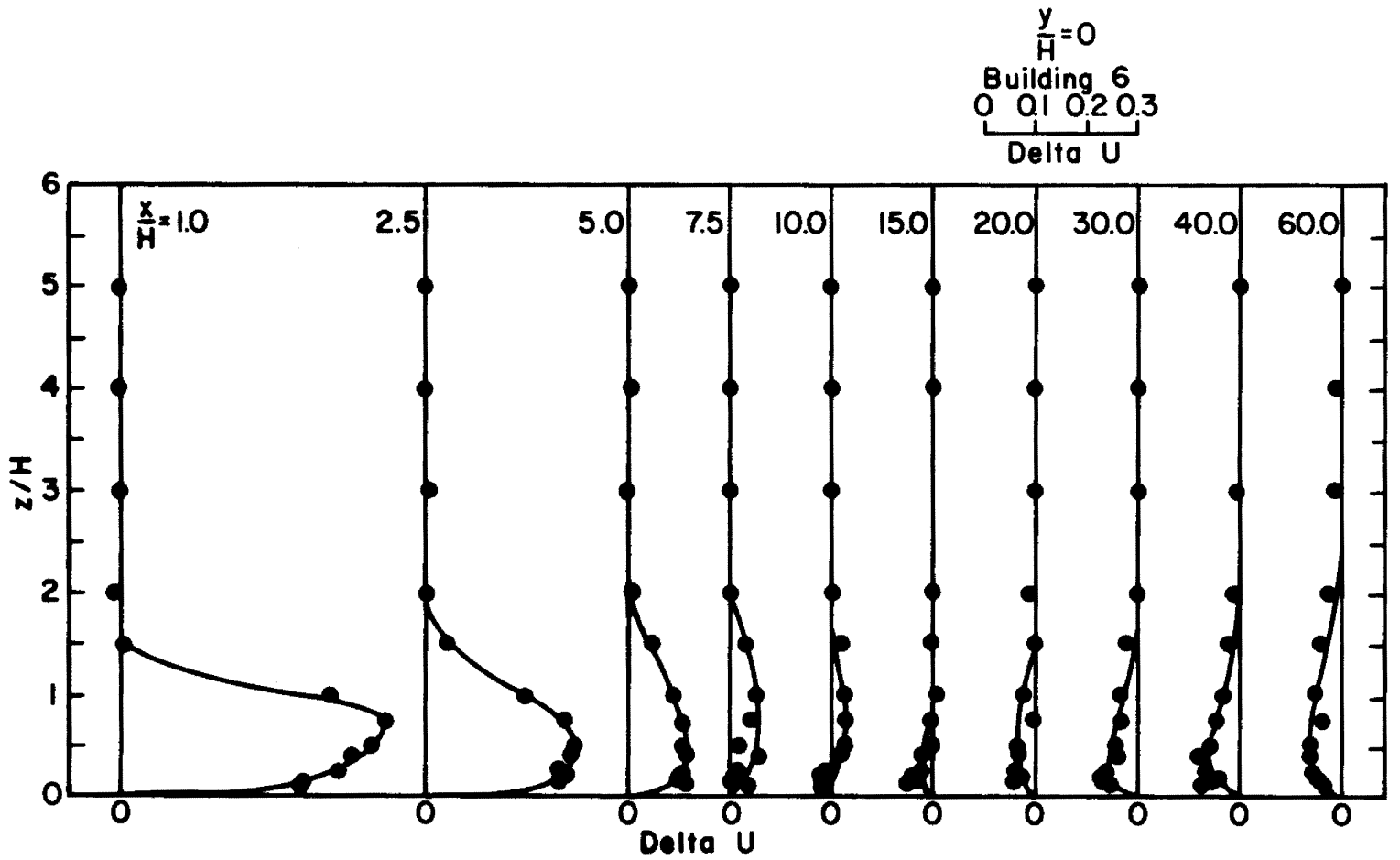

Figure 15. Vertical profiles of mean velocity defect behind building 6.

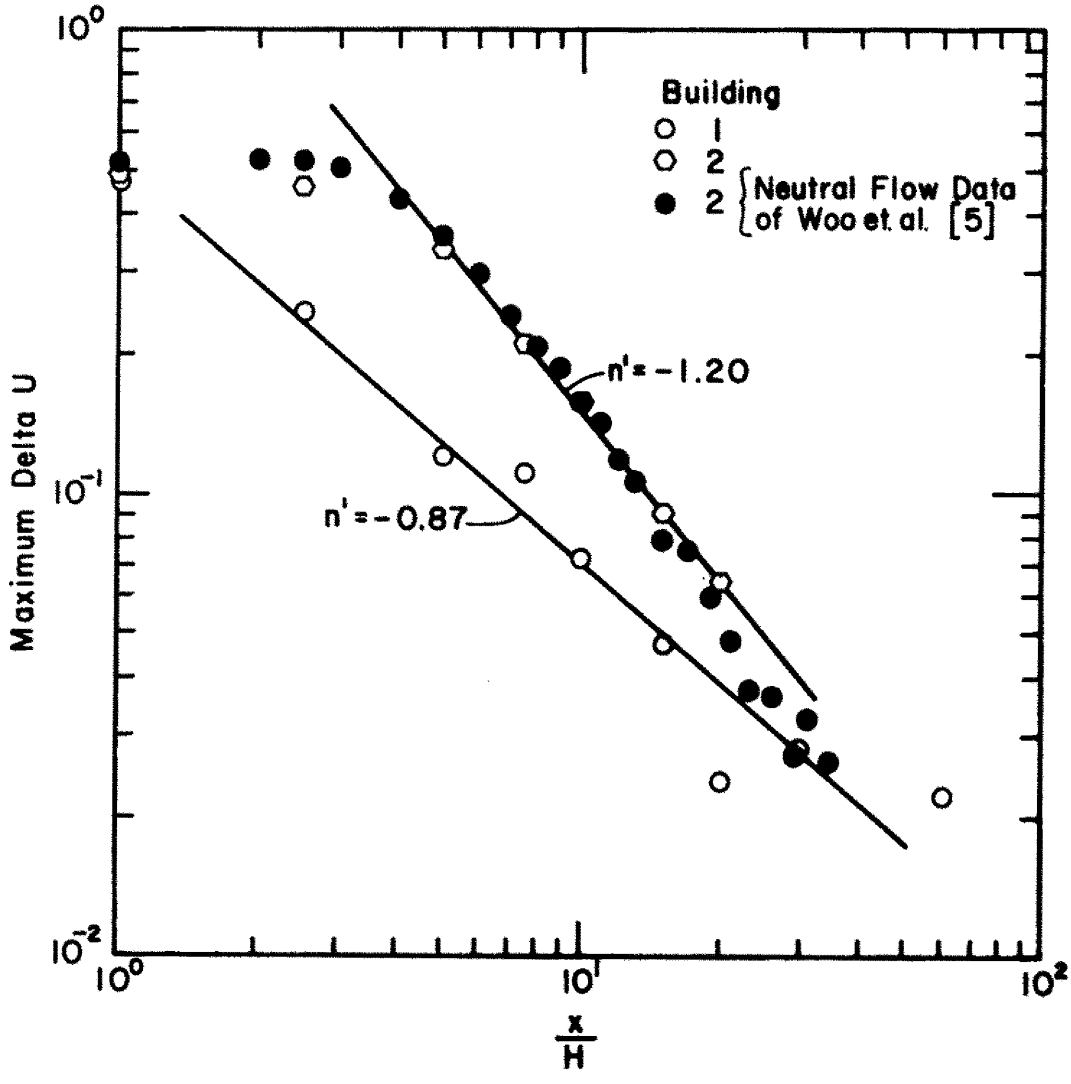

Figure 16. Comparison of decay rates of mean velocity defect in the wakes of buildings 1 and 2 with Woo et al., [5].

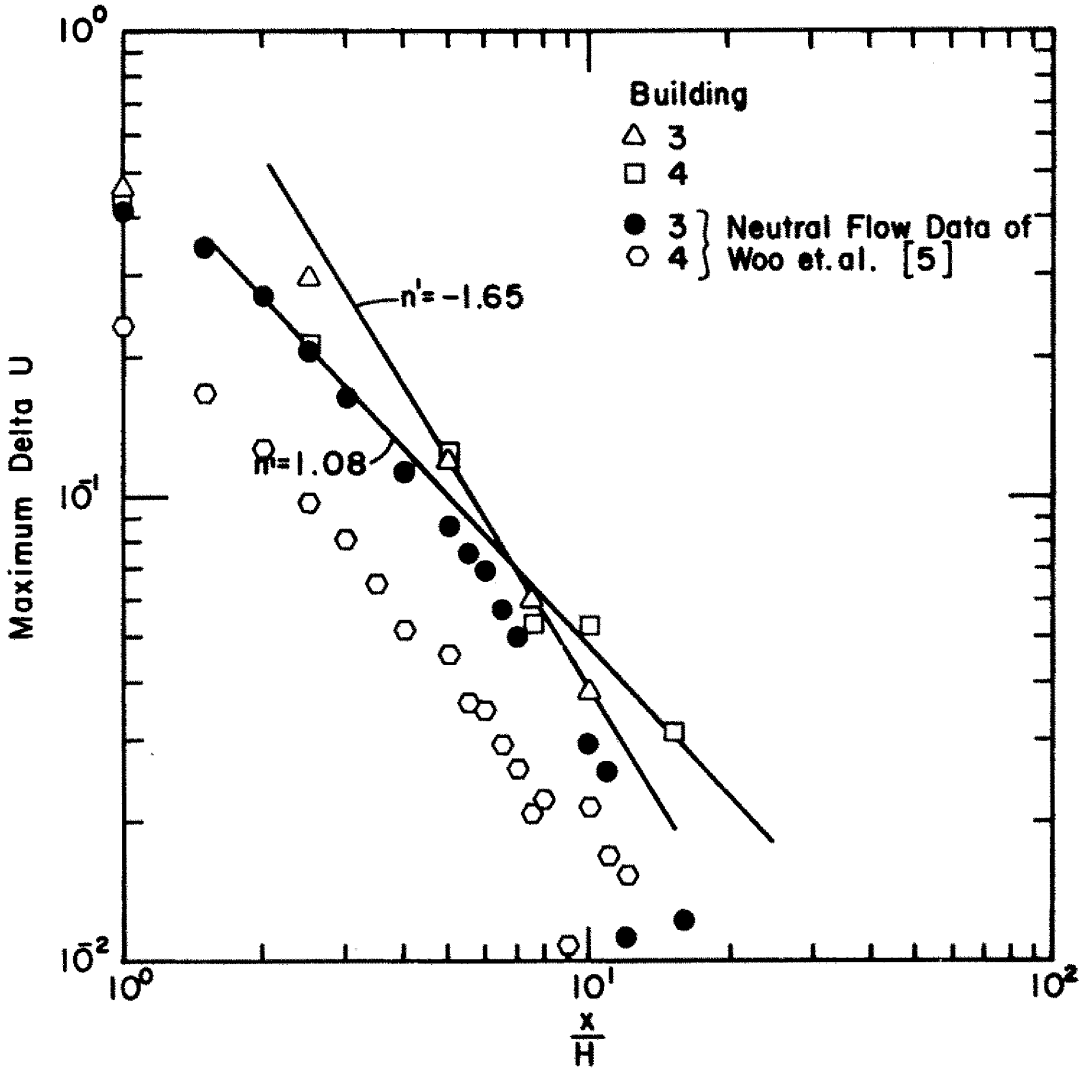

Figure 17. Comparison of decay rates of mean velocity defect in the wakes of buildings 3 and 4 with Woo et al., [5].

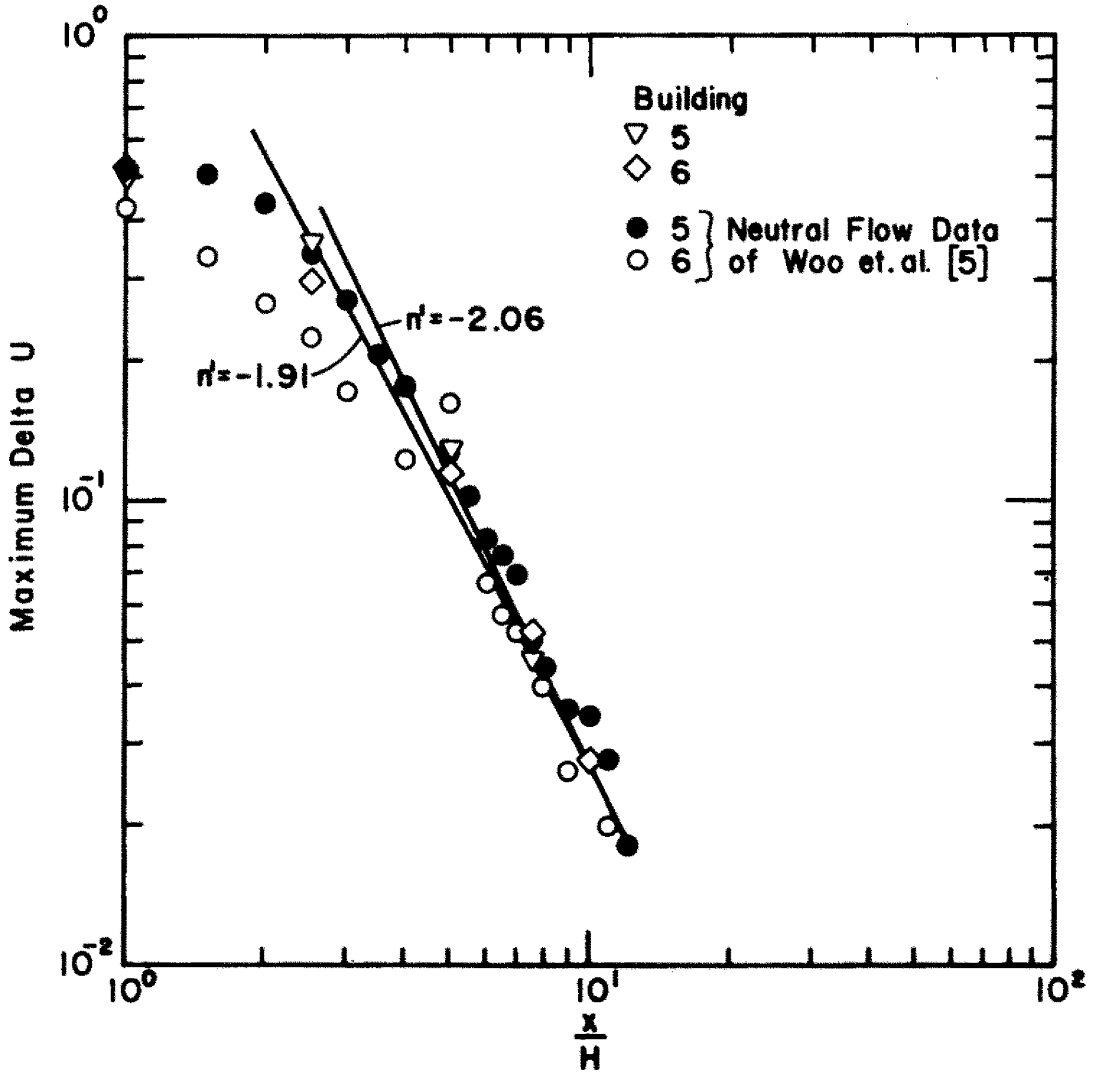

Figure 18. Comparison of decay rates of mean velocity defect in the wakes of buildings 5 and 6 with Woo et al., [5].

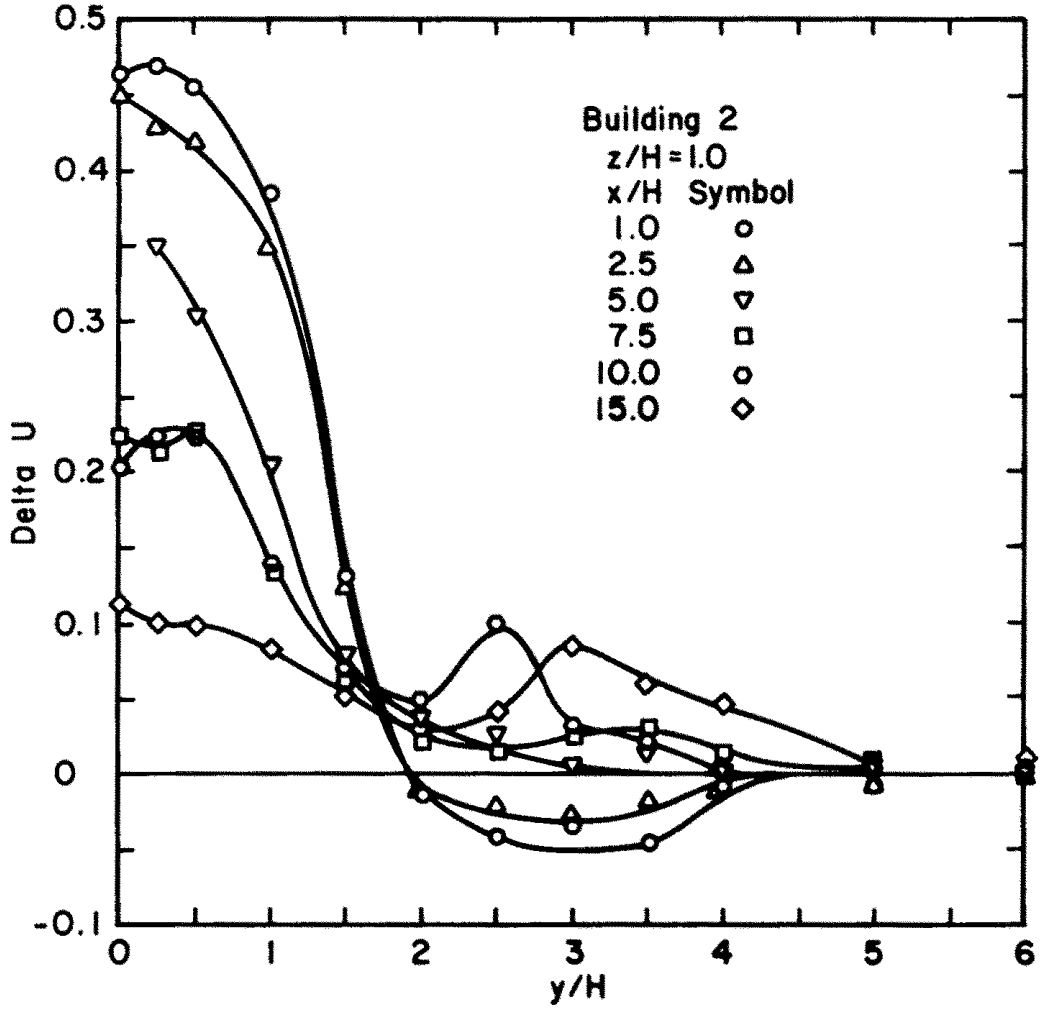

Figure 19. Horizontal profiles of mean velocity defect behind building 2.

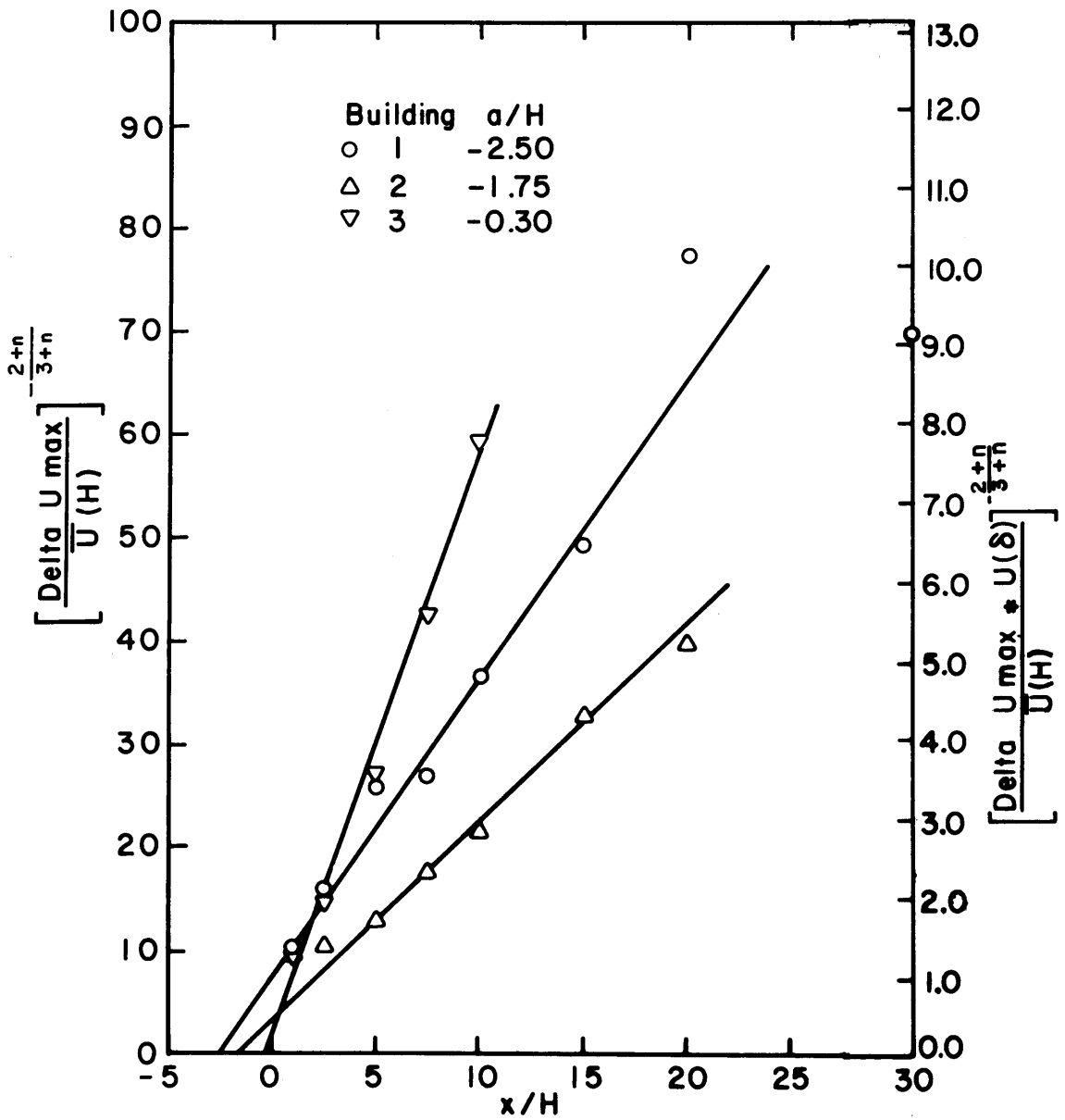

Figure 20. Determination of virtual origin for buildings 1, 2 and 3.

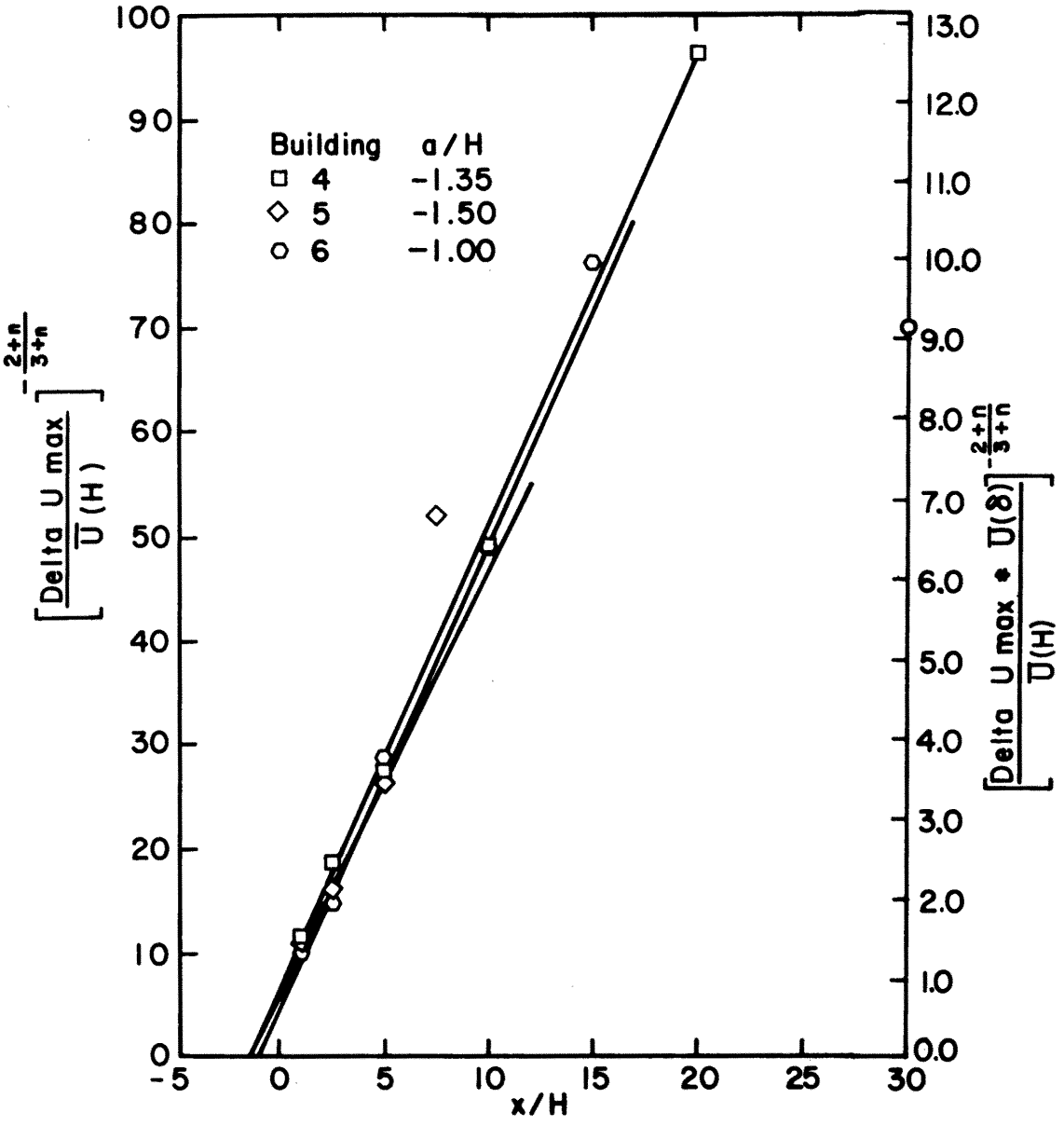

Figure 21. Determination of virtual origin for buildings 4, 5 and 6.

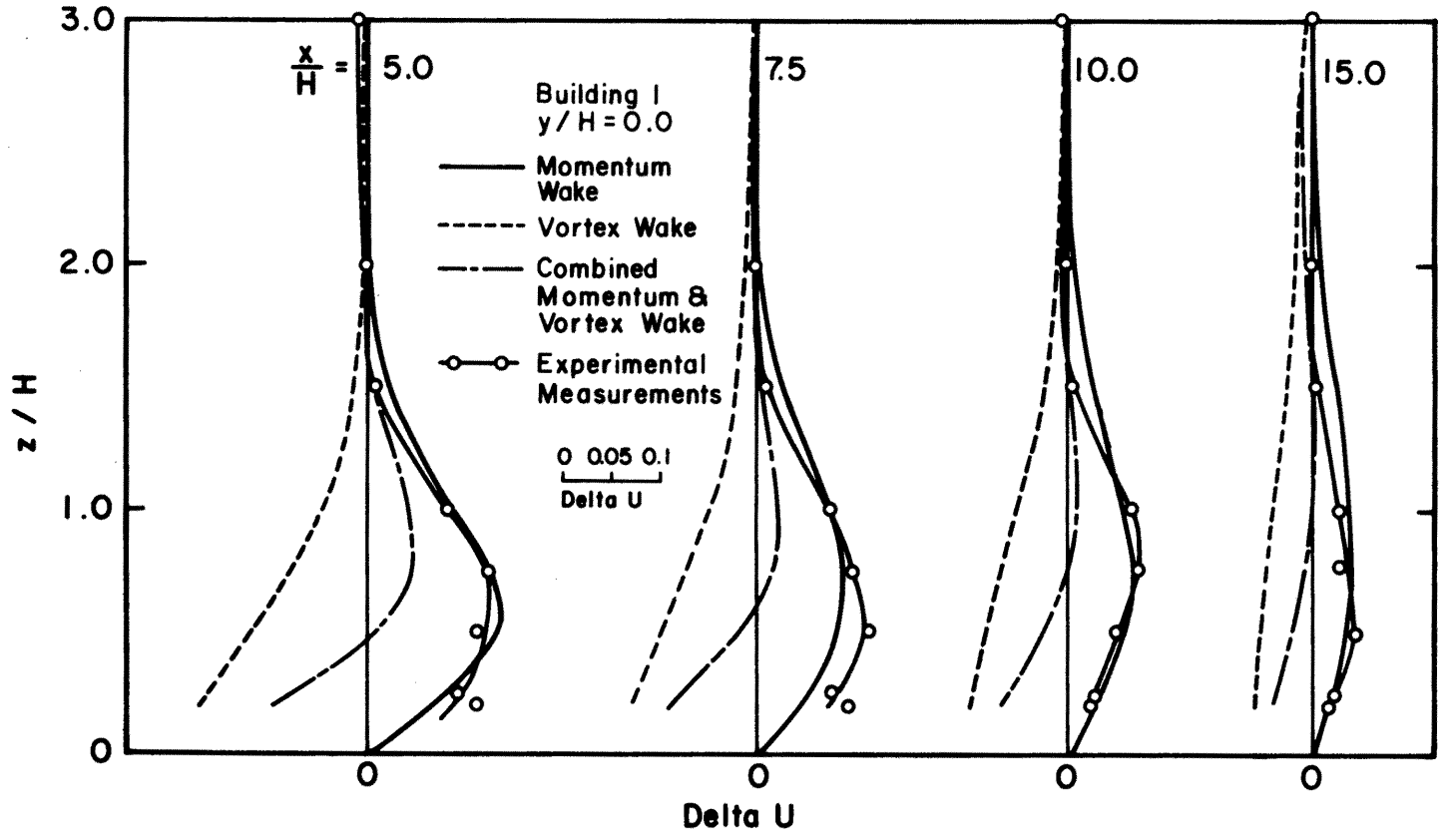

Figure 22. Comparison of the measured vertical profiles of velocity defect on the building 1 centerline with the momentum and vortex wake theory of Hunt.

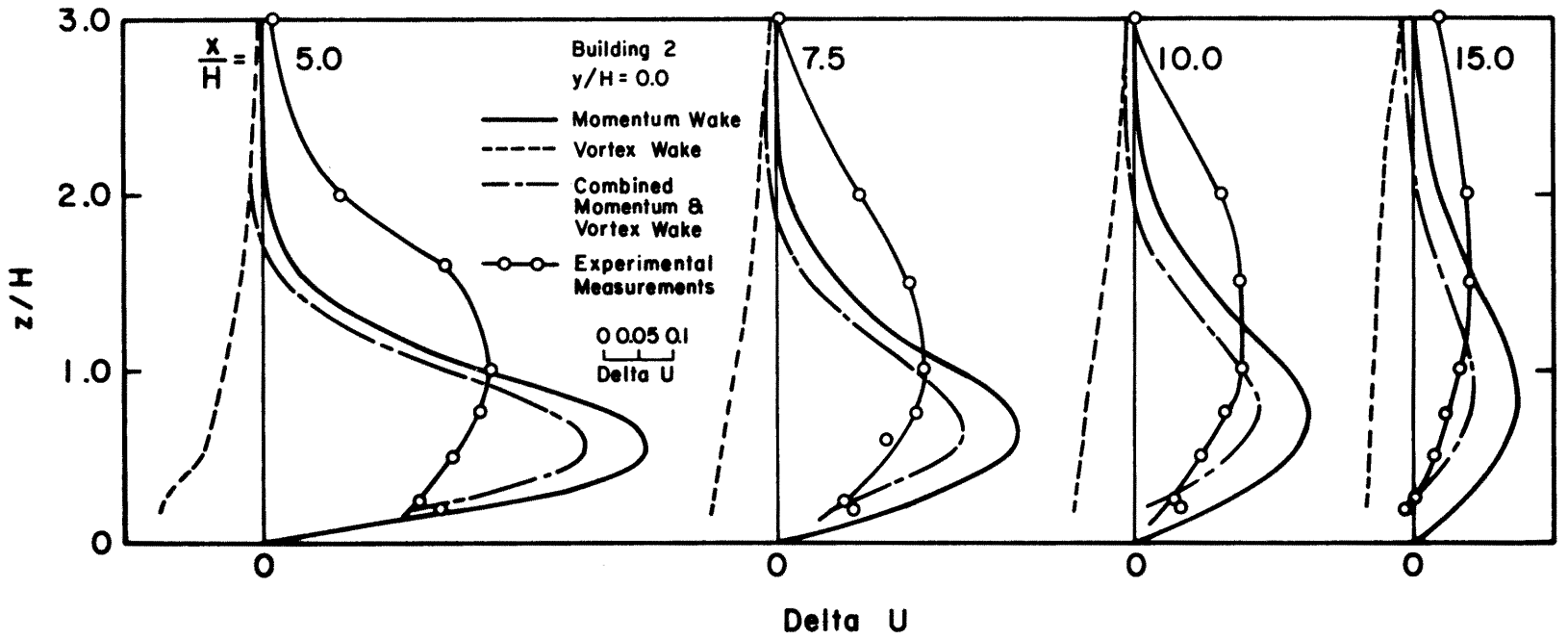

Figure 23. Comparison of the measured vertical profiles of velocity defect on the building 2 centerline with the momentum and vortex wake theory of Hunt.

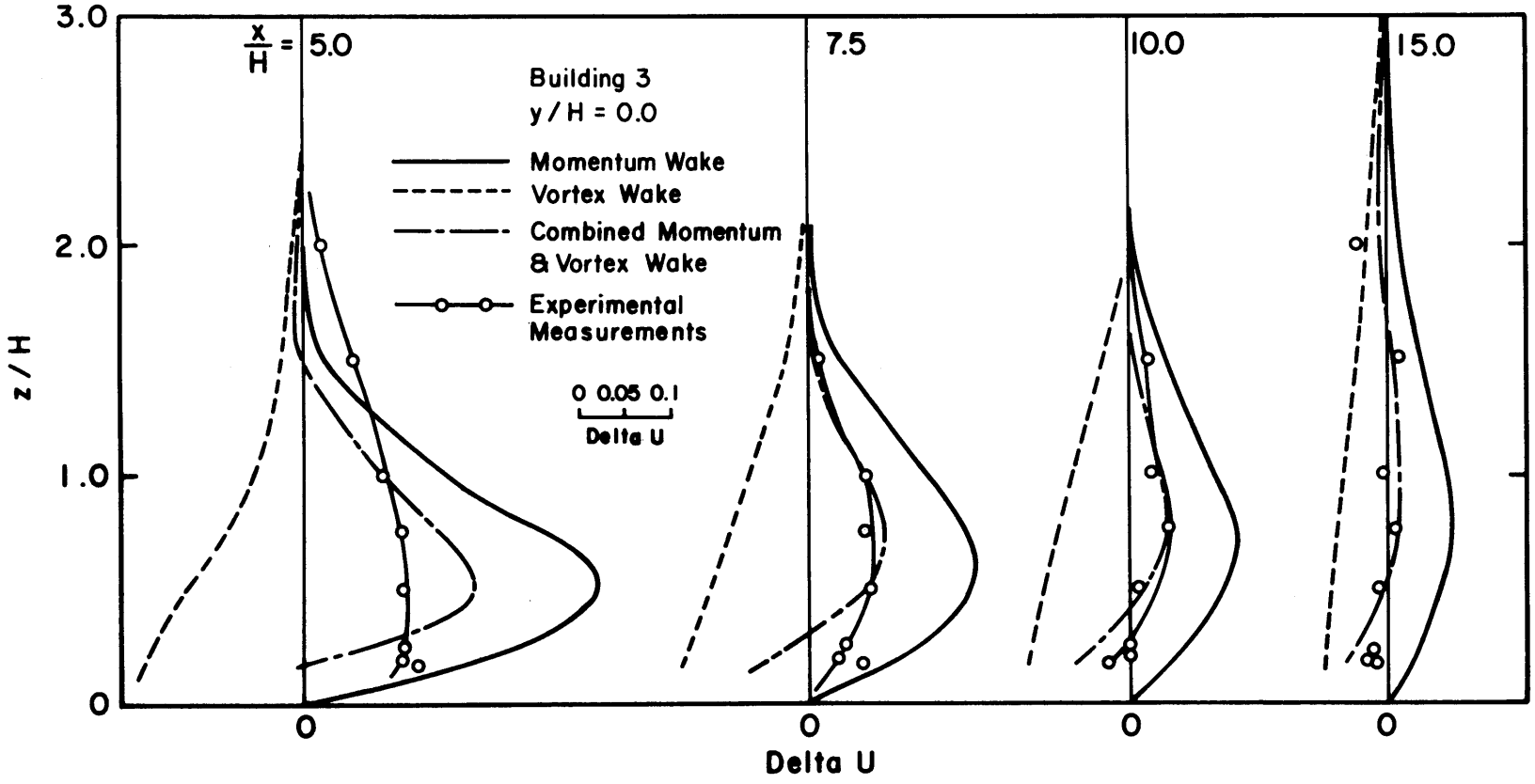

Figure 24. Comparison of the measured vertical profiles of velocity defect on the building 3 centerline with the momentum and vortex wake theory of Hunt.

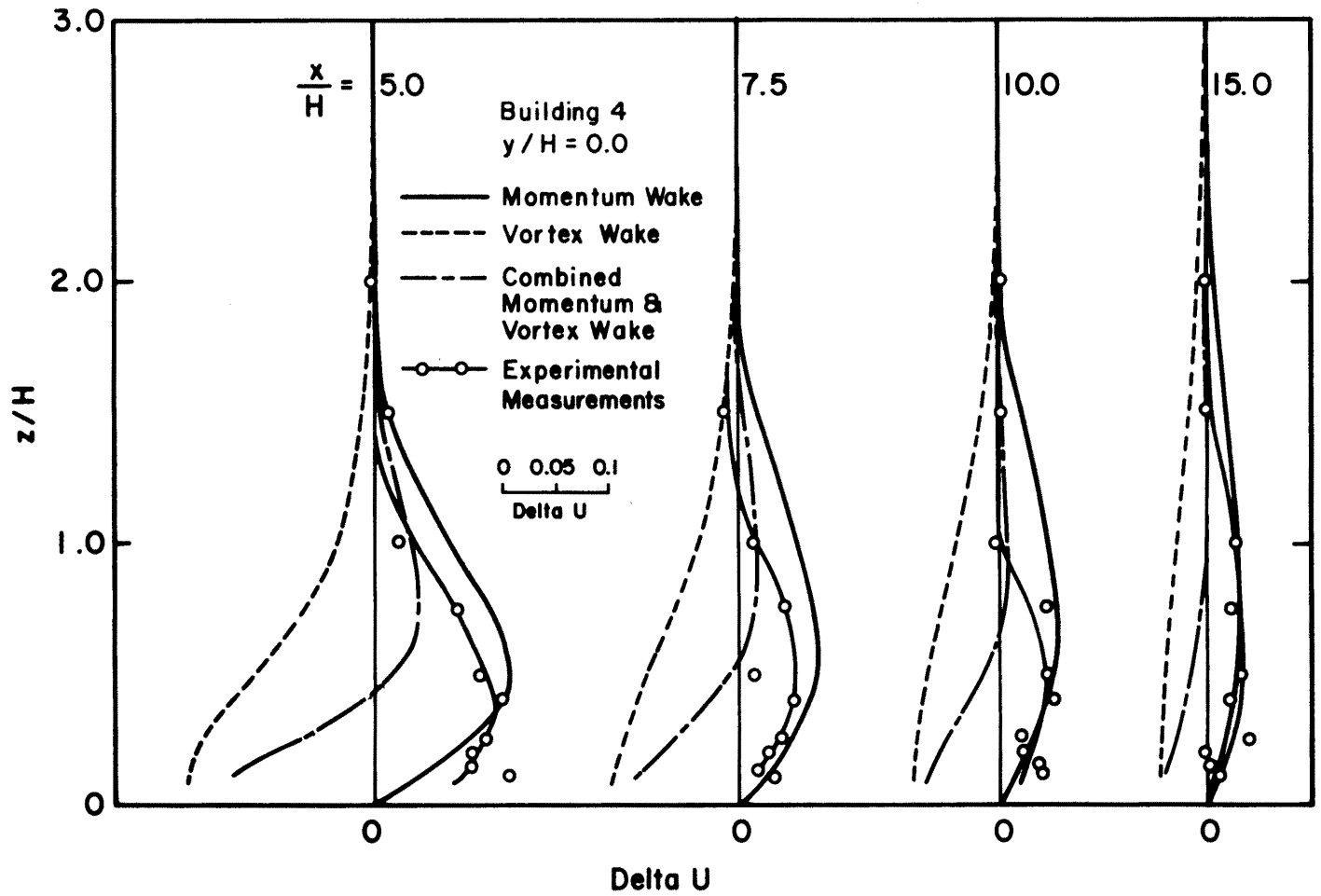

Figure 25. Comparison of the measured vertical profiles of velocity defect on the building 4 centerline with the momentum and vortex wake theory of Hunt.

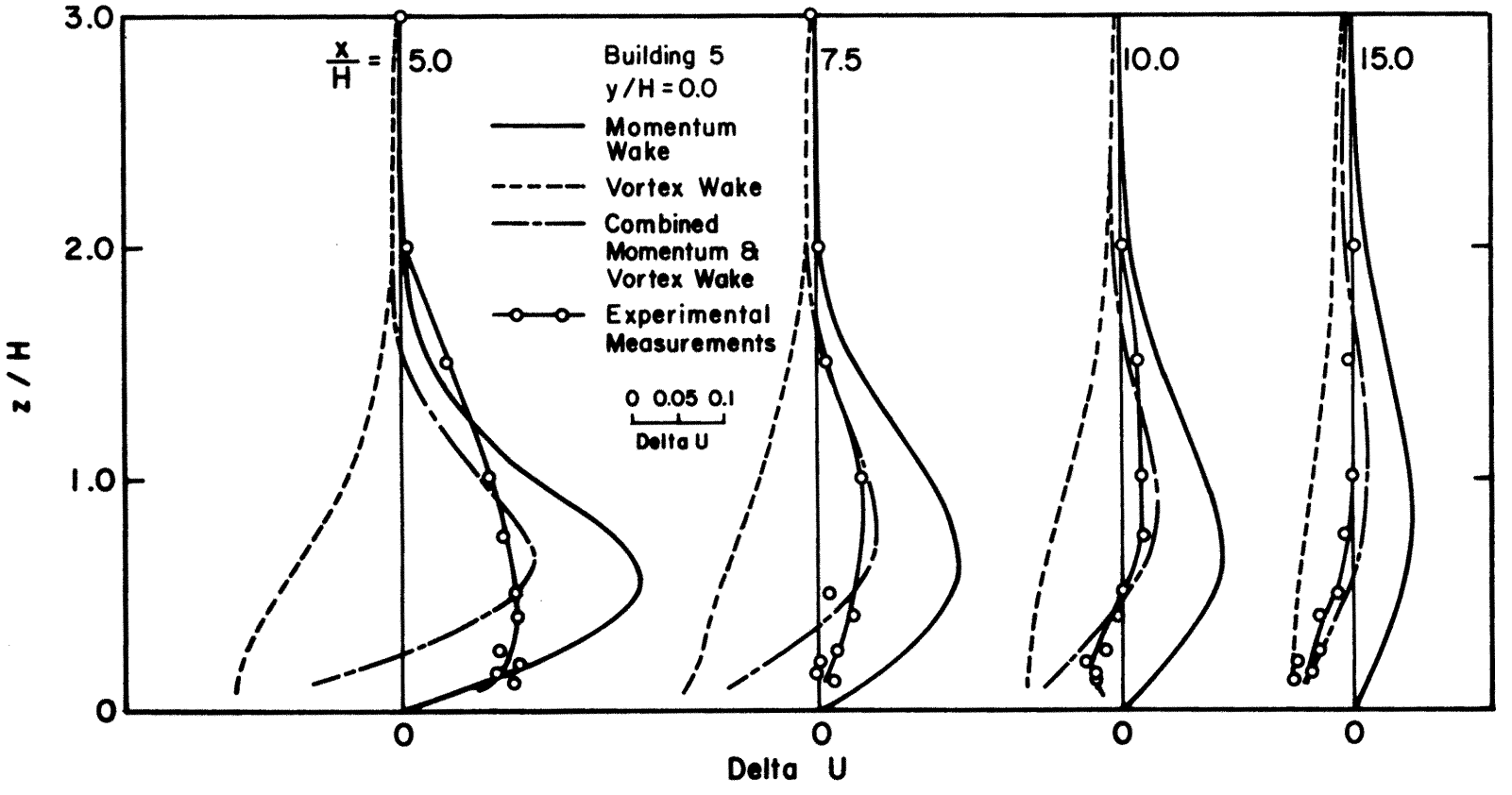

Figure 26. Comparison of the measured vertical profiles of velocity defect on the building 5 centerline with the momentum and vortex wake theory of Hunt.

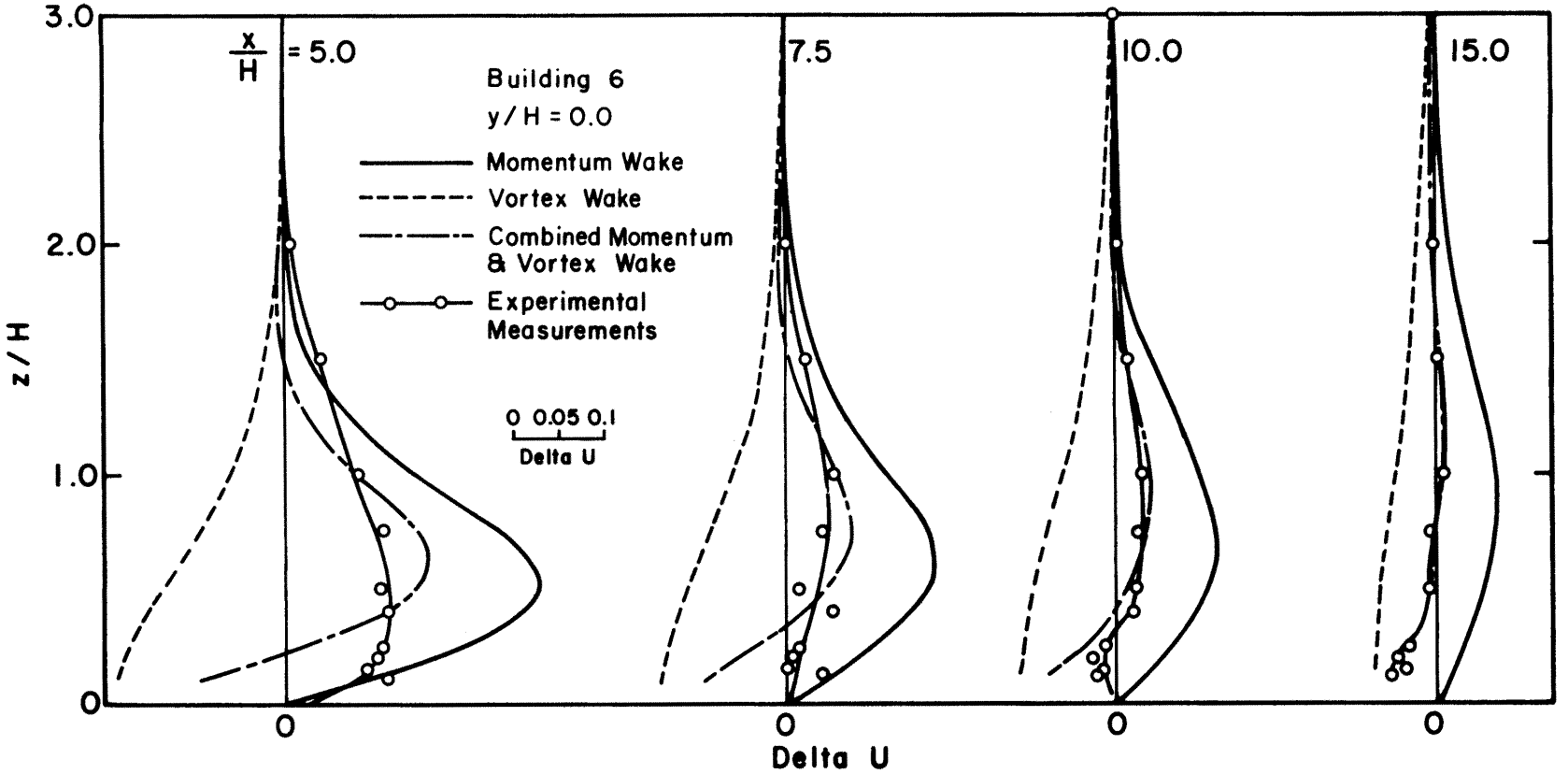

Figure 27. Comparison of the measured vertical profiles of velocity defect on building 6 centerline with the momentum and vortex wake theory of Hunt.

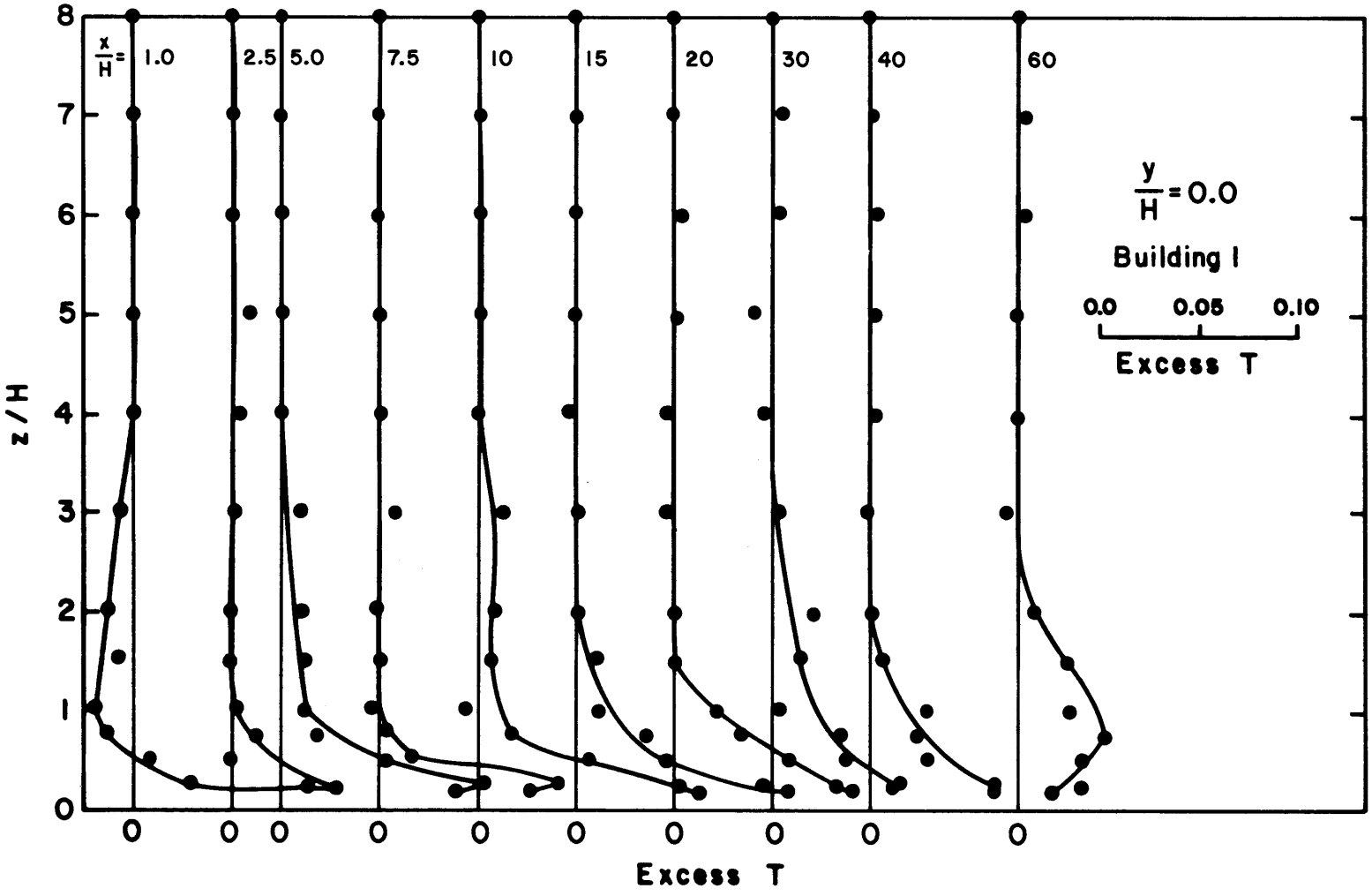

Figure 28. Vertical profiles of mean temperature excess behind building 1.

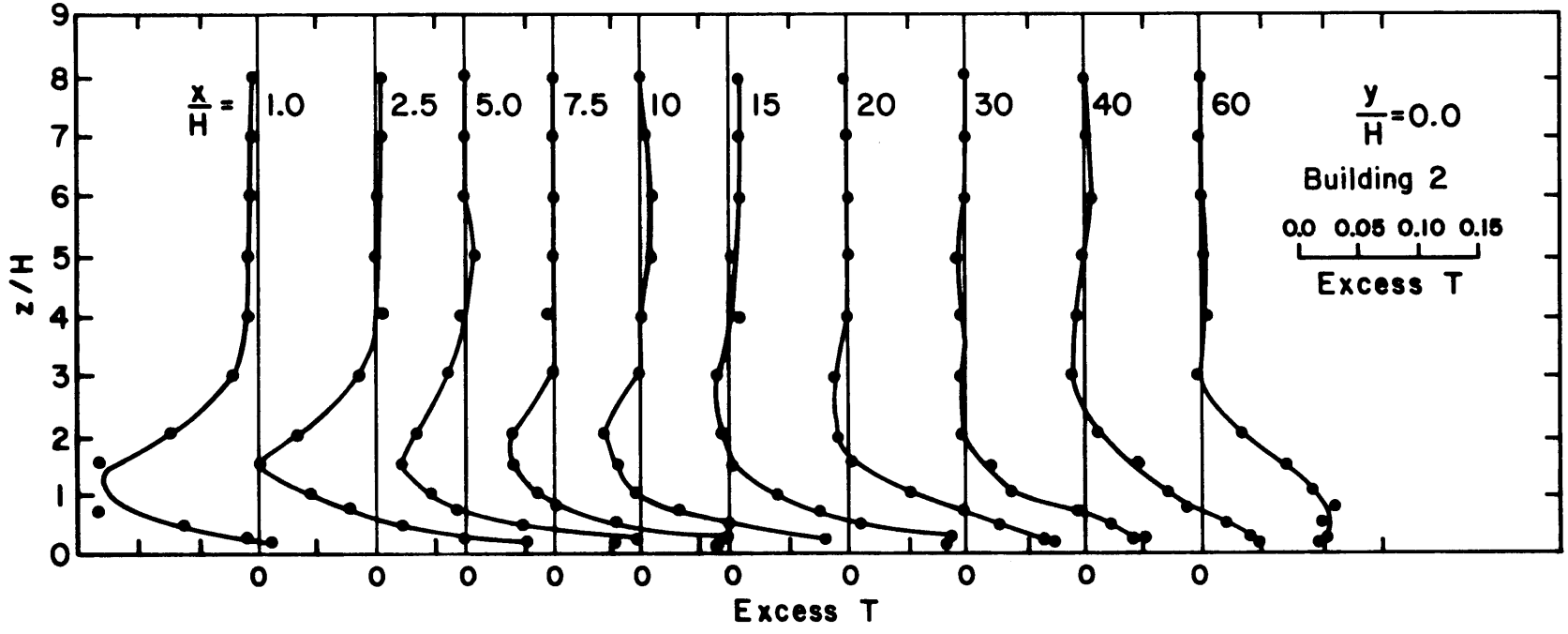

Figure 29. Vertical profiles of mean temperature excess behind building 2.

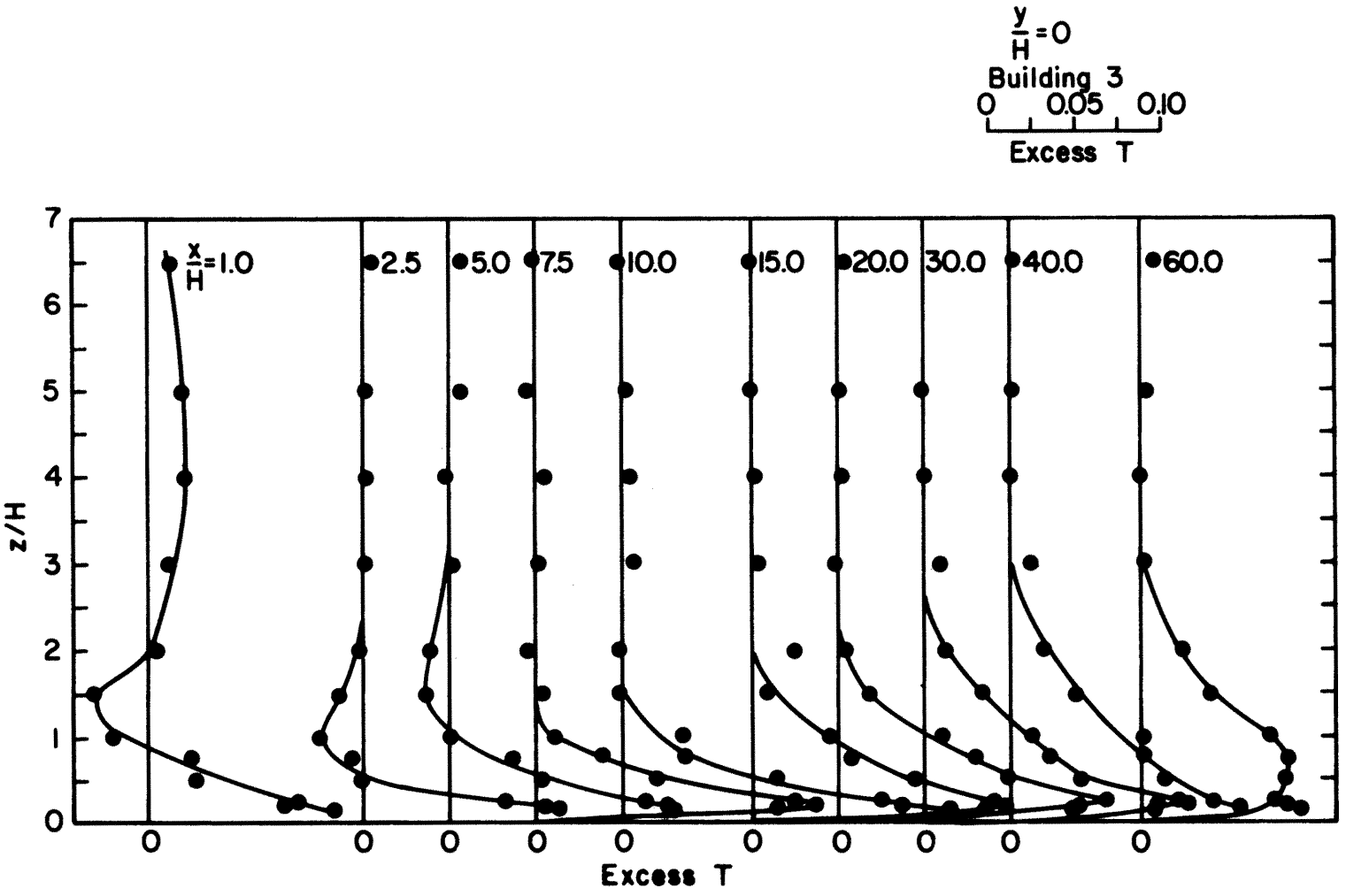

Figure 30. Vertical profiles of mean temperature excess behind building 3.

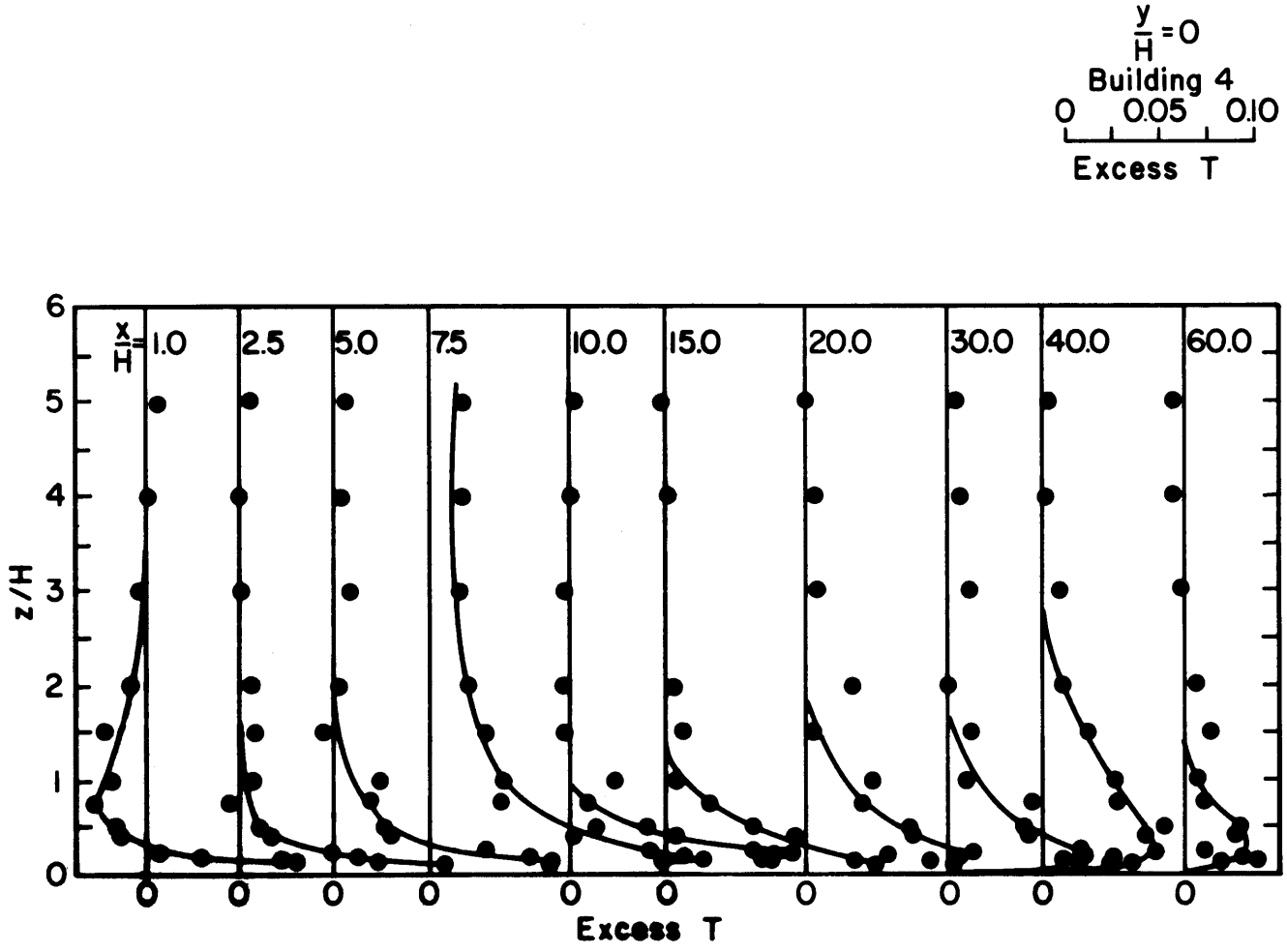

Figure 31. Vertical profiles of mean temperature excess behind building 4.

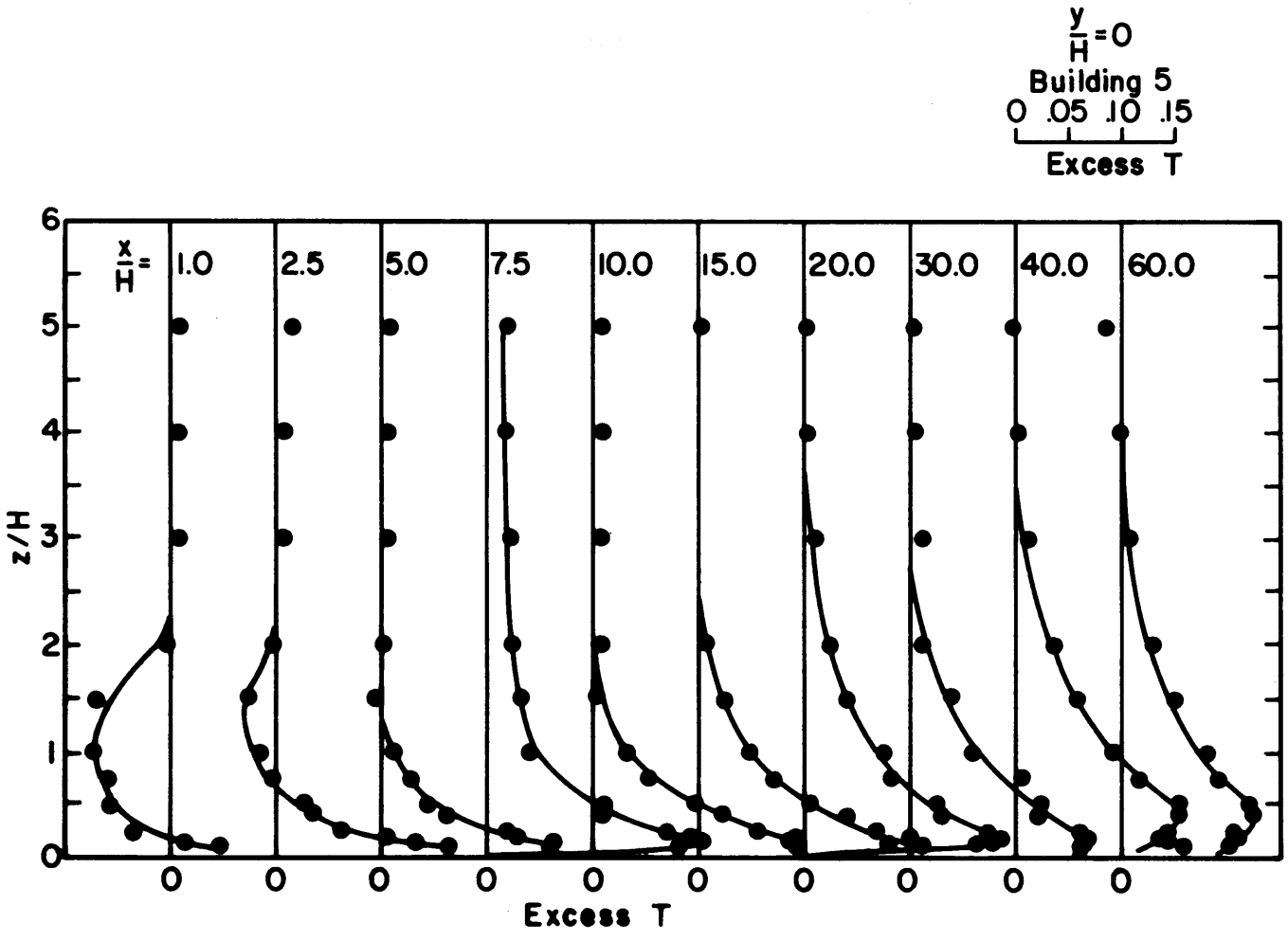

Figure 32. Vertical profiles of mean temperature excess behind building 5.

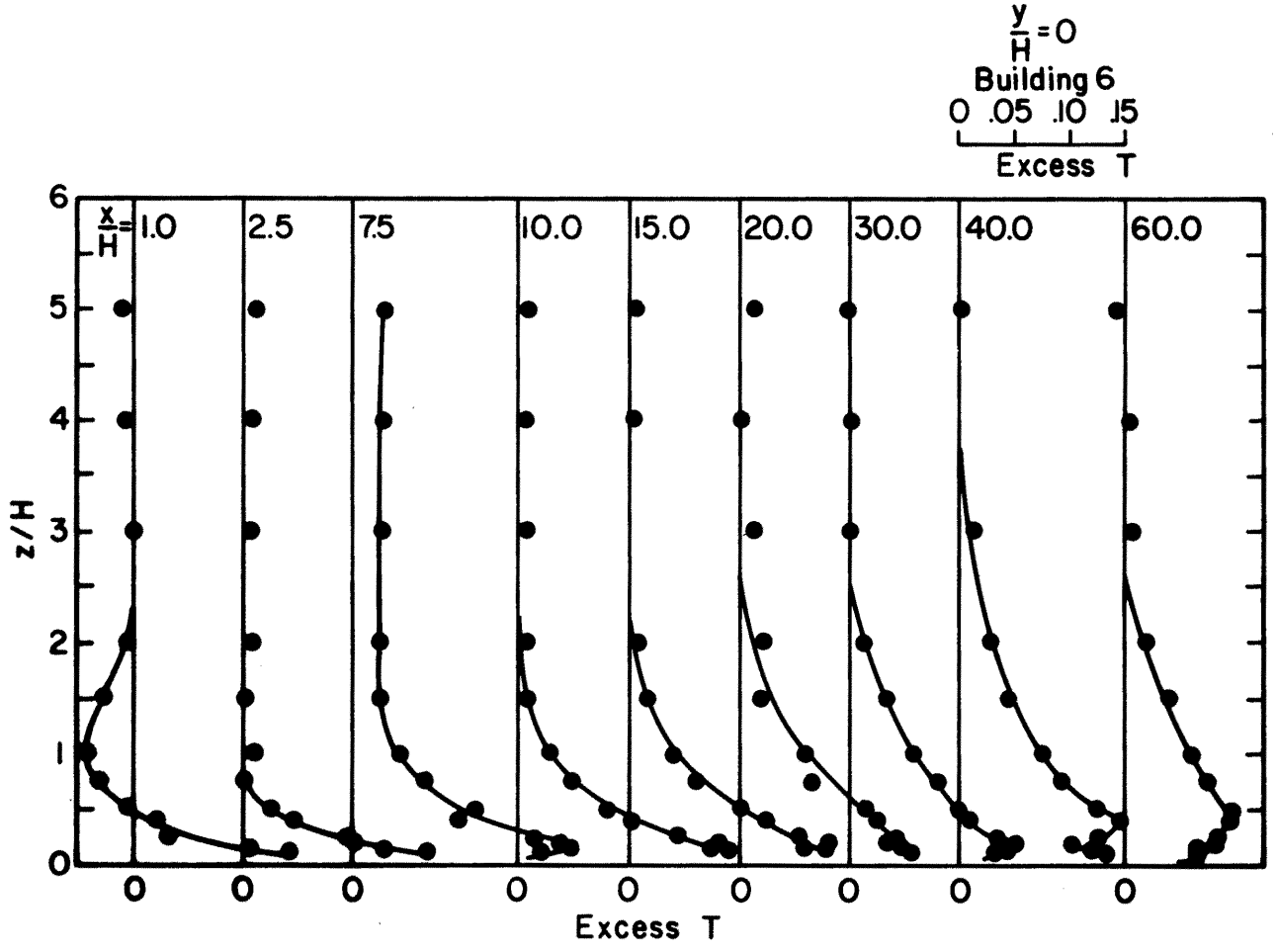

Figure 33. Vertical profiles of mean temperature excess behind building 6.

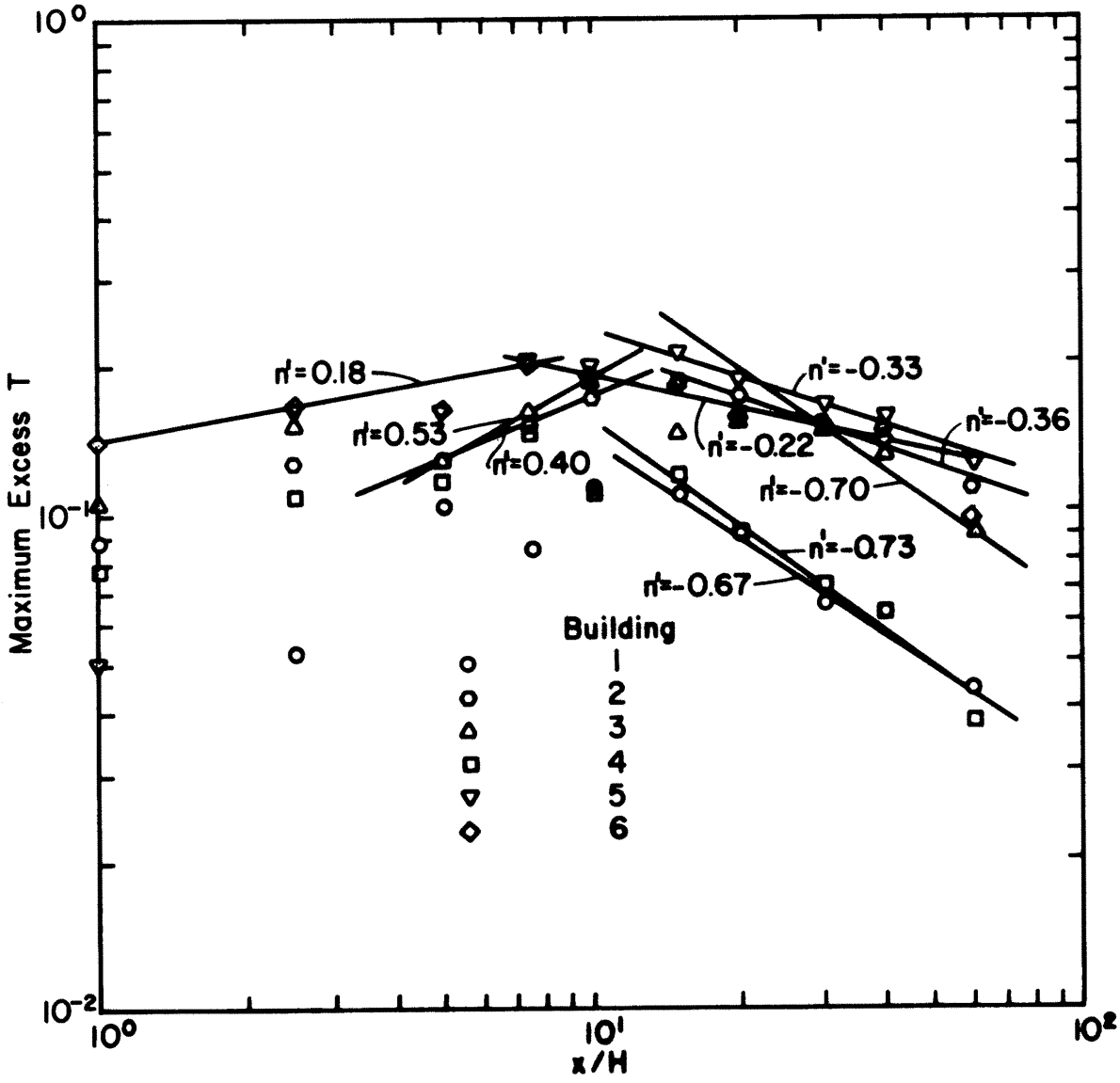

Figure 34. Variation of mean temperature excess in the wake of buildings.

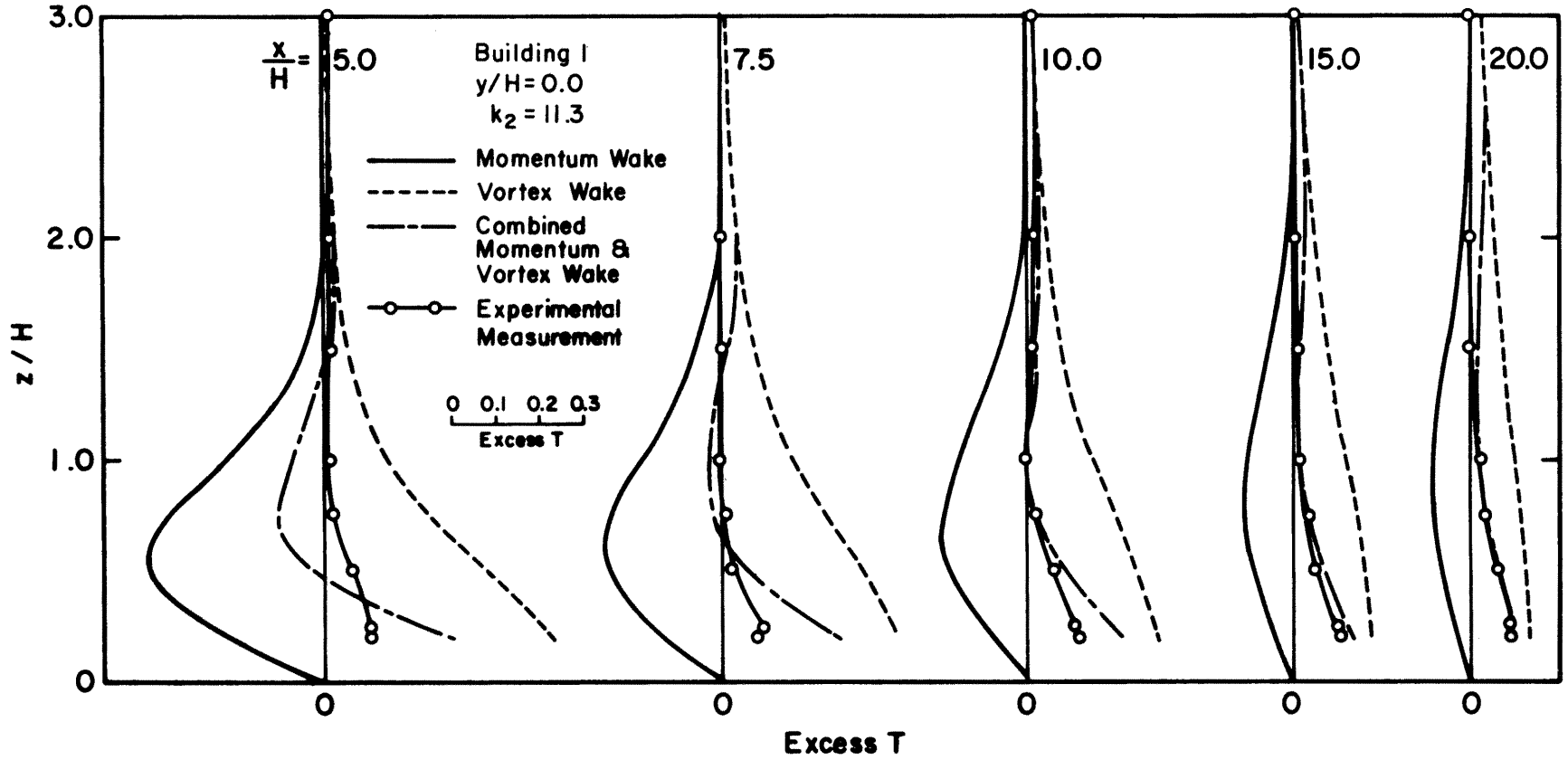

Figure 35. Comparison of the measured vertical profiles of temperature excess on the building 1 centerline with the present theory.

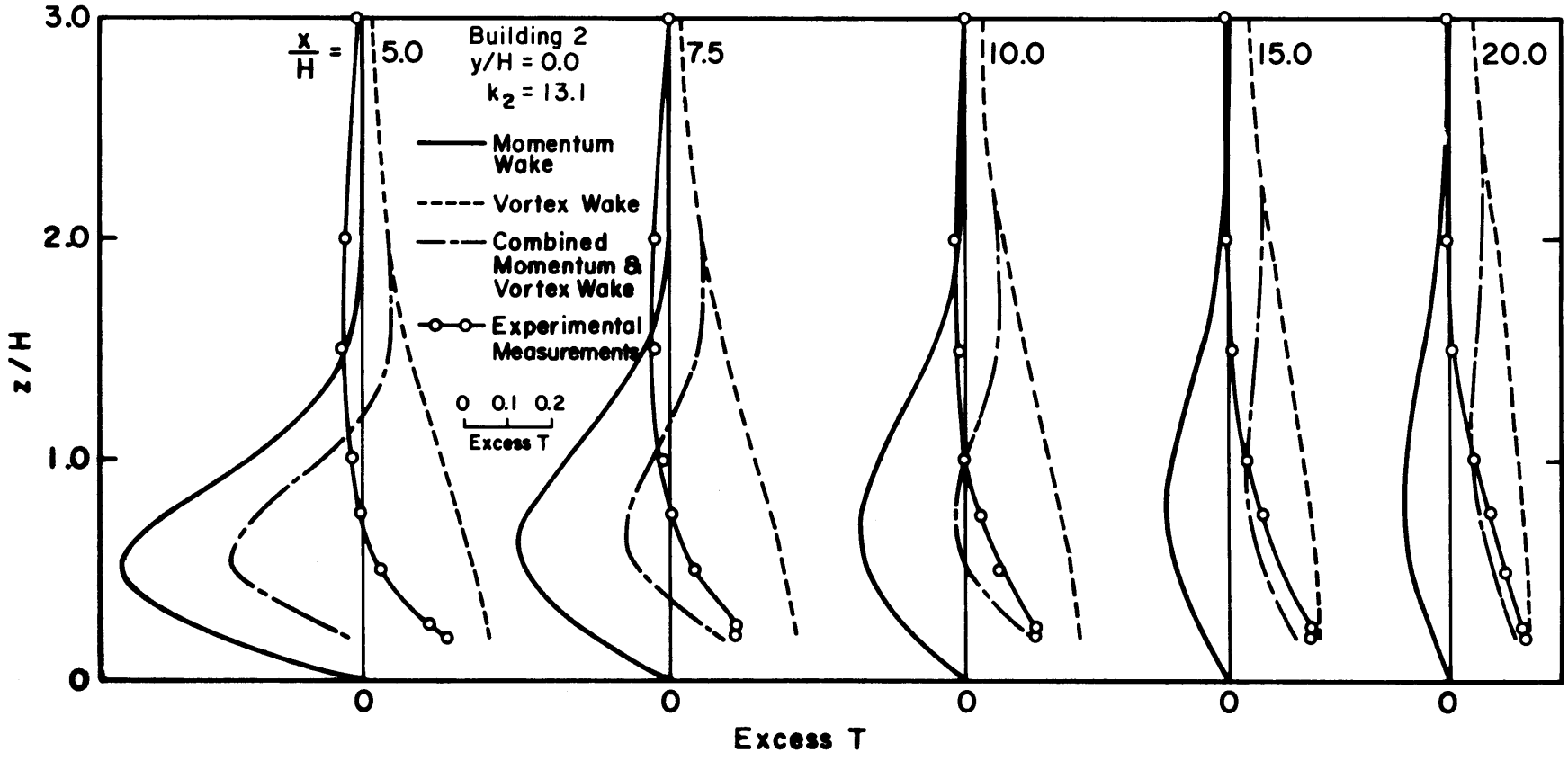

Figure 36. Comparison of the measured vertical profiles of temperature excess on the building 2 centerline with the present theory.

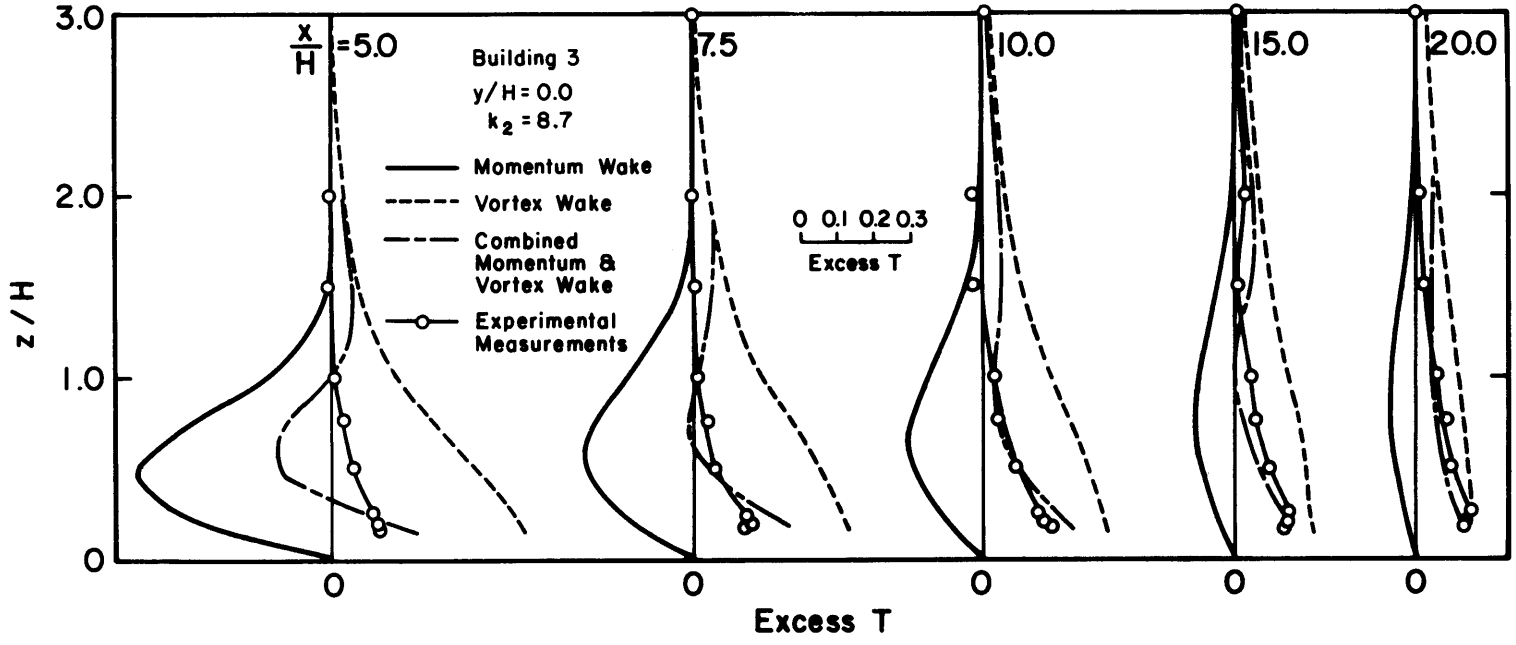

Figure 37. Comparison of the measured vertical profiles of temperature excess on the building 3 centerline with the present theory.

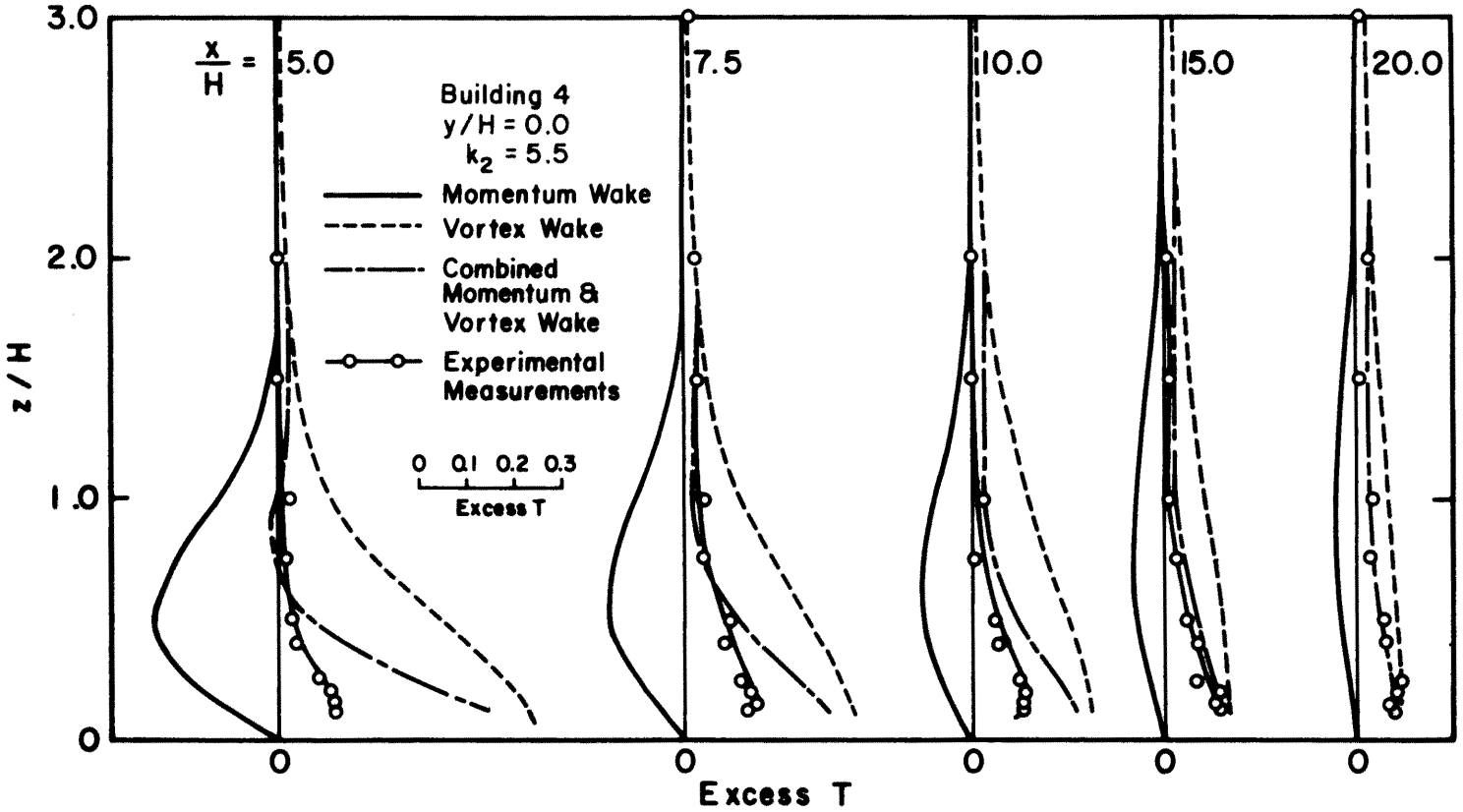

Figure 38. Comparison of the measured vertical profiles of temperature excess on the building 4 centerline with the present theory.

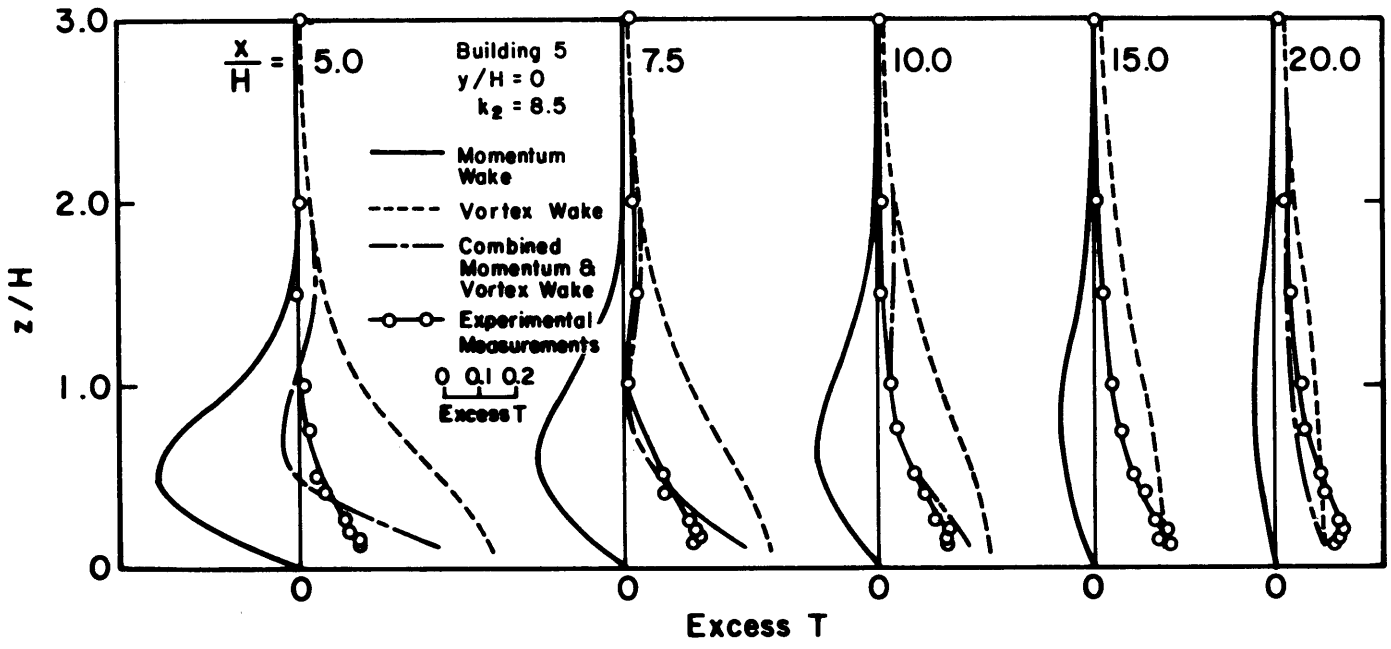

Figure 39. Comparison of the measured vertical profiles of temperature excess on the building 5 centerline with the present theory.

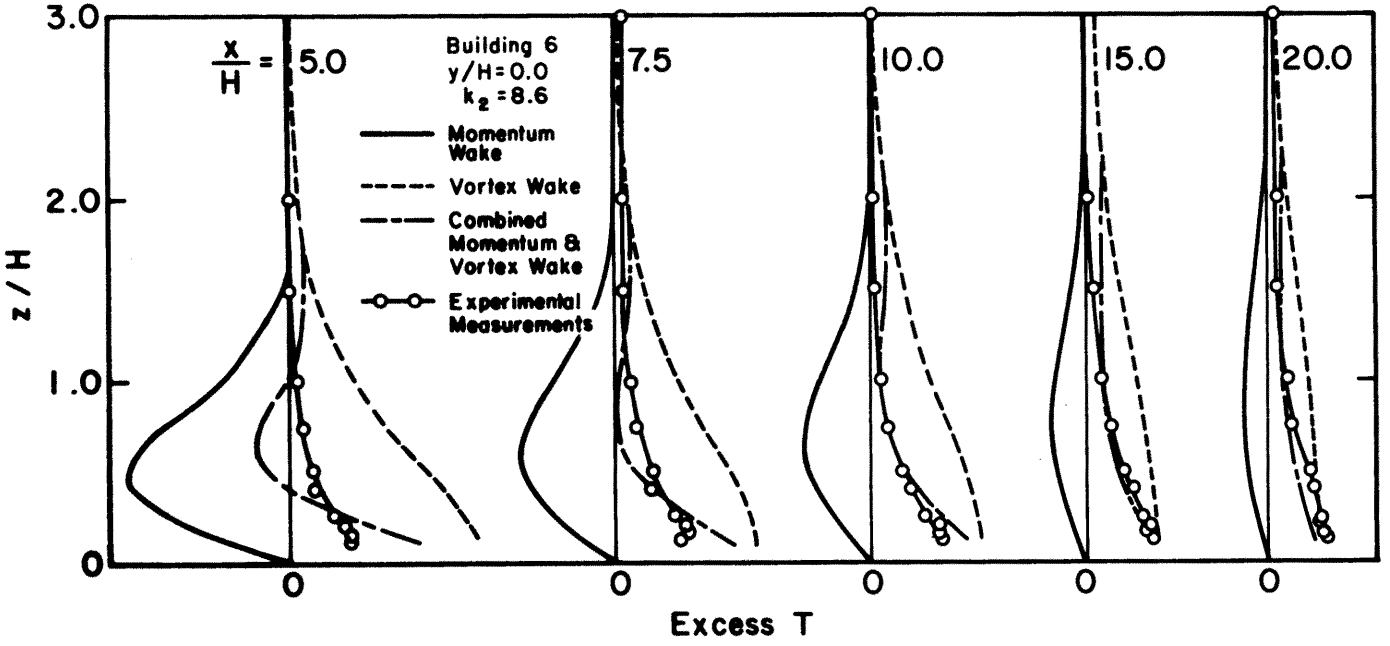

Figure 40. Comparison of the measured vertical profiles of temperature excess on the building 6 centerline with the present theory.

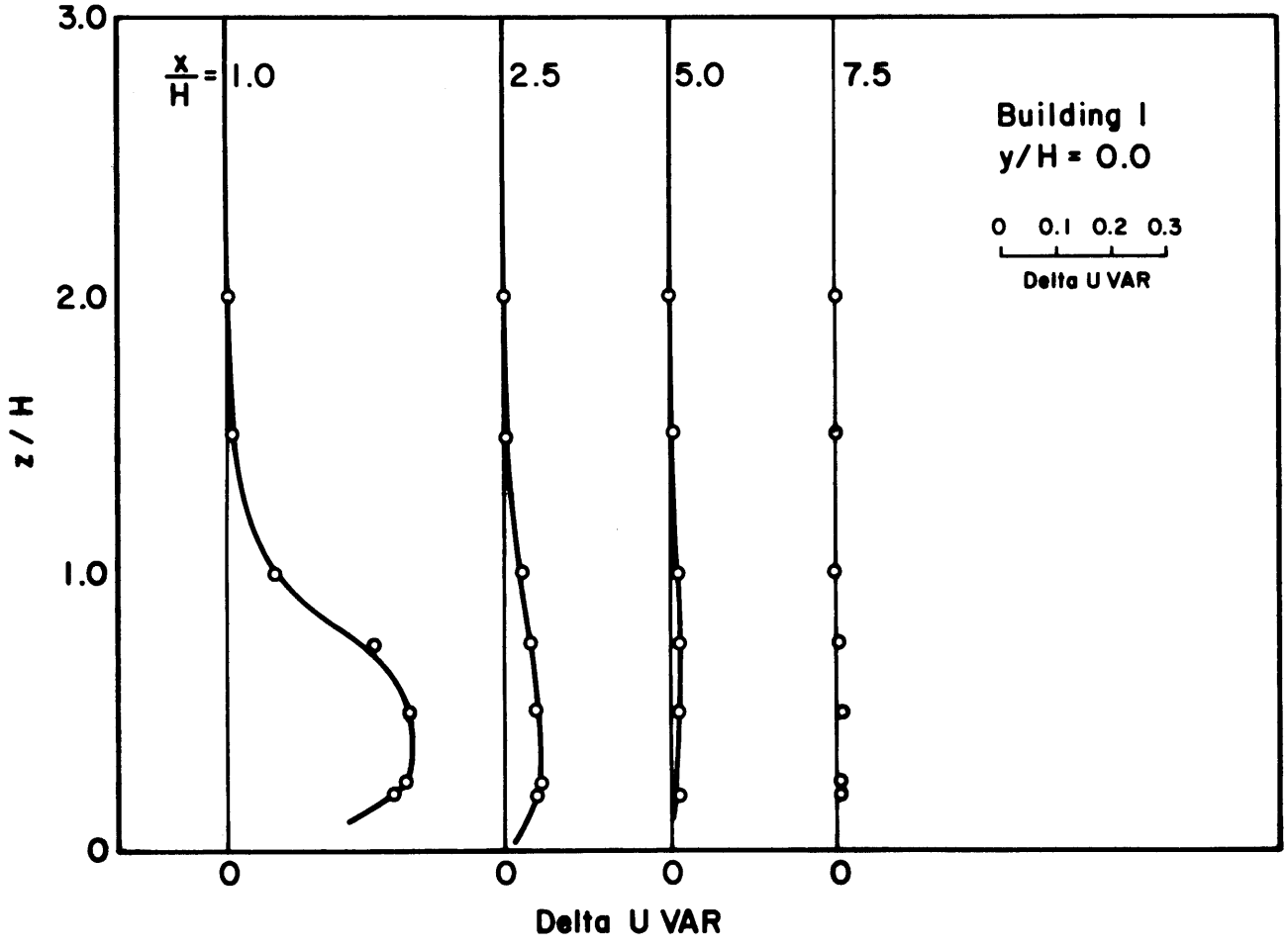

Figure 41. Vertical profiles of turbulence intensity excess variance on the centerline of building 1.

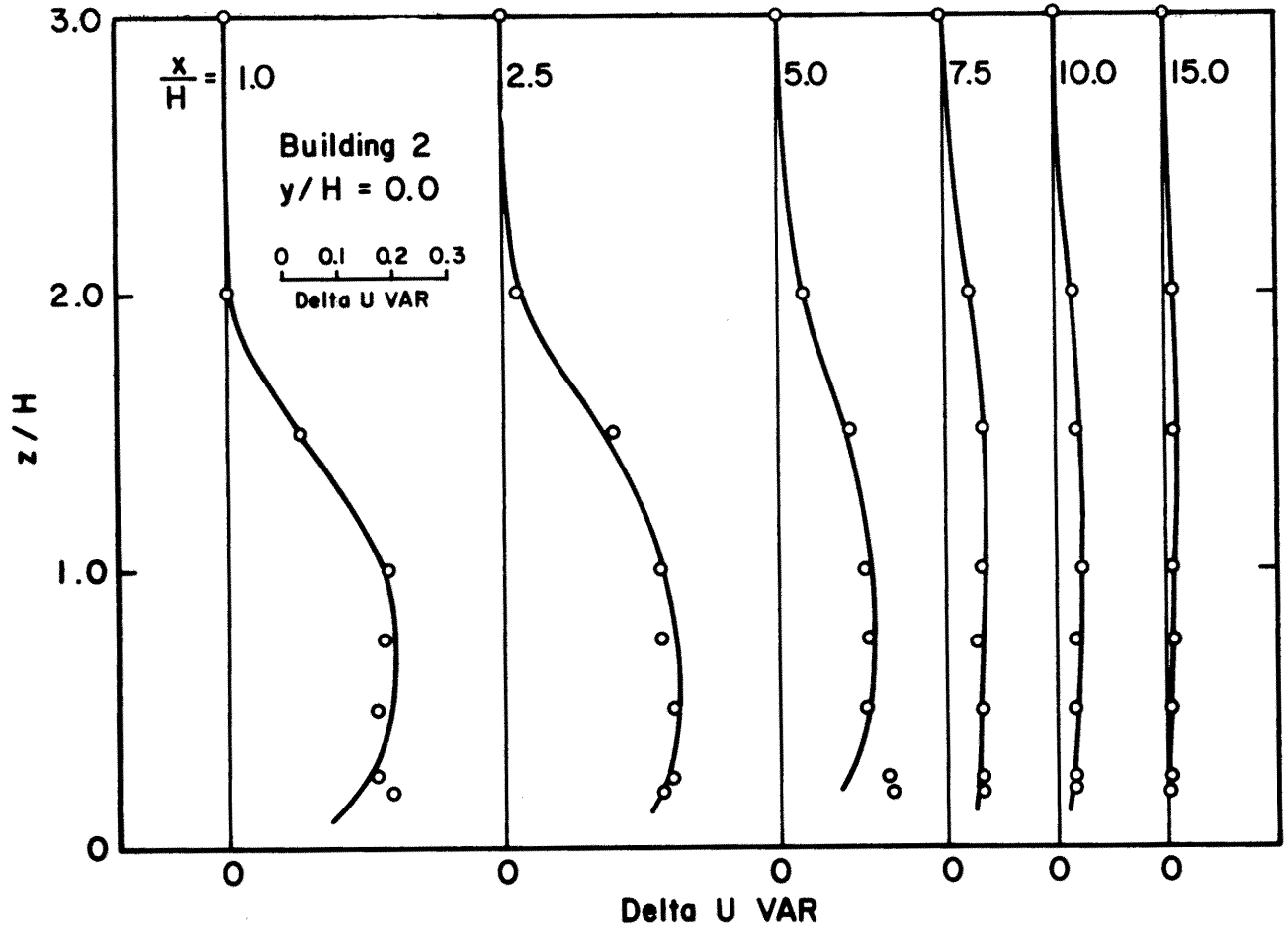

Figure 42. Vertical profiles of turbulence intensity excess variance on the centerline of building 2.

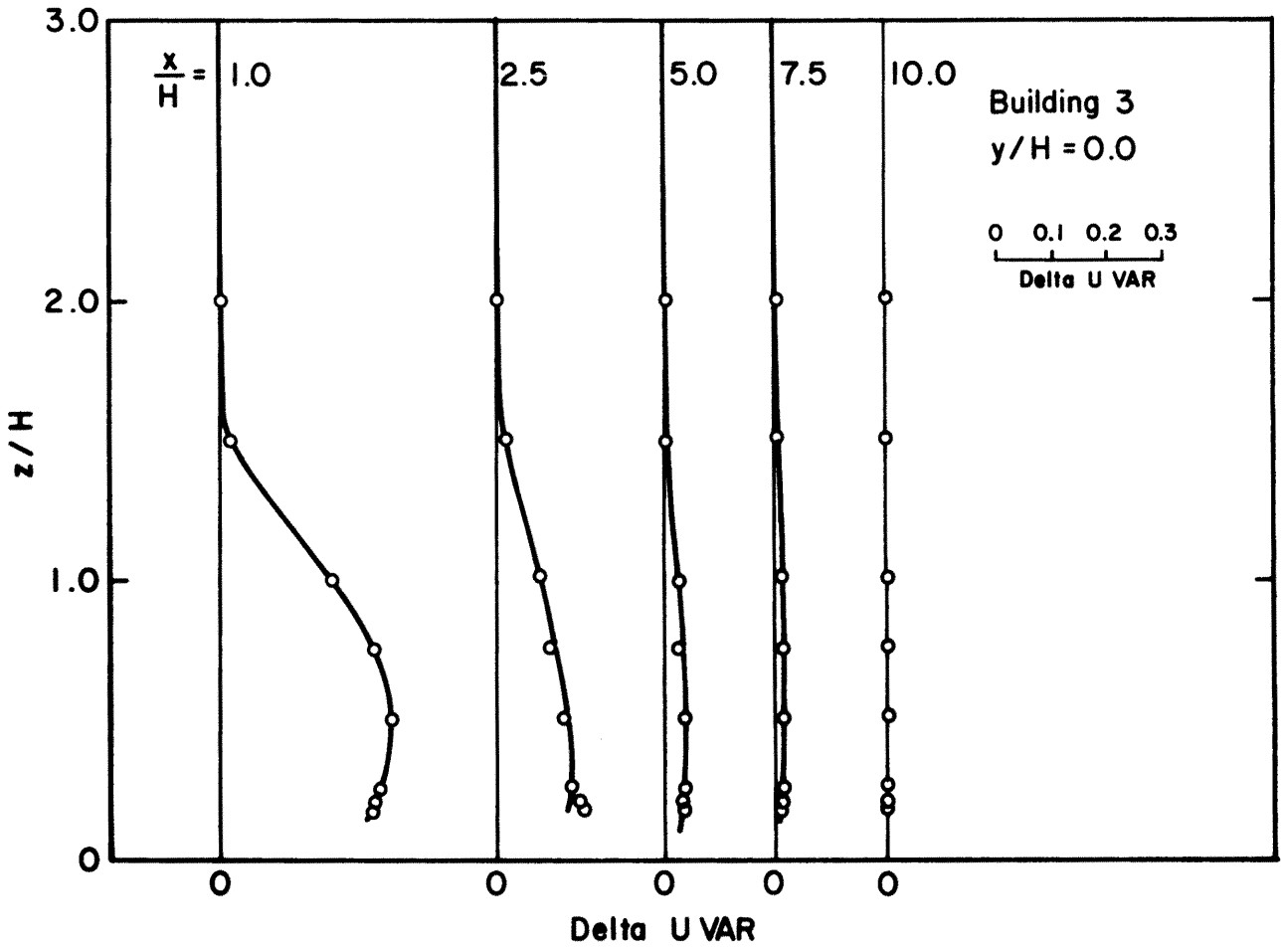

Figure 43. Vertical profiles of turbulence intensity excess variance on the centerline of building 3.

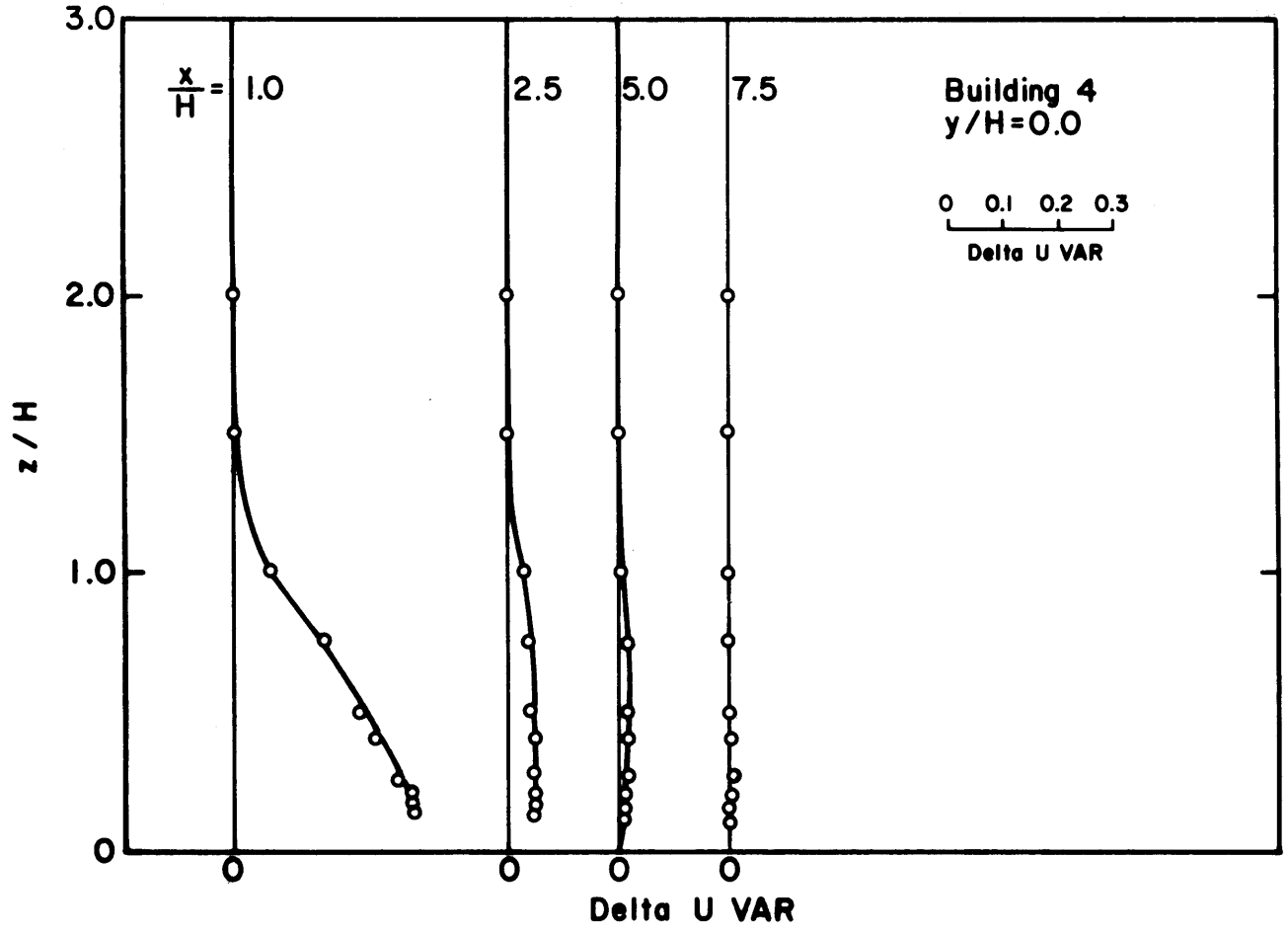

Figure 44. Vertical profiles of turbulence intensity excess variance on the centerline of building 4.

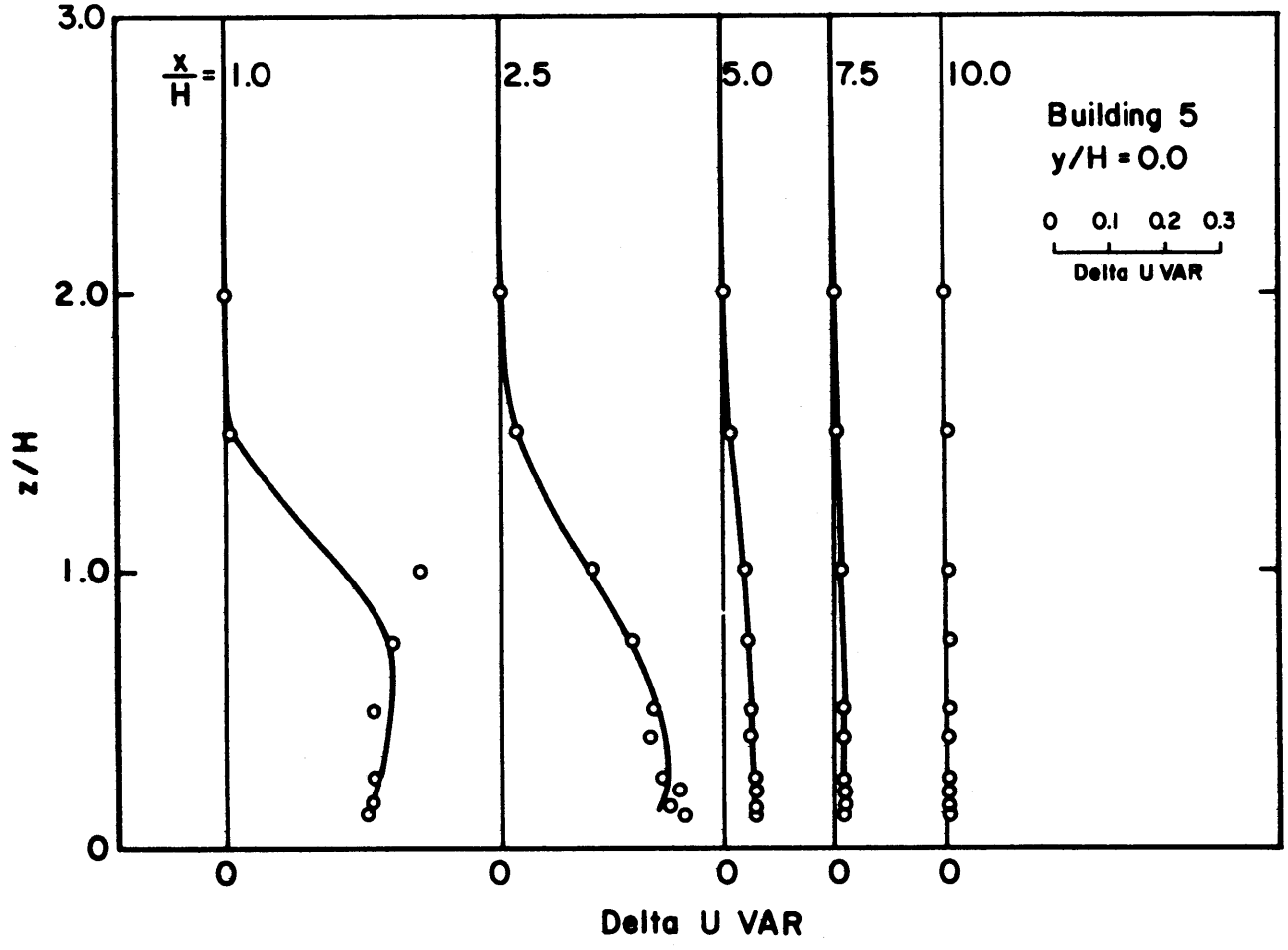

Figure 45. Vertical profiles of turbulence intensity excess variance on the centerline of building 5.

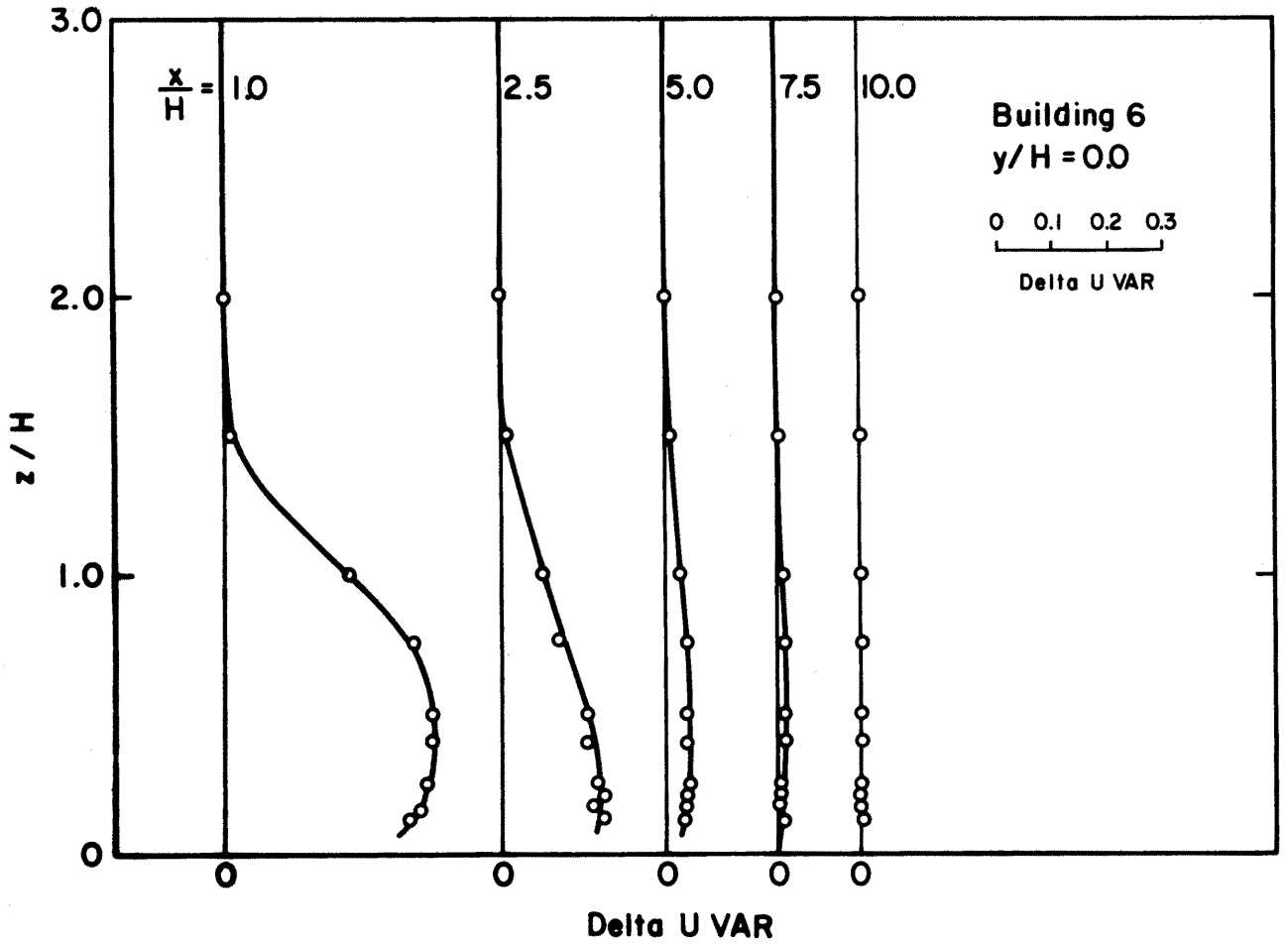

Figure 46. Vertical profiles of turbulence intensity excess variance on the centerline of building 6.

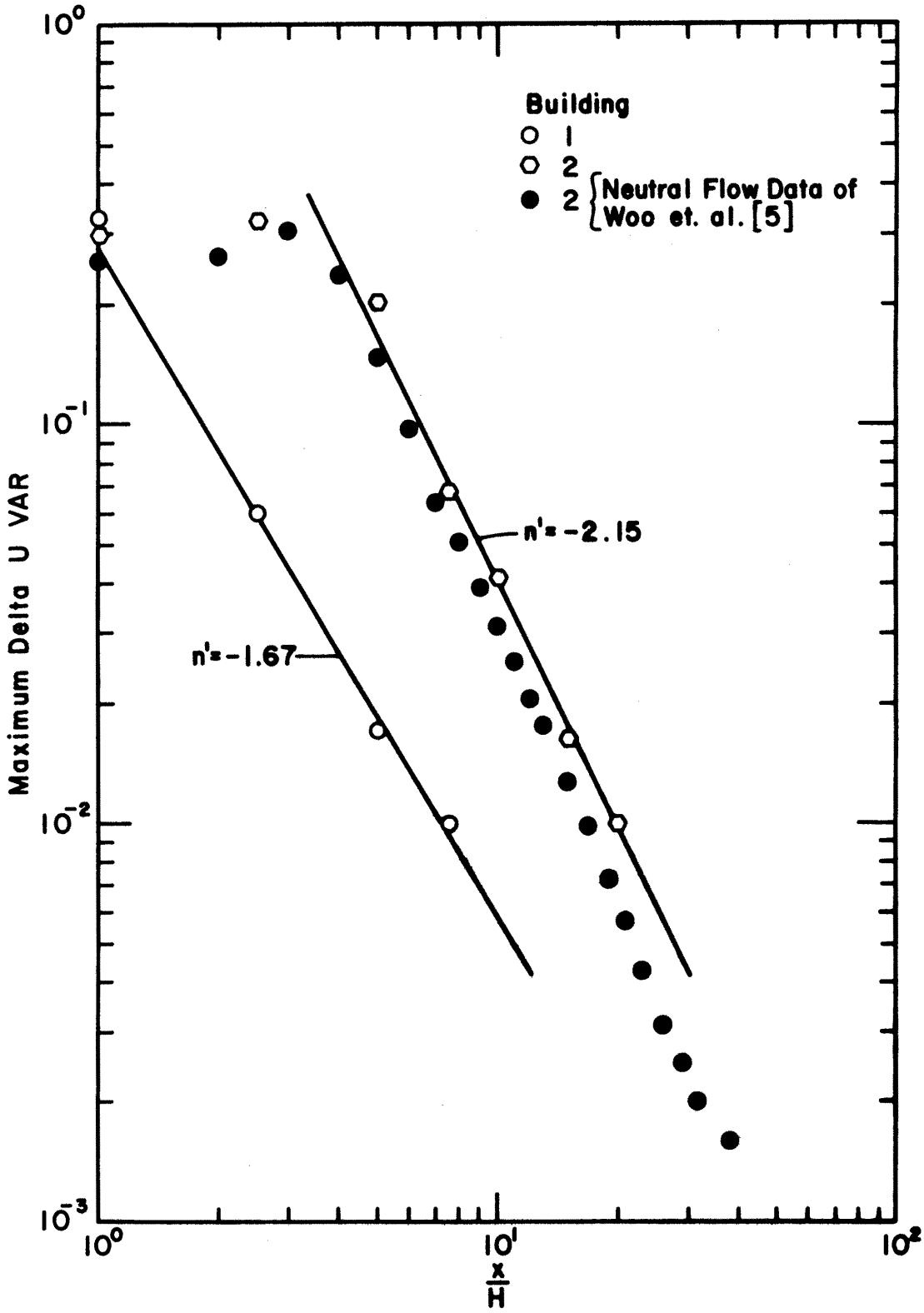

Figure 47. Comparison of the decay rates of turbulence intensity excess variance behind buildings 1 and 2 with Woo et al., [5].

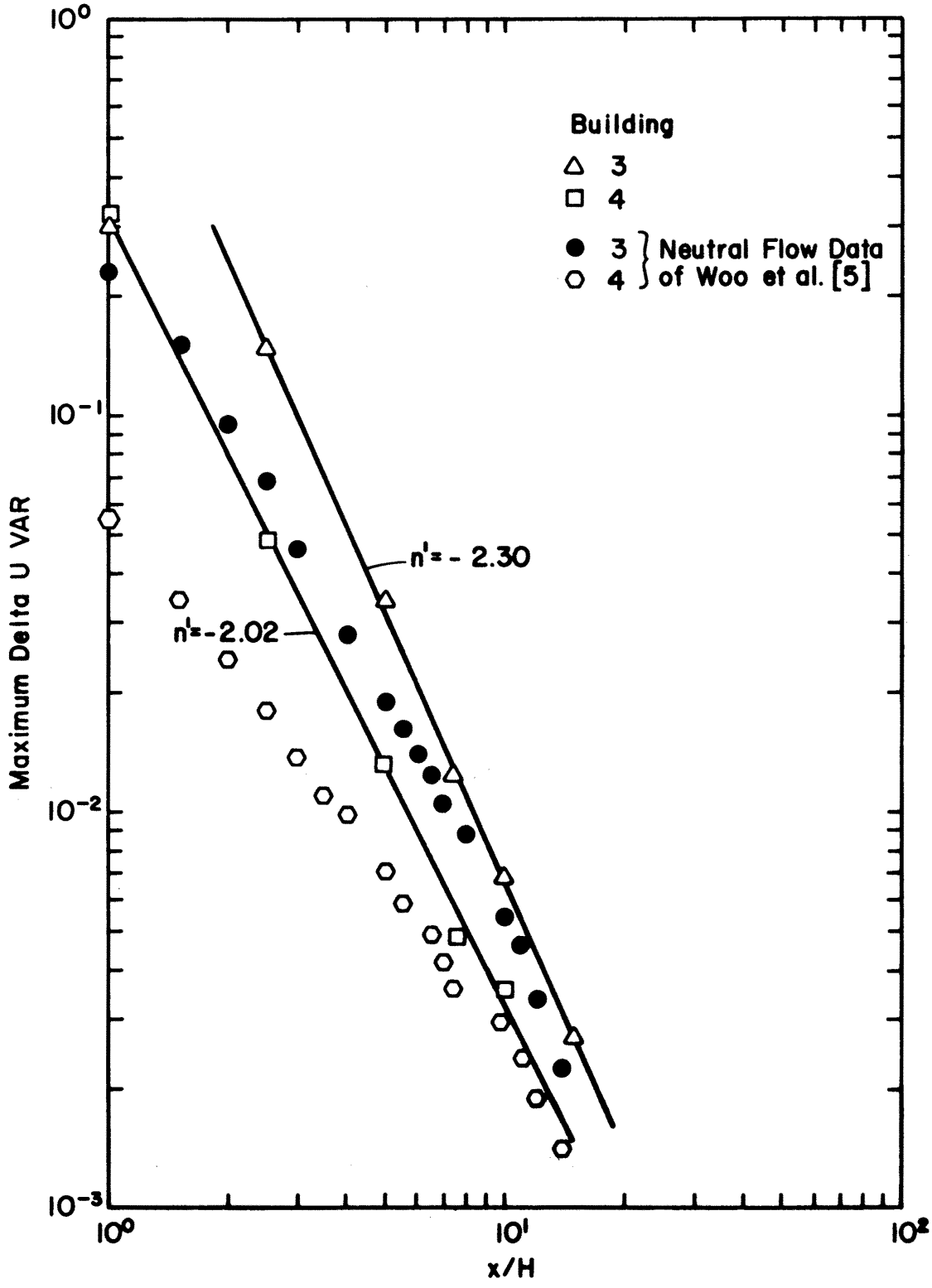

Figure 48. Comparison of the decay rates of turbulence intensity excess variance behind buildings 3 and 4 with Woo et al., [5].

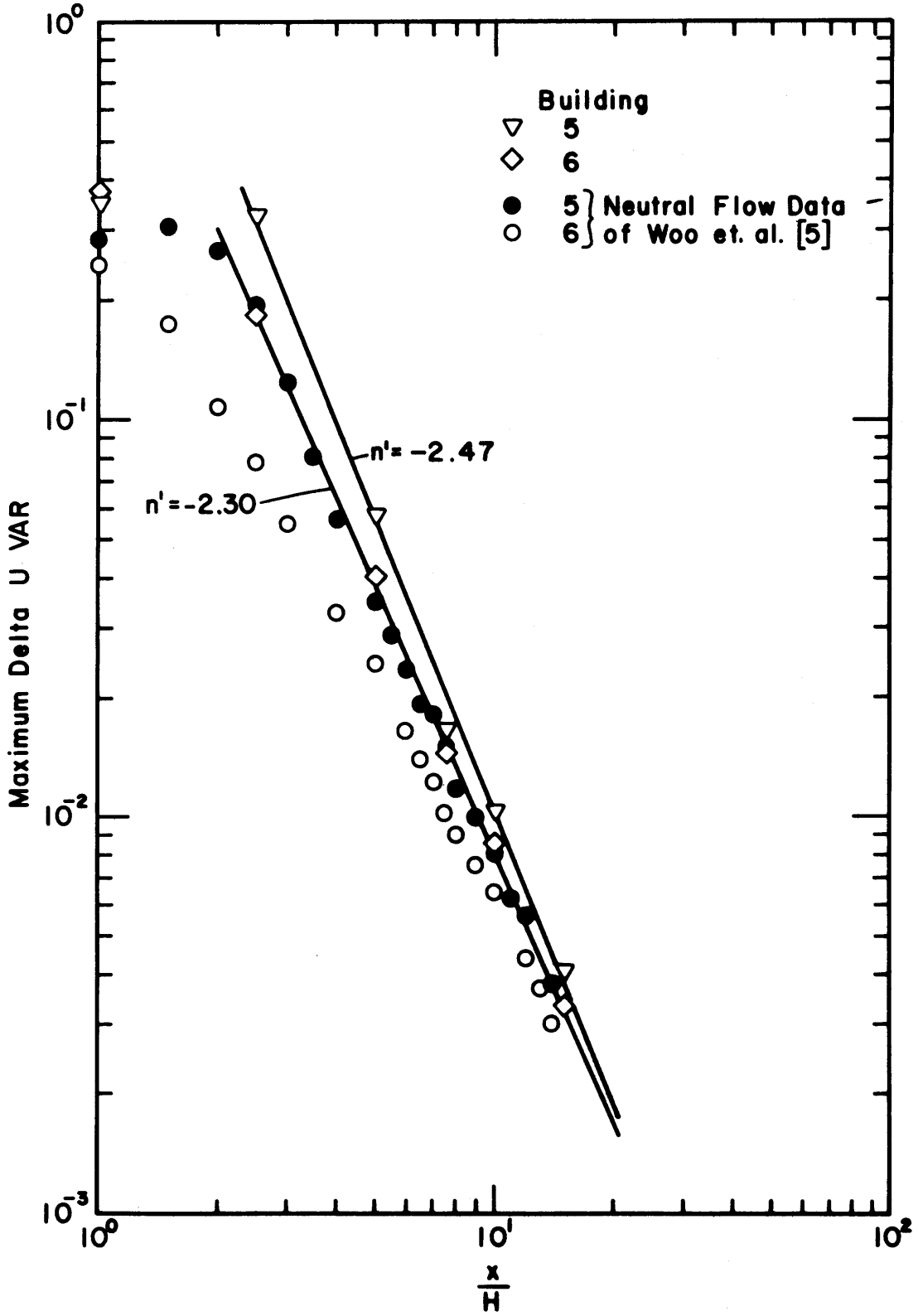

Figure 49. Comparison of the decay rates of turbulence intensity excess variance behind buildings 5 and 6 with Woo et al., [5].

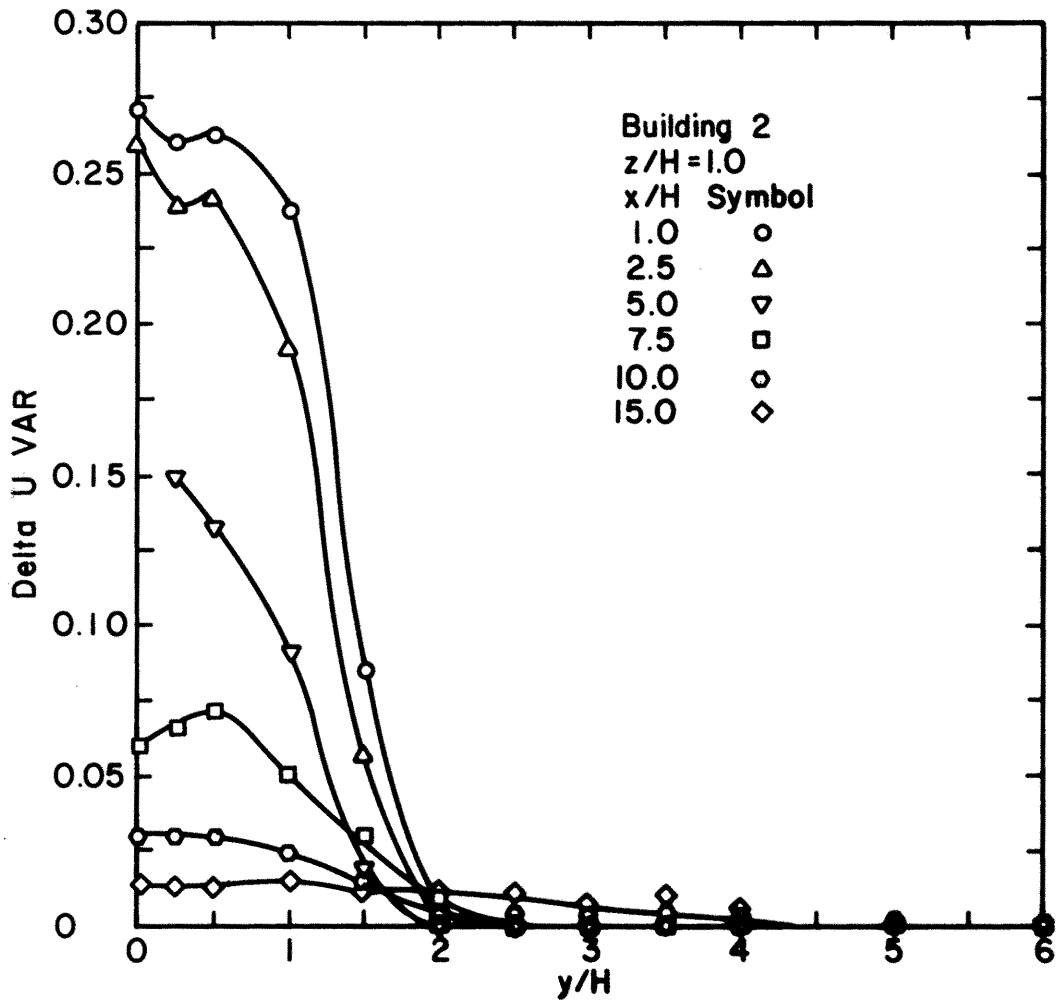

Figure 50. Horizontal profiles of turbulence intensity excess variance behind building 2.

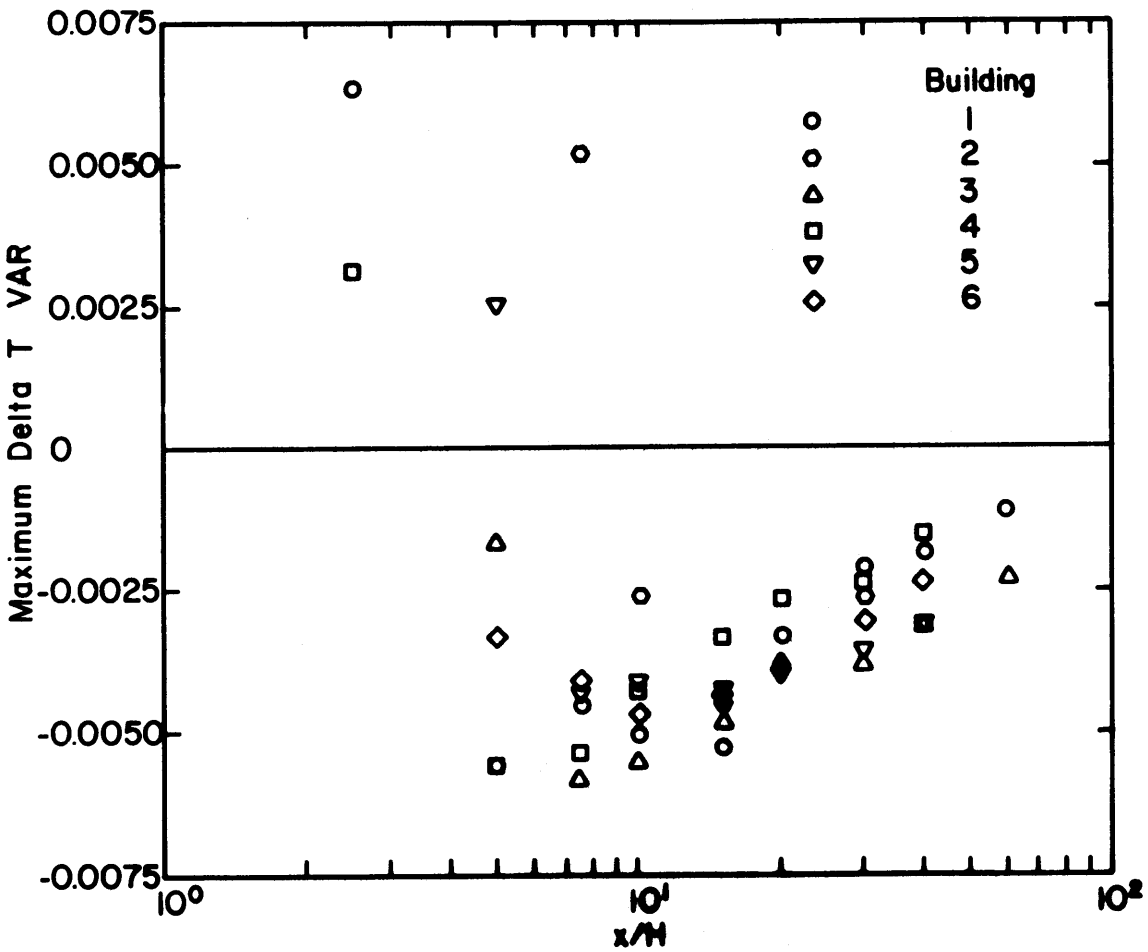

Figure 51. Decay of temperature excess variance in the wake of buildings.

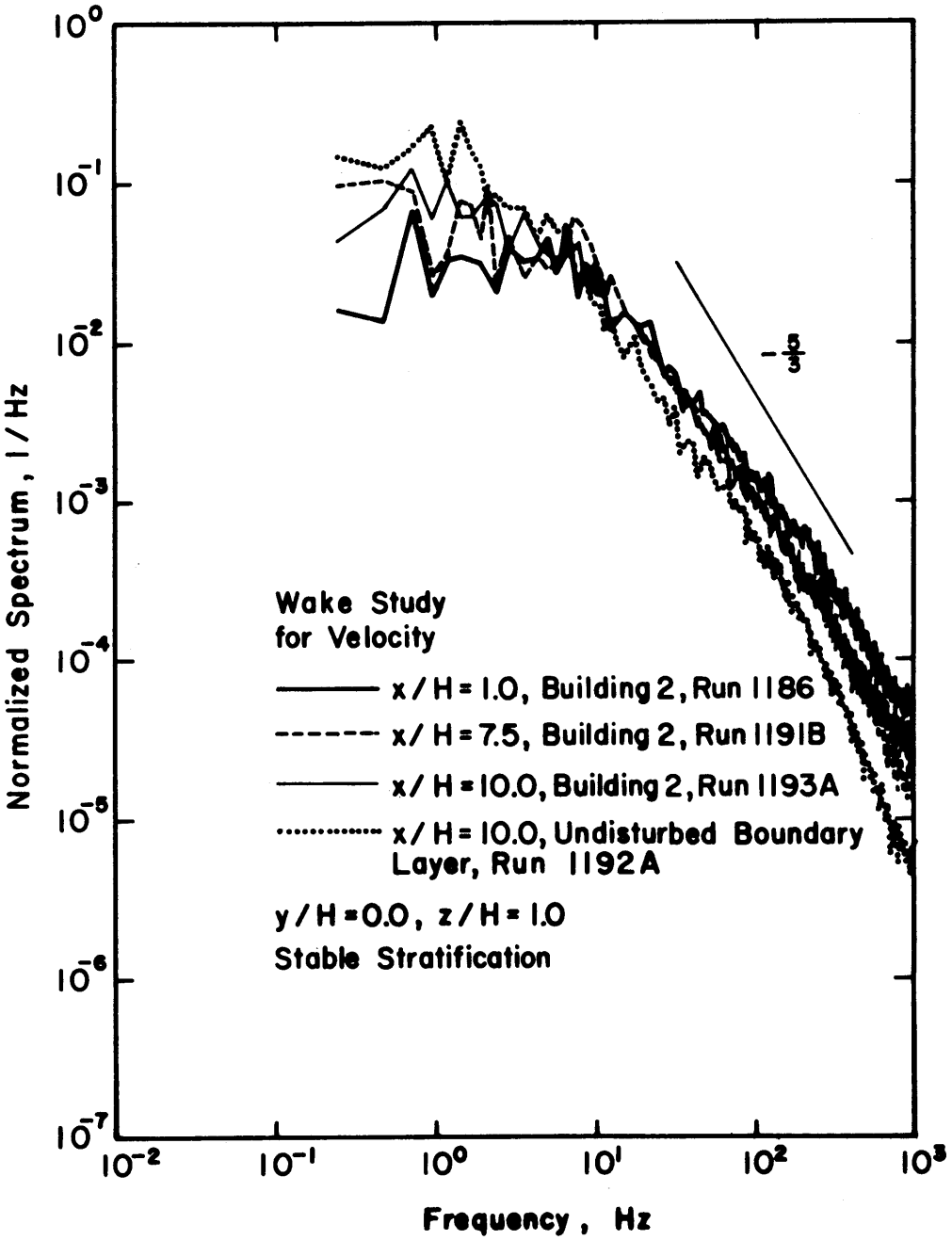

Figure 52. Comparison of normalized longitudinal velocity spectra behind building 2 with undisturbed boundary layer spectrum.

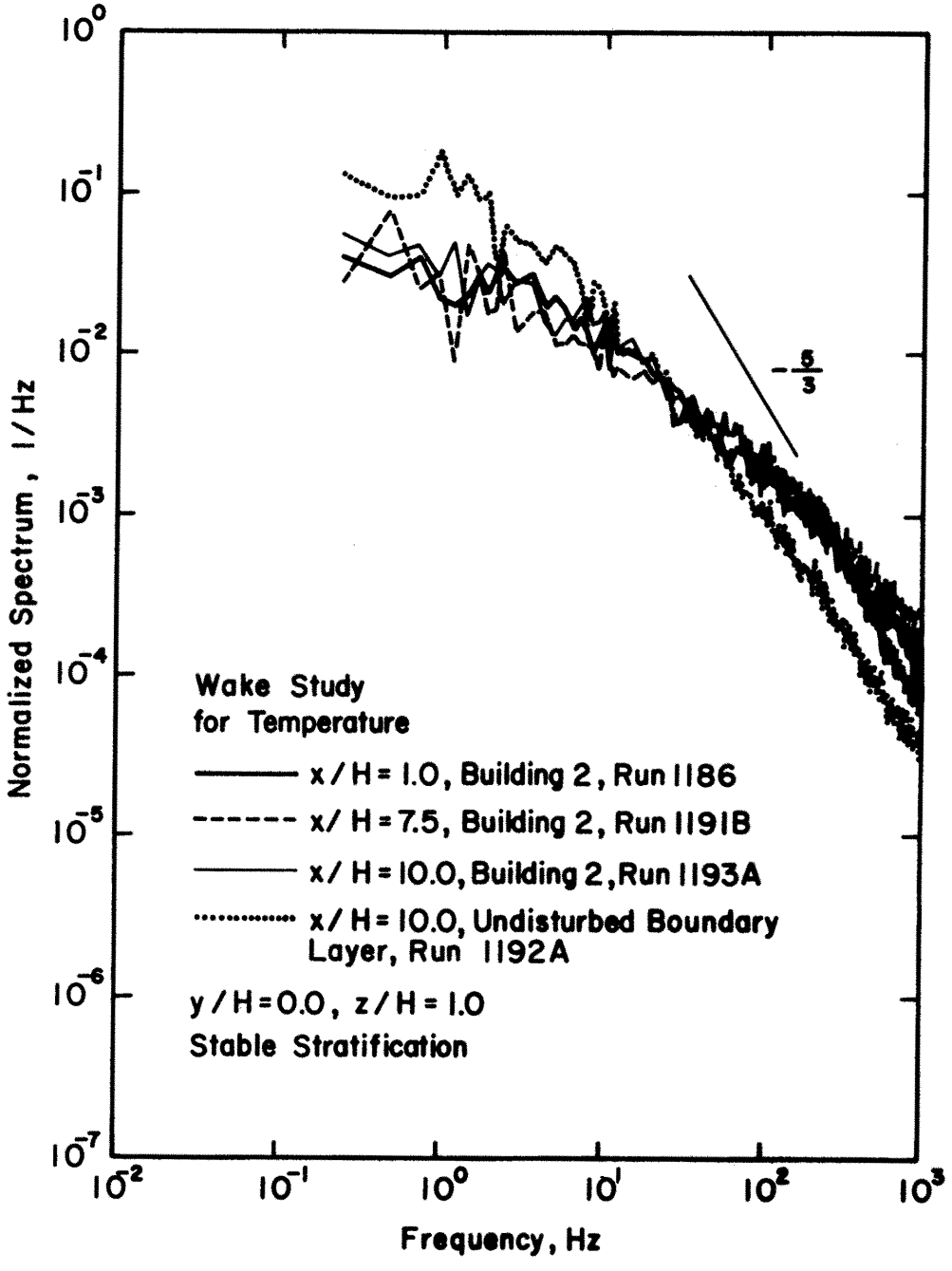

Figure 53. Comparison of normalized temperature spectra behind building 2 with undisturbed boundary layer spectrum.

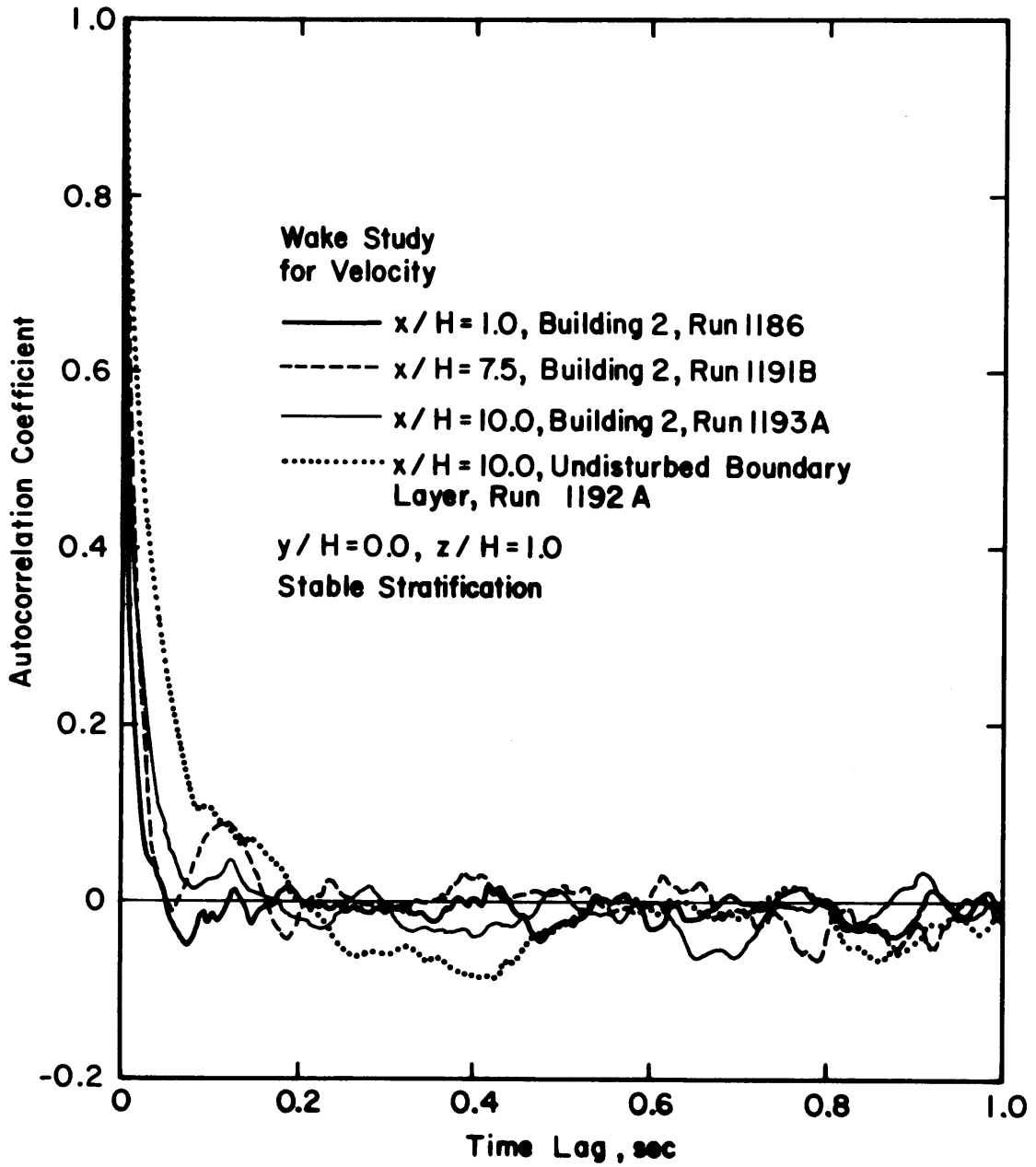

Figure 54. Comparison of auto-correlation coefficients derived from velocity spectra behind building 2 with undisturbed boundary layer auto-correlation coefficients.

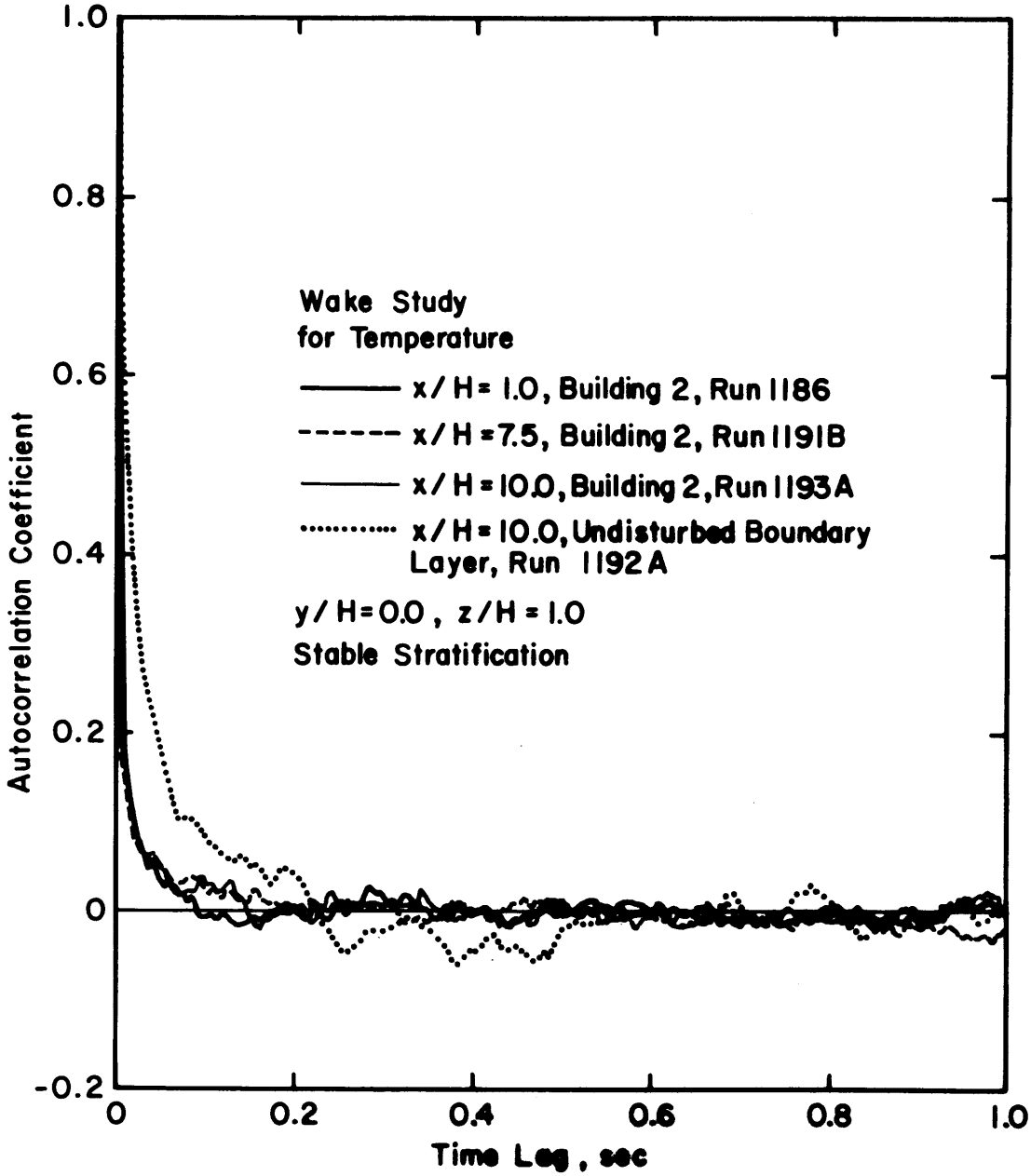

Figure 55. Comparison of auto-correlation coefficients derived from temperature spectra behind building 2 with undisturbed boundary layer auto-correlation coefficients.

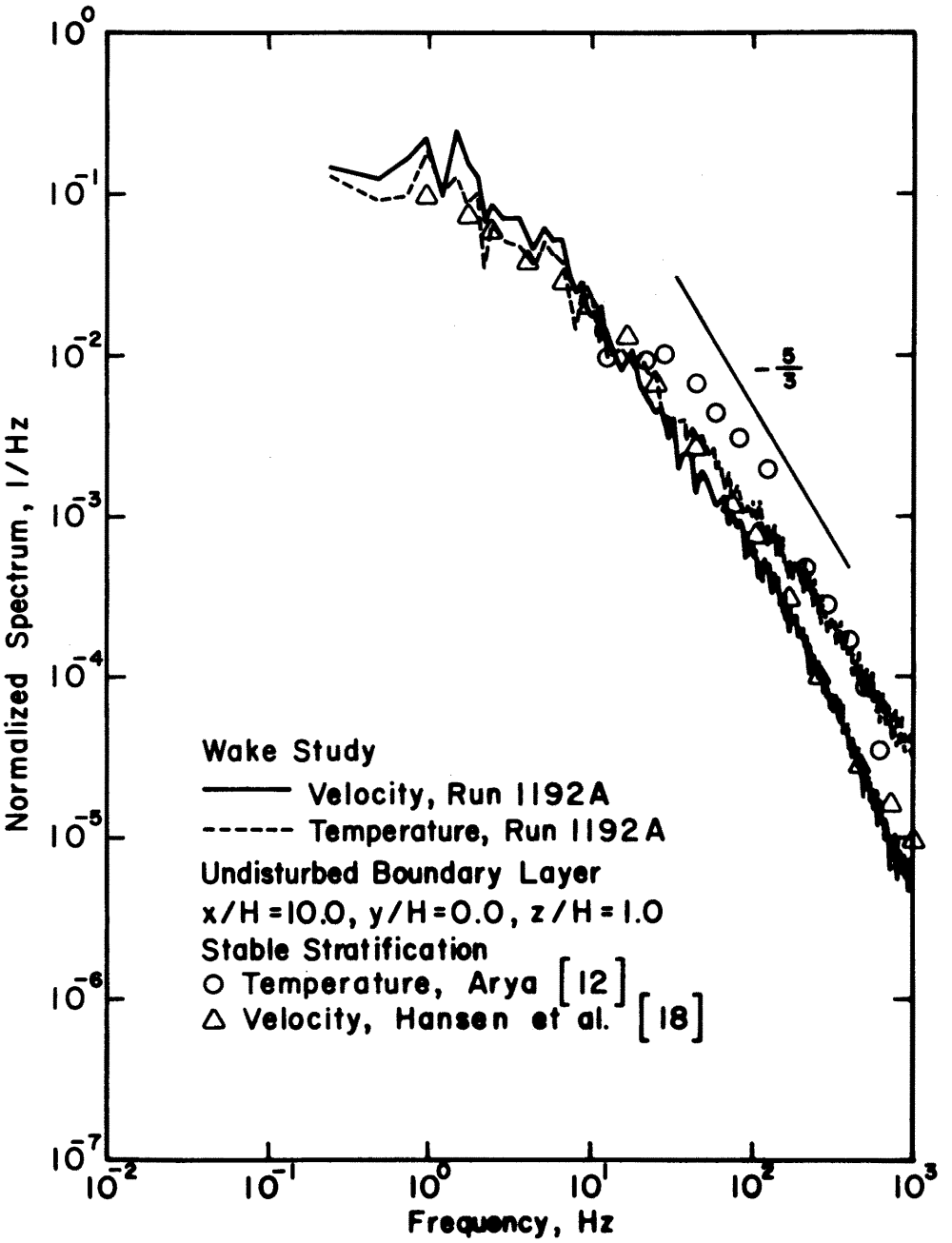

Figure 56. Comparison of longitudinal velocity spectrum with temperature spectrum in undisturbed boundary layer.

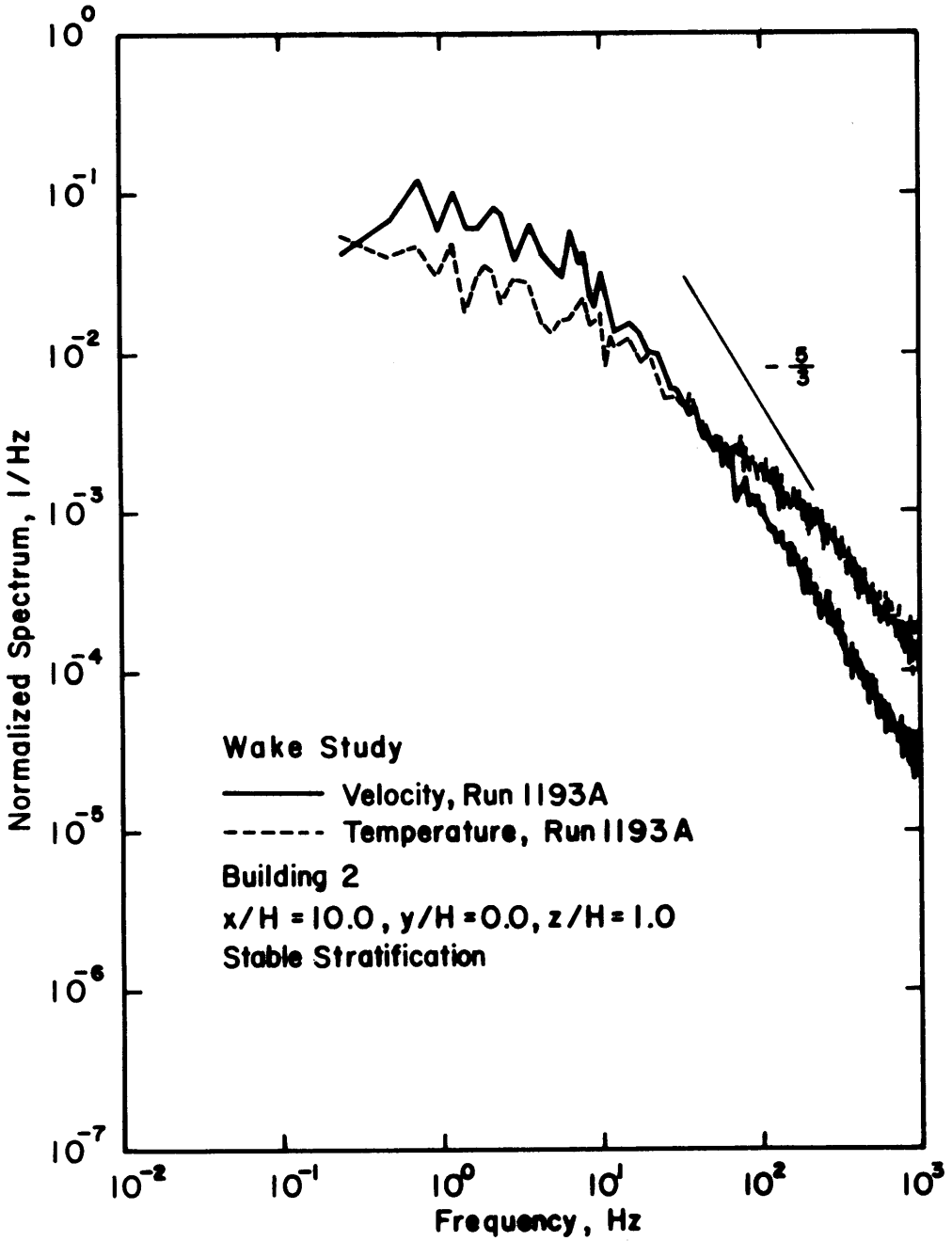

Figure 57. Comparison of longitudinal velocity spectrum with temperature spectrum behind building 2.

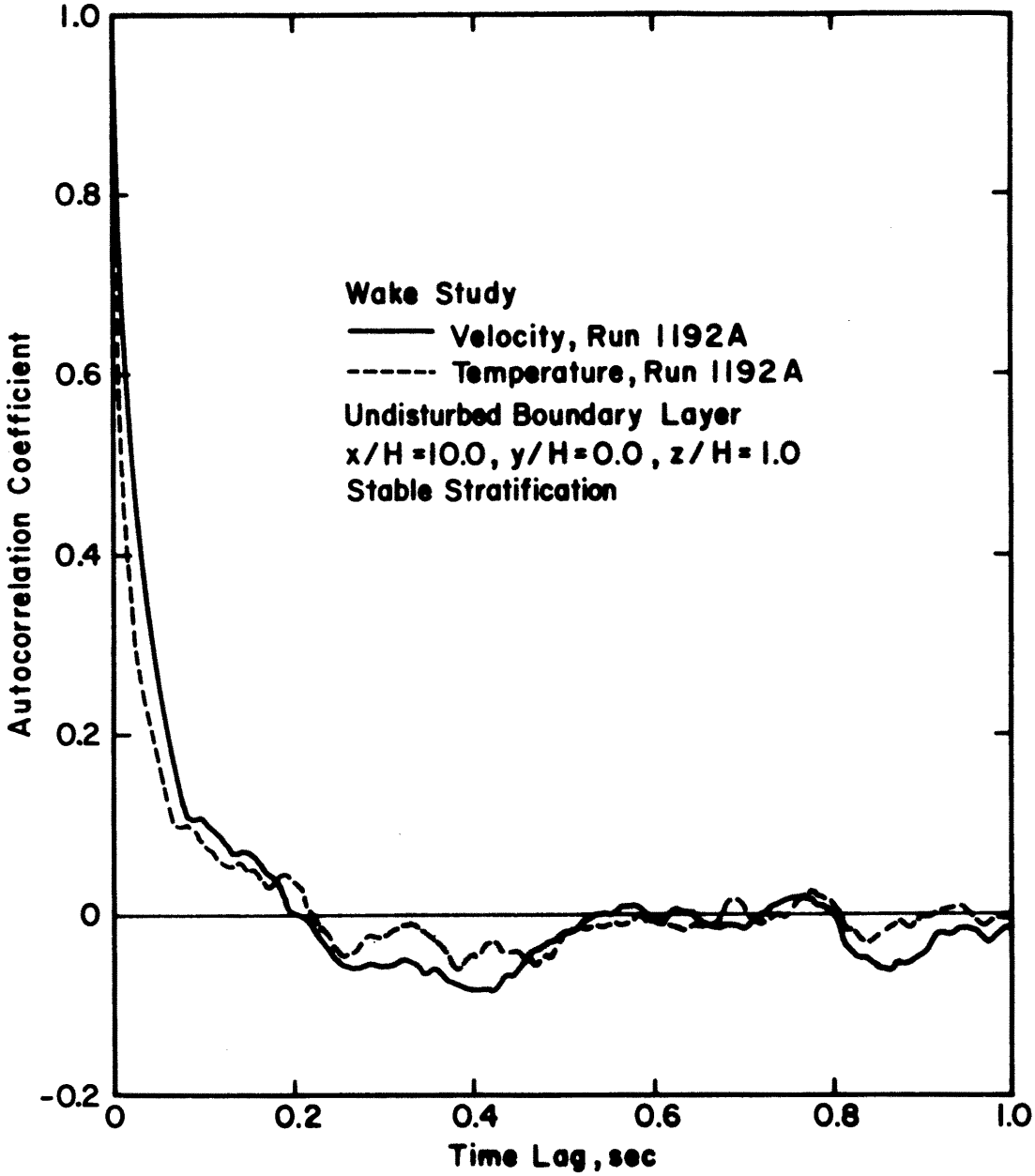

Figure 58. Comparison of auto-correlation coefficients derived from velocity and temperature spectrum in undisturbed boundary layer.

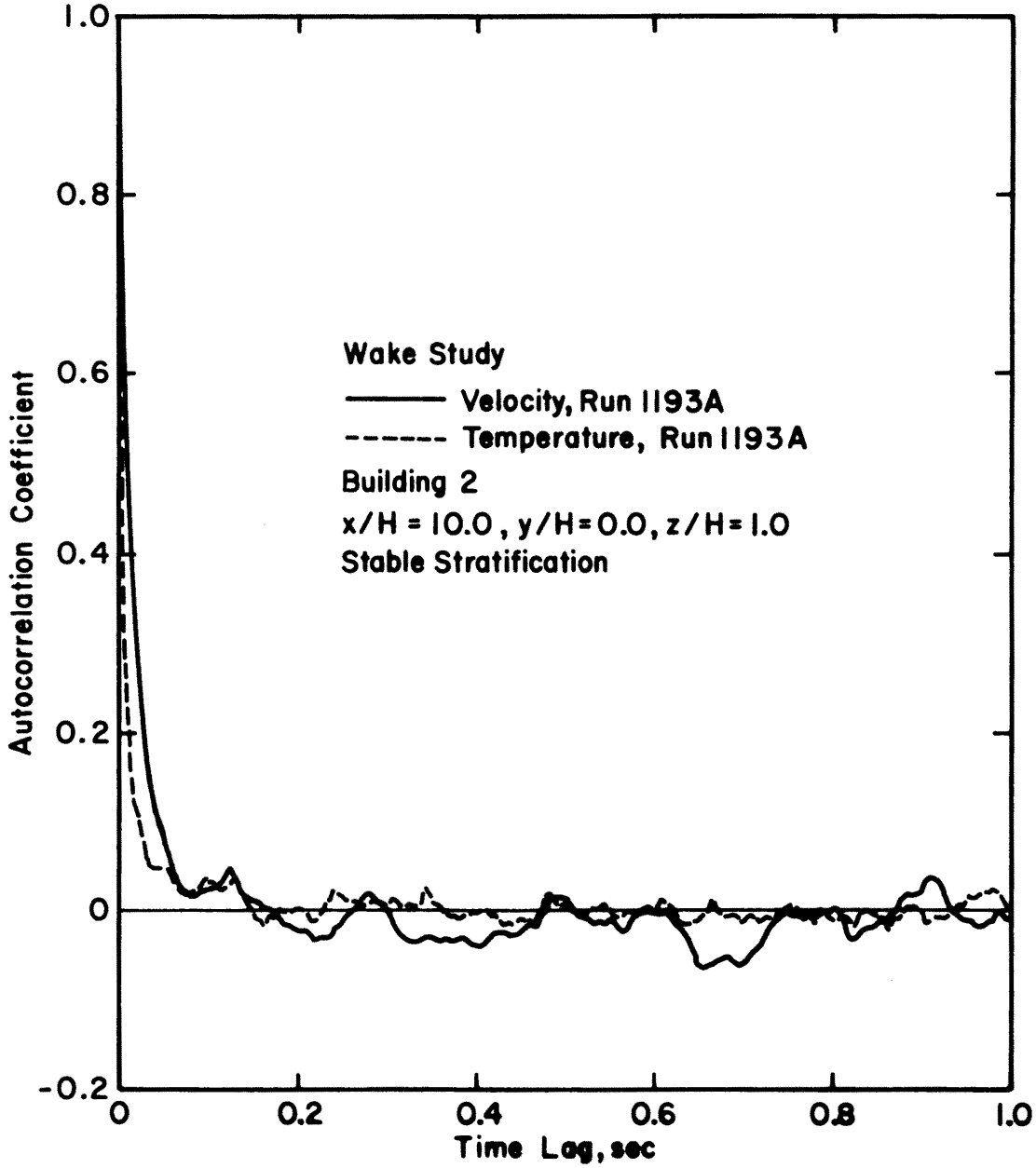

Figure 59. Comparison of auto-correlation coefficients derived from velocity and temperature spectrum behind building 2.